Appendix 9

Hydrodynamic, Morphodynamic, and Dredge Plume modelling reports

Hydrodynamic Modelling Update

Effects of Proposed Reclamation and Dredging Layout on Hydrodynamics

Report prepared for Northport

August 2022

MetOcean
SOLUTIONS

Document History

Versions

Version	Revision Date	Summary	Reviewed by
0.1	01/07/2022	Initial document created	Watson
0.2	16/07/2022	Draft for internal review	Berthot/Watson
0.3	18/07/2022	Draft for Client review	Berthot
0.4	26/08/2022	Draft for Client addressing review comments	Watson/Berthot

Distribution

Version	Date	Distribution
1.0		

Document ID: P0519 - 10

Authors

Berthot A., Watson H.

Contributors

MetOcean Solutions is a Division of Meteorological Services of New Zealand Ltd, MetraWeather (Australia) Pty Ltd [ACN 126 850 904], MetraWeather (UK) Ltd [No. 04833498] and MetraWeather (Thailand) Ltd [No. 0105558115059] are wholly owned subsidiaries of Meteorological Service of New Zealand Ltd (MetService).

Contents

List of Figures

List of Tables

1. Introduction

Northport is a deep-water commercial port strategically situated at Marsden Point near Whangarei in Northland, New Zealand (Figure 1-1). Northport's current footprint totals 58 hectares, with 570 linear metres of berthage consisting of three berths, 30 hectares paved and being used for cargo operations, and berth with a depth at Chart Datum (CD) of 13 m at berth 1 and 2, and 14.5 m at berth 3 (Northport, 2020).

Northport is planning to expand the port's capacity by reclaiming land and building additional berths. MetOcean Solutions (MOS, a division of the Meteorological Service of New Zealand) has already undertaken a number of a number of numerical hydrodynamic and morphological modelling simulations and dredged plume dispersion simulations related to this project, with results presented in MOS reports P0367-01 to P0367-06 (MetOcean Solutions Ltd, 2018a, 2018b, 2018c, 2018d, 2018e, 2018f) and P0519-01 to P0519-03 (MetOcean Solutions Ltd, 2021a, 2021b, 2021c). The proposed dredging footprint and depth are displayed in Figure 1-2.

This technical report provides the outcomes of hydrodynamic modelling for the Eastern Reclamation which include the following tasks:

- Review grid spacing in the area around the Eastern Reclamation and revised dredge footprint, including refining the hydrodynamic grid to ensure structures and batterslopes are accurately captured within the numerical model.
- Simulations of hydrodynamic with the Eastern Reclamation and comparison to simulations with the existing bathymetry (updated with the latest survey). Runs over a full month of hydrodynamic (2 spring/neap cycles) modelling and an assessment of change in currents over a typical spring and neap tidal cycle.

The structure of this report is organised as follows. Section 2 presents a summary of previous study undertaken at the site. Section 3 describes the methodology. In Section 4, results of hydrodynamic modelling from both existing and proposed bathymetry layout are presented. Section 5 provides a summary of this report. A list of references is given in the last section of the document.

Figure 1-1 Location of Northport within Whangarei Harbour.

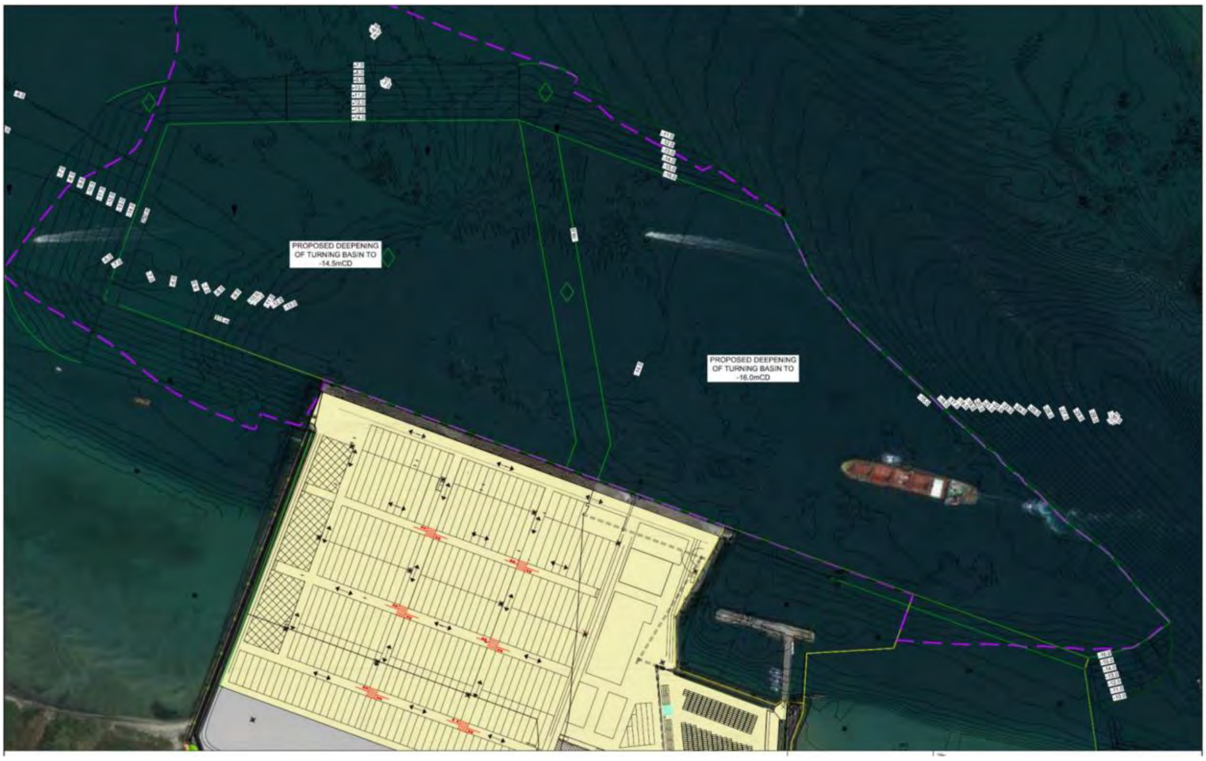

Figure 1-2 Eastern Reclamation concept drawing for the proposed area to be dredged and reclaimed.

2. Previous Studies

Over the last 11 years, MetOcean Solutions has undertaken several modelling studies of the Whangarei Harbour. The characterisation of the physical environment of the Whangarei Harbour and the establishment of wave, current and sediment dynamics numerical models initiated in 2015-2016 with the Refining New Zealand (RNZ) proposed deepening of the shipping channel to Marsden Point Refinery (MetOcean Solutions Ltd, 2016).

Each of the model software used in the studies was selected for a specific technical requirement and a flow diagram of the overall modelling process is presented in Figure 2-1. The numerical models included:

- SWAN[1] (Simulating Waves Nearshore) wave model (Holthuijsen et al., 2007)
- ROMS hydrodynamic model, (Regional Ocean Modelling System, described in (Haidvogel, D.B et al., 2008))
- SELFE/SCHISM hydrodynamic model (Zhang and Baptista, 2008)
- Delft3D Hydrodynamic/Wave/Sediment Transport suite (Deltares, 2018a, 2018b).
- ERcore Lagrangian particle tracking model.

The models were calibrated and validated with available measured data. Details and examples of the model validation extracted from the previous reports can be found in previous reports (MetOcean Solutions Ltd, 2021a, 2018b). The work presented in this report was built upon the existing knowledge and previous model setups and development.

Effects of proposed reclamations layouts on hydrodynamics using the calibrated and validated SCHISM model was undertaken previously and presented in MOS report P0519-01 (MetOcean Solutions Ltd, 2021a). The potential changes to hydrodynamics of the area were evaluated against existing bathymetry for three layouts, Full Vision for Growth scenario (VFG), Western reclamation only, Eastern reclamation only. The same model setup/configurations were used from the previous studies including computational domain extent, model forcing terms.

An evaluation of sensitivity to wind driven currents was also undertaken. The outcome was that wind-driven currents are not significant within the proposed dredging and reclamation regions and tidal current are expected to dominate there. However, the wind field can trigger additional current speed of 0.3m/s in shallow areas of the harbour and

[1] Modified from SWAN version of the 40.91 release (publicly available code)

along the port entrance. Therefore, it was recommended that the atmospheric forcing is included in the SCHISM model and they were included in the 2021 study.

Results from the study found that changes in the current field were confined to the region where the dredging and reclamation works would be undertaken and changes in current speed during a spring tide were expected to be typically less than 0.1m/s. There was also a small decrease in predicted currents near the Western and Eastern reclamation ends which indicated a potential for increase in sedimentation in this area.

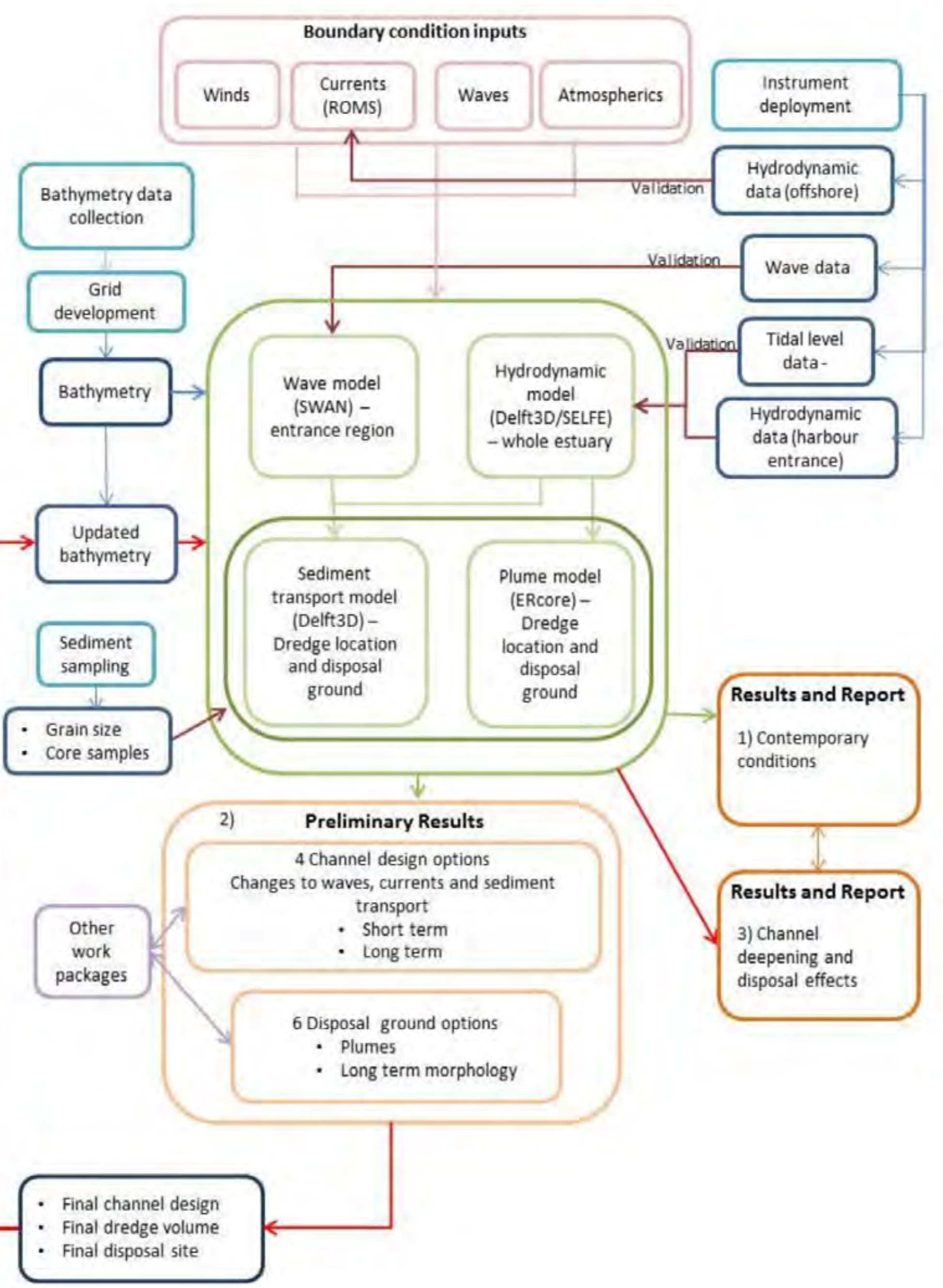

Figure 2-1 Flow chart showing the numerical modelling process and model development for the 2016 RNZ Whangarei study

3.Methodology

The present study applied the same model setup/configurations used in the previous studies including computational domain extent and model forcing terms (MetOcean Solutions Ltd, 2021a, 2018b). By doing so, it is expected that all the previous model features and calibration could be retained. Compared to previous studies, the only differences in the model configurations of the present investigation are the use of the updated bathymetry provided by the Port and the mesh refinement around the proposed layout (described in Section 3.2). The purpose of refining the mesh around the proposed dredging and reclamation areas is to capture the shape of the new designed batter slope and the proposed layout. The following sections briefly describe the numerical model framework, computational domain, model forcing inputs, model verification applied for the present study.

3.1 Model description

This study uses the open-sourced hydrodynamic modelling system: Semi-implicit Crossscale Hydroscience Integrated System Model (SCHISM) based on Zhang and Baptista (2008); Zhang et al. (2016). It is based on unstructured grid algorithms with the robustness and computational efficiency designed to address various applications across creek-lake-river-estuary-shelf-ocean scales with high accurate levels. Specifically, SCHISM does not require any splitting mode and thus excludes the splitting errors which often procedure between internal and external modes. It employs the semi-implicit time stepping with Eulerian-Lagrangian treatment of advection (Zhang and Baptista, 2008) with an implicit transport solver using two limiter functions which have been shown to work with different Courant numbers (Zhang et al., 2016).

The major challenge to coastal modelling is to resolve the complex shoreline and bathymetry in horizontal space. The unstructured models are ideal for this. However, many unstructured grid models use explicit splitting methods which are restricted to the Courant conditions. The stability of these models often requires a small timestep. Further, in 3D ocean modelling, the restriction is often related to the numerical scheme used to solve the vertical dimension. Due to small grid size in the vertical layer, the explicit scheme which is also subjected to the Courant criterion requires a large number of sub-iterations. Generally, explicit ocean models are often computationally more expensive.

Additionally, in 3D mode, SCHISM utilises the Localised Sigma Coordinates (Zhang et al., 2014) (described in a latter section) which allow to maximise the benefits from the traditional Z and terrain-following coordinate system while excluding their limitations. Therefore, SCHISM is an ideal modelling system to simulate hydrodynamics for dredging applications required in the present study. For reference, the reader may refer to several international studies[2] that used SCHISM model to address dredging impacts including those done by Lopes et al. (2009), Mendes, Fortunato, and Pires-Silva (2016) and Ye et al. (2018b).

3.2 Model domain

The model domain is defined by the horizontal grid shown in Figure 3-1. The grid extends into Bream Bay with the water depth of 60m to capture ocean tides. The mesh resolution varies from a coarse mesh size of approximately 300 m at the open boundary to the finest size of approximately 5 m located nearshore and in the proposed dredged and reclamation areas. To reflect changes in the bathymetry between the existing and the proposed Eastern Reclamation, the same computational grid was used for both simulations. Figure 3-2 and Figure 3-3 present the interpolated bathymetry captured by the computational grid for the existing and proposed Eastern Reclamation (named Design East in simulations) respectively. The reporting locations for the model outputs are displayed in Figure 3-2 and Figure 3-3.

[2] http://ccrm.vims.edu/schismweb/schism_pubs.html

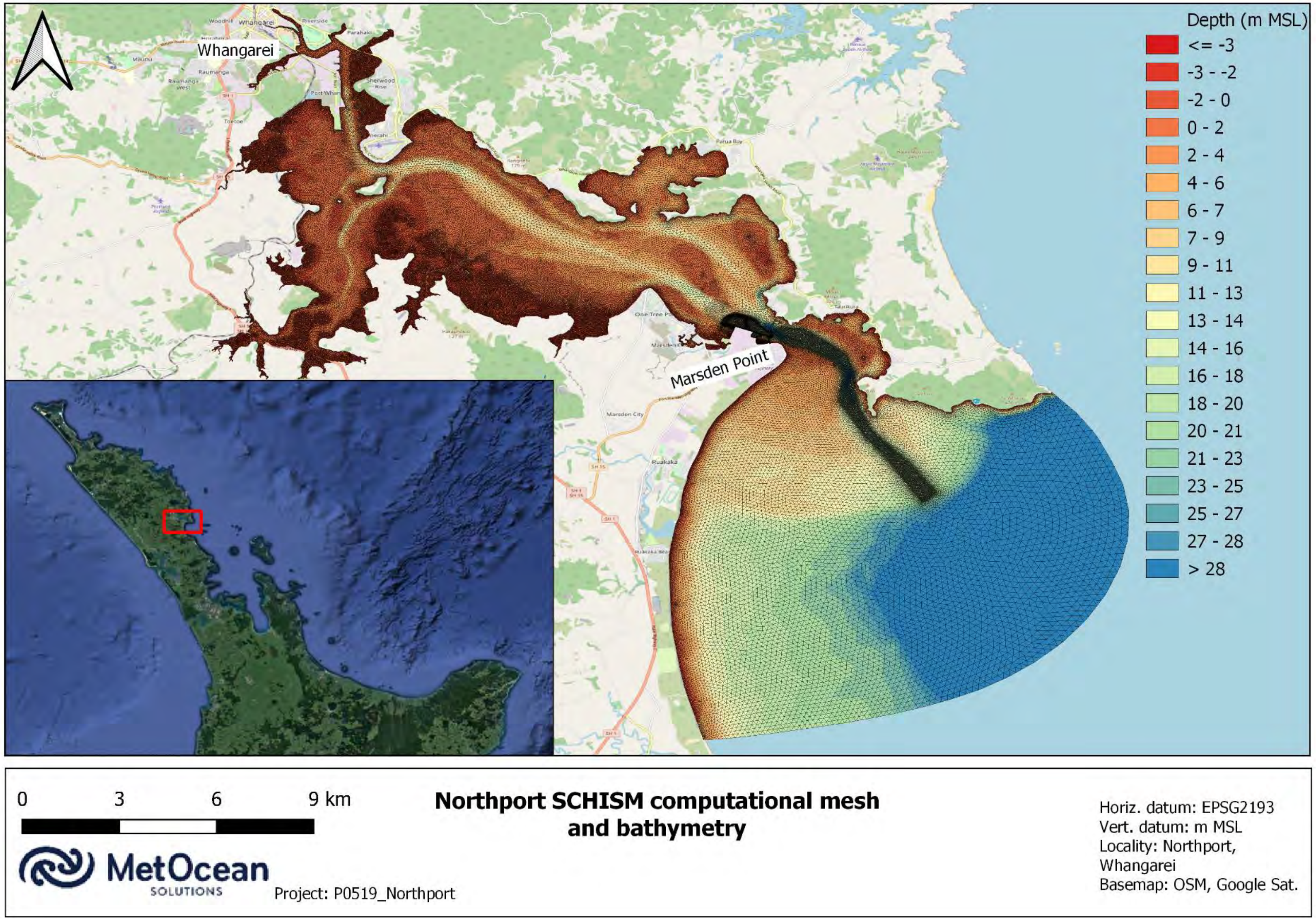

Figure 3-1 SCHISM computational mesh and bathymetry.

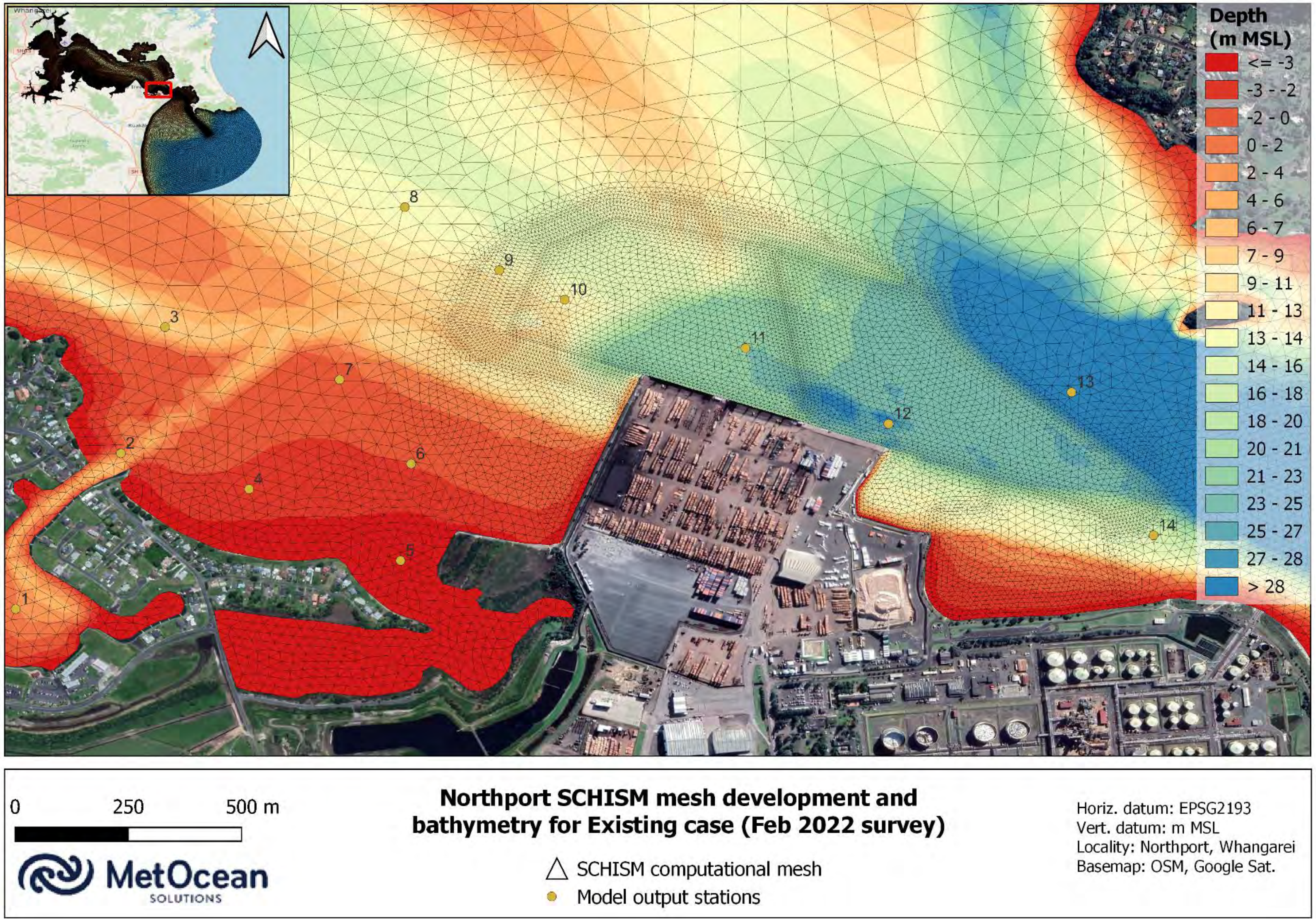

Figure 3-2 SCHISM computational mesh and bathymetry for the Existing case.

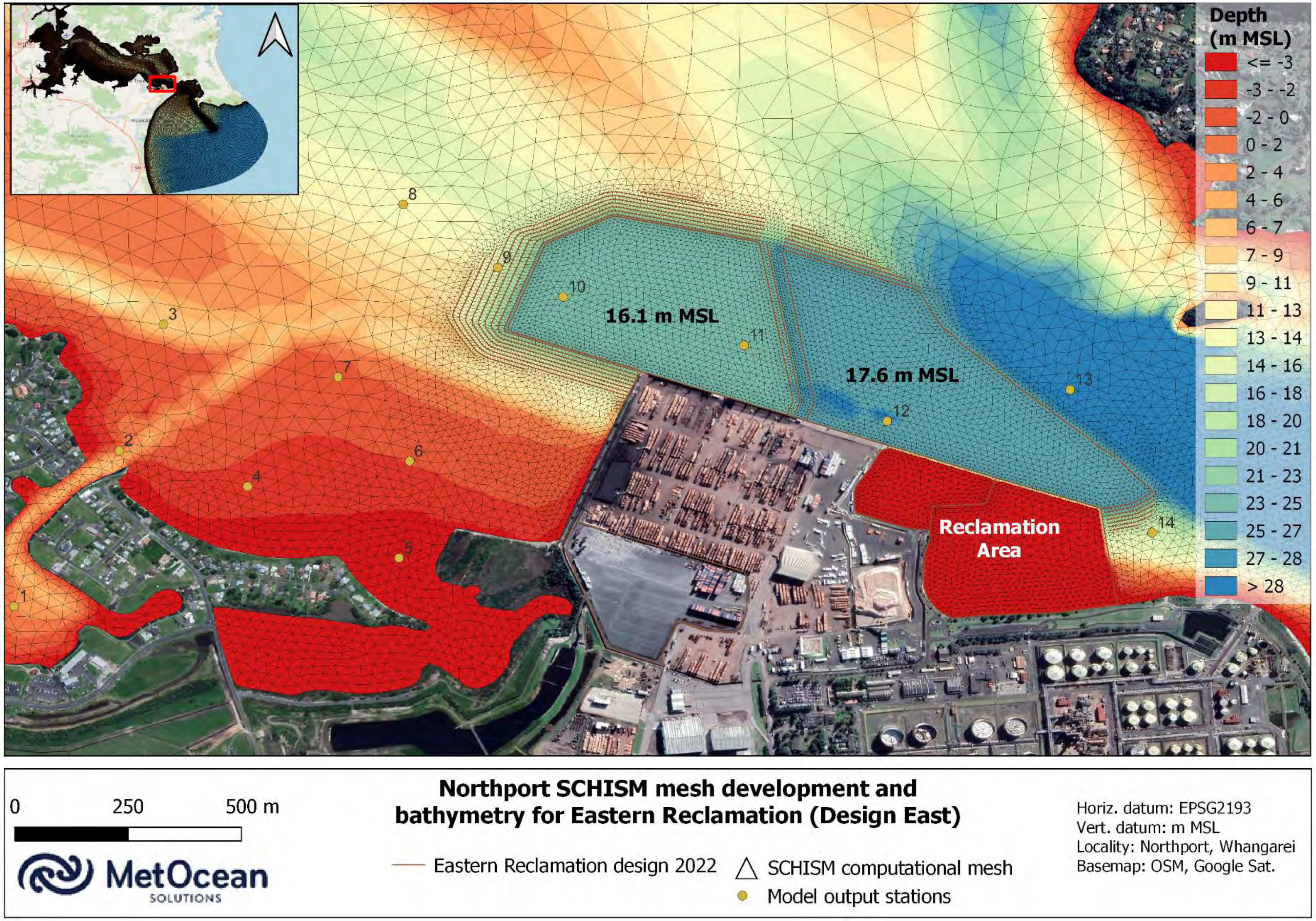

Figure 3-3 SCHISM computational mesh and bathymetry for the Eastern Reclamation design case (Design East).

3.3 Vertical grid

In this study, SCHISM was configured in 3D mode, and thus requires a vertical grid or vertical coordinate system to be designed. In ocean modelling, the importance of the vertical coordinate system has long been identified. Currently, there are three commonly used vertical coordinates namely Z, terrain-following, and pressure coordinates. However, these coordinate systems come up with its own problems (e.g. see Song and Hou (2006) for a review). For instance, Z-coordinates often creates an artificial staircases resulting in artificial drag. Similarly, the terrain-following coordinate systems often have a problem with the pressure gradient discretization leading to spurious flow. For the least commonly used vertical coordinates, the isopycnal or pressure-coordinate system faces a problem about the mass preservation in the well-mixed zones. Therefore, all of the mentioned coordinates were not chosen for the present study.

A Localised Sigma Coordinates with Shaved Cell (LSC^2) developed by Zhang et al. (2014) is used to eliminate the above issues. After this development, the LSC^2 vertical grid has been widely used in the SCHISM modelling community[3] including those done by Ye et al. (2016), Ye et al. (2018a), Zhang et al. (2020) and Liu et al. (2020). This is the most advanced vertical grid system which has benefits from both the terrain-following and Z-coordinate systems making 3D SCHISM models very efficient in terms of computational resources. Furthermore, smoothness features in the LSC^2grid are designed to eliminate the staircase problem caused by the mismatch between vertical layers. This problem is commonly found in other traditional vertical grid systems applied for coastal domains where the bathymetry is often complex. An example for the LSC^2grid used in this project is shown in Figure 3-4.

[3] http://ccrm.vims.edu/schismweb/

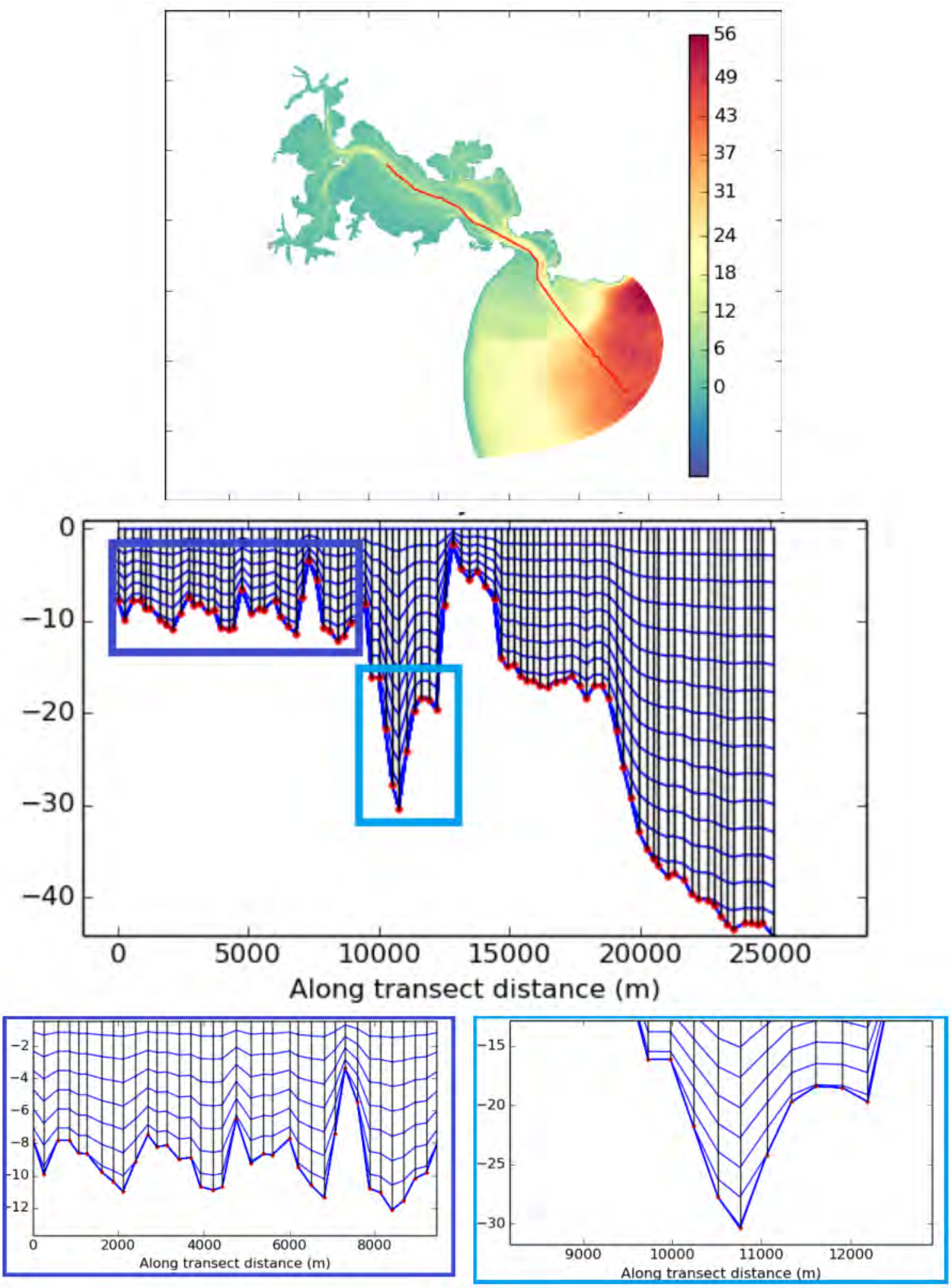

Figure 3-4 The design of a LSC2 vertical grid for 3D SCHISM model. The top panel presents a cross section (red line) along the main channel over the horizontal domain. The vertical grid along this section shows in the middle panel. Two zoomed sections (in rectangular boxes) are plotted in the bottom panel.

3.4 Model inputs

Bathymetry is an important input of numerical models. In this study, MOS has compiled different bathymetry datasets as described in the previous report (MetOcean Solutions Ltd, 2018b) and updates to the existing bathymetry in 2020 (MetOcean Solutions Ltd, 2021a).

These data were updated with the most recent surveys provided by the Port at Marsden Point and upstream in Portland Channel and Wellington Reach both undertaken in February-March 2022 at 2m resolution in CD. The updated existing bathymetry were used as the base for the existing model layout shown in Figure 3-2. The existing bathymetry layout was then modified to account for the proposed reclamation and dredging option detailed in Figure 1-2 (depths also given in CD). The bathymetry used for the Eastern Reclamation is displayed in Figure 3-3. It is noted that the bathymetry attached to the numerical mesh was in mean sea level (MSL) using the linear interpolation method.

The computational domain has an open boundary on the ocean side which requires tidal conditions to be prescribed. In the present study, SCHISM was forced with tidal constituents at open boundary grid points. These constituents were derived from one-year ROMS model within Whangarei domain with a spatial resolution of 0.3 km. The velocity, residual components, salinity, and temperature were also interpolated into the 3D SCHISM grid from the same ROMS model.

Sensitivity analysis undertaken as part of the previous hydrodynamic modelling (MetOcean Solutions Ltd, 2021a) assessed the effects of wind forcing on currents and described the subsequent inclusion of wind forcing in the simulations. As in the previous modelling, the near-surface wind field was prescribed by a 36-year (1979-2014) regional atmospheric hindcast carried out by MOS. The WRF (Weather Research and Forecasting) model was established over all of New Zealand at hourly intervals and approximately 12 km resolution. The hindcast was specifically tuned to provide highly accurate marine wind fields for metocean studies around New Zealand. The WRF model boundaries were sourced from the CFSR (Climate Forecast System Reanalysis) dataset distributed by NOAA (Saha et al., 2010), which was available at hourly intervals and 0.31° spatial resolution.

While the WRF hindcast produced atmospheric parameters at hourly intervals over the 36 years, only the near surface wind field (i.e. 10 minute mean at 10 m elevation) are used in the study. Validation of the WRF reanalysis has been undertaken at various locations around New Zealand. More details about model inputs can be found in the final report written for Refining New Zealand project (MetOcean Solutions Ltd, 2019).

3.5 Model calibration and validation

Model calibration and validation has been was undertaken in the previous Whangarei Harbour studies done by MOS for Refining New Zealand (MetOcean Solutions Ltd, 2019, 2016) and for Northport (MetOcean Solutions Ltd, 2018a, 2018b, 2018c, 2018d, 2018e, 2018f). Reporting of sensitivity tests undertaken in the MOS 2021 updated of the SCHISM model to ensure the updated SCHISM mesh show consistent results with the existing DELFT3D model along with sensitivity analysis of wind driven currents can be found in MOS report P0519-01 (2021a).

However, due to the further mesh refinement in the SCHISM computational grid at the proposed site, sensitivity tests were undertaken to ensure the updated SCHISM mesh show consistent results within the present study. Comparison of water level and current timeseries and maps for the simulations of existing bathymetry between the 2021 mesh and the present studies refined mesh with 2022 bathymetry survey are presented in Figure 3-5 and Figure 3-6 for a spring flood and ebb tide respectively. No notable differences are evident between the two existing simulations during a spring tide.

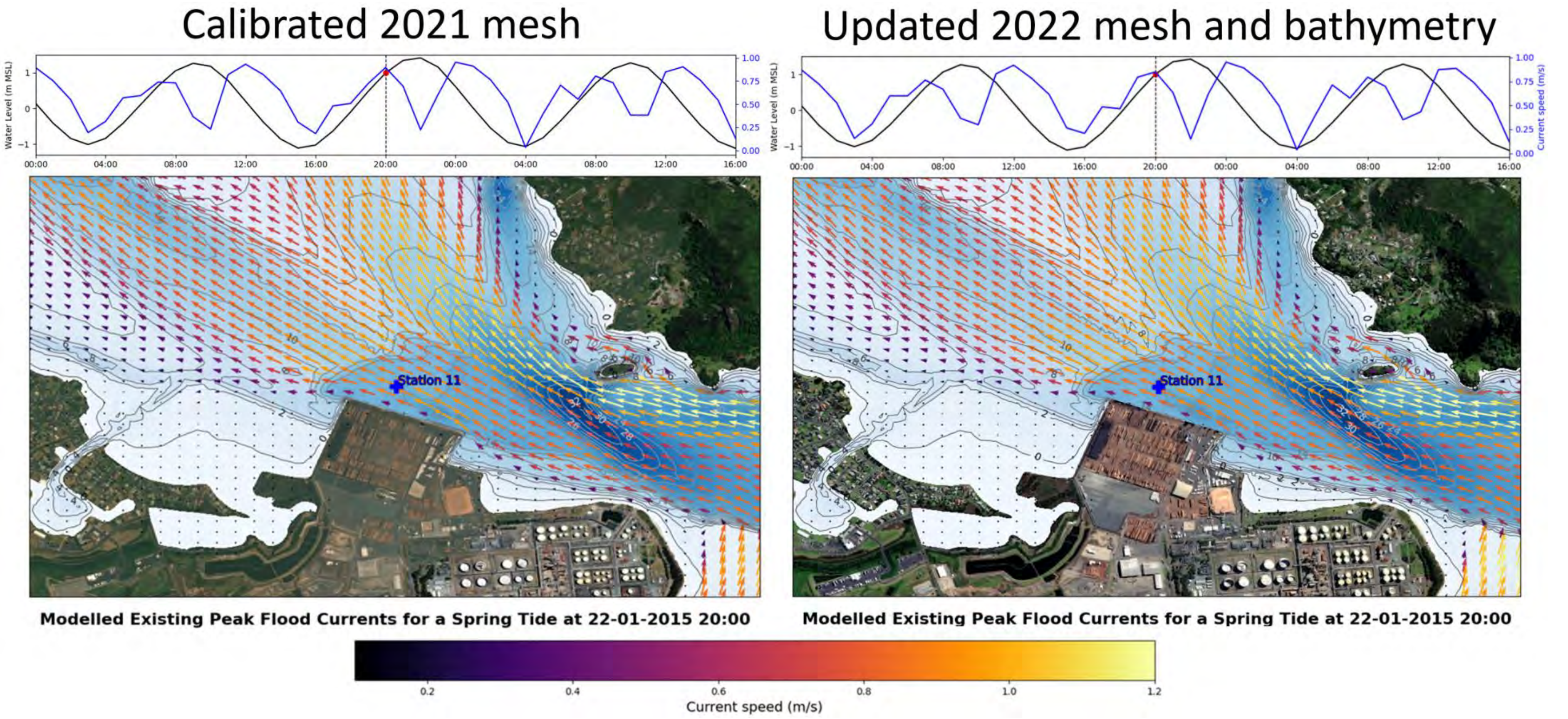

Figure 3-5 Comparison of peak ebb current maps for a spring tide of the Existing simulations from the 2021 model and the updated mesh and bathymetry used in the present study

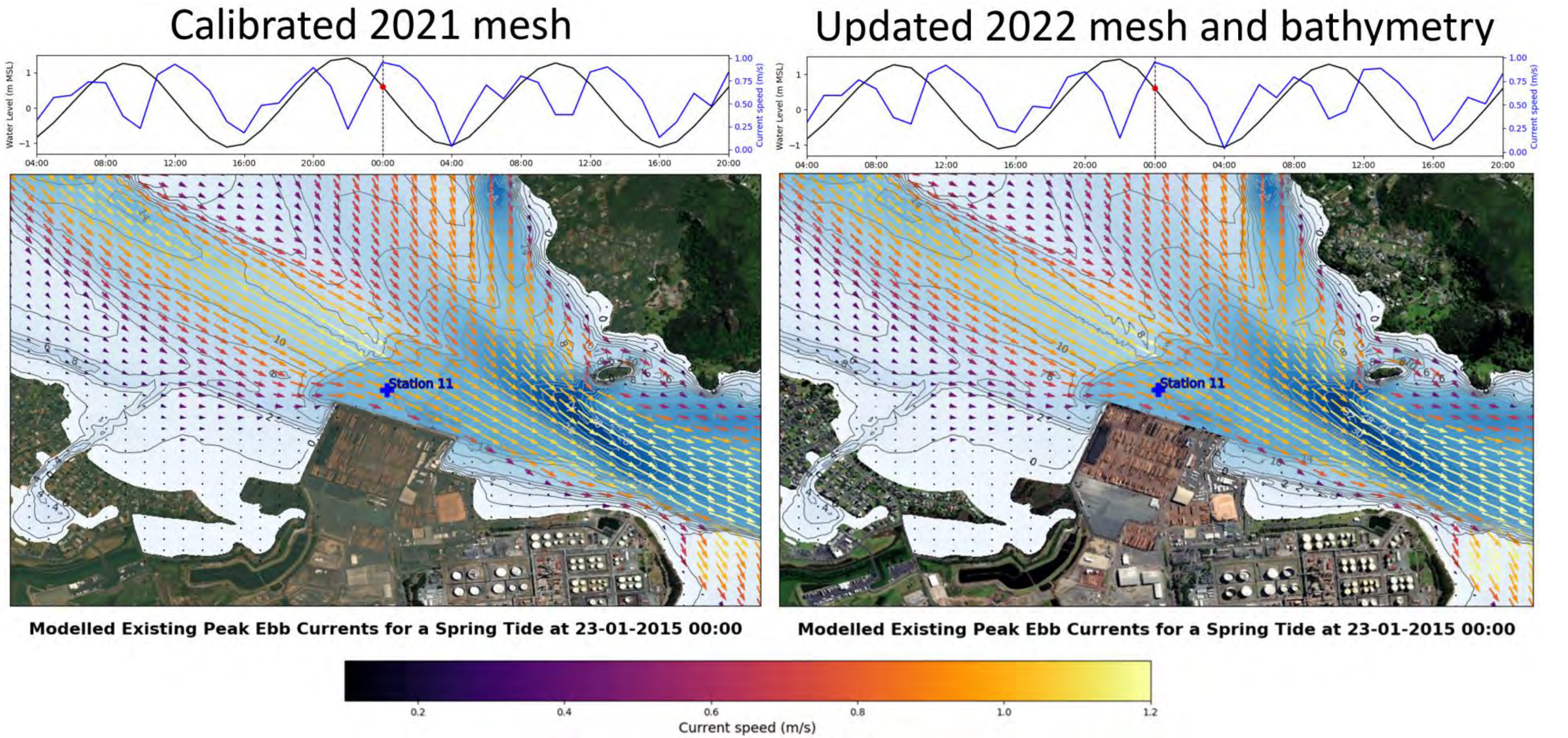

Figure 3-6 Comparison of peak ebb current maps for a spring tide of the Existing simulations from the 2021 model and the updated mesh and bathymetry used in the present study.

4. Results

As tidal forcing dominates the climatology at the site, hydrodynamic simulations were undertaken over a 29-day full lunar cycle (2 spring/neap cycles). The modelled period was retained from the previous modelling reports of 1st -30th January 2015. Simulations of the proposed Eastern Reclamation (named Design East in simulations) were compared to existing simulations to determine any potential impacts of the proposed design on hydrodynamics at the site.

4.1 Effects of Eastern Reclamation layout on hydrodynamics

Comparison of the modelled water levels and currents between the existing and design (Eastern Reclamation) simulations over the full simulation period are assessed at selected station output locations. Station output locations and depths are displayed in Figure 3-2 and Figure 3-3. The tidal planes at two stations are displayed in Table 4-1, showing no changes at station 3 in Blacksmith Creek and at station 10 within the dredge footprint only 0.01m decrease in the LAT.

A statistical analysis of the current speeds at selected stations is displayed in Table 4-2. The largest change in current speeds is at station 10 with the 98th percentile current speeds of 1.03 m.s^{-1} and 0.85 m.s^{-1} for the existing and design simulations respectively. The percentage difference in mean current speeds is a 29.6% reduction due to the change of depth between the two simulations from 8.4 m to 16.1 m (MSL). Stations 12 near the berth pocket and station 14 to the east of the proposed reclamation also show a reduction in current speeds with the 98th percentile values reducing from 1.02 m.s^{-1} to 0.91 m.s^{-1} at station 12 and 0.95 m.s^{-1} to 0.79 m.s^{-1} at station 14. There is only a 6.7% increase in mean current speeds at station 3. Timeseries of the modelled existing and design (Eastern Reclamation) water levels, current speeds and directions for the full simulation period at selected stations where the largest change occurred are displayed in Figure 4-1, Figure 4-2 and Figure 4-3.

Table 4-1 Tidal planes (m) relative to MSL for existing and design (Eastern Reclamation) simulations derived over 29-day lunar cycle for selected stations.

Parameter	**Station 3**		**Station 10**	
	Existing	Design	Existing	Design
HAT (Highest Astronomical Tide)	1.30	1.30	1.29	1.29
MHWS (Mean High Water Springs (M2+S2))	1.03	1.03	1.02	1.02
MHWN (Mean High Water Neaps (M2-S2))	0.77	0.77	0.76	0.76
MSL (Mean Sea Level)	0.00	0.00	0.00	0.00
MLWN (Mean Low Water Neaps (-M2+S2))	-0.77	-0.77	-0.76	-0.76
MLWS (Mean Low Water Springs (-M2-S2))	-1.03	-1.03	-1.02	-1.02
LAT (Lowest Astronomical Tide)	-1.31	-1.31	-1.29	-1.30

Table 4-2 Current speed statistics (m. s^{-1}) for existing and design (Eastern Reclamation) simulations derived over 29-day lunar cycle for selected stations.

Station	**Simulation**	**Mean**	**80th %tile**	**90th %tile**	**95th %tile**	**98th %tile**	**Max**	**% diff. in mean**
Station 3	Existing	0.15	0.21	0.27	0.31	0.34	0.41	6.7%
	Design	0.16	0.22	0.27	0.31	0.35	0.42	
Station 8	Existing	0.52	0.74	0.83	0.91	0.98	1.09	0.0%
	Design	0.52	0.74	0.85	0.93	1.01	1.11	
Station 10	Existing	0.54	0.77	0.87	0.96	1.03	1.17	-29.6%
	Design	0.38	0.57	0.68	0.77	0.85	0.95	
Station 11	Existing	0.53	0.75	0.89	0.99	1.07	1.21	-7.5%
	Design	0.49	0.70	0.83	0.93	1.02	1.16	
Station 12	Existing	0.47	0.66	0.78	0.91	1.02	1.21	-19.1%
	Design	0.38	0.55	0.69	0.78	0.91	1.13	
Station 13	Existing	0.54	0.75	0.90	1.02	1.15	1.31	1.9%
	Design	0.55	0.77	0.89	0.99	1.08	1.29	
Station 14	Existing	0.42	0.61	0.73	0.82	0.95	1.24	-19.0%
	Design	0.34	0.51	0.60	0.67	0.79	1.05	

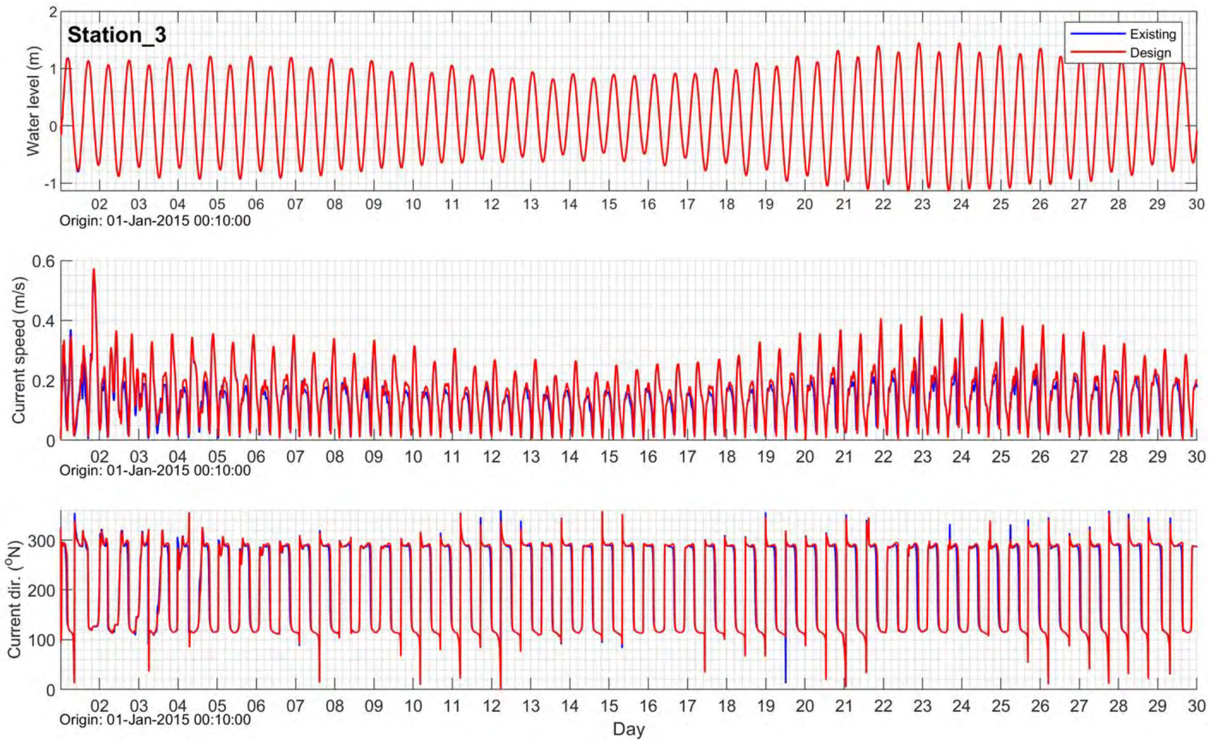

Figure 4-1 Comparison of existing and design (Eastern Reclamation) water levels, current speeds and directions for the full simulation period at station 3.

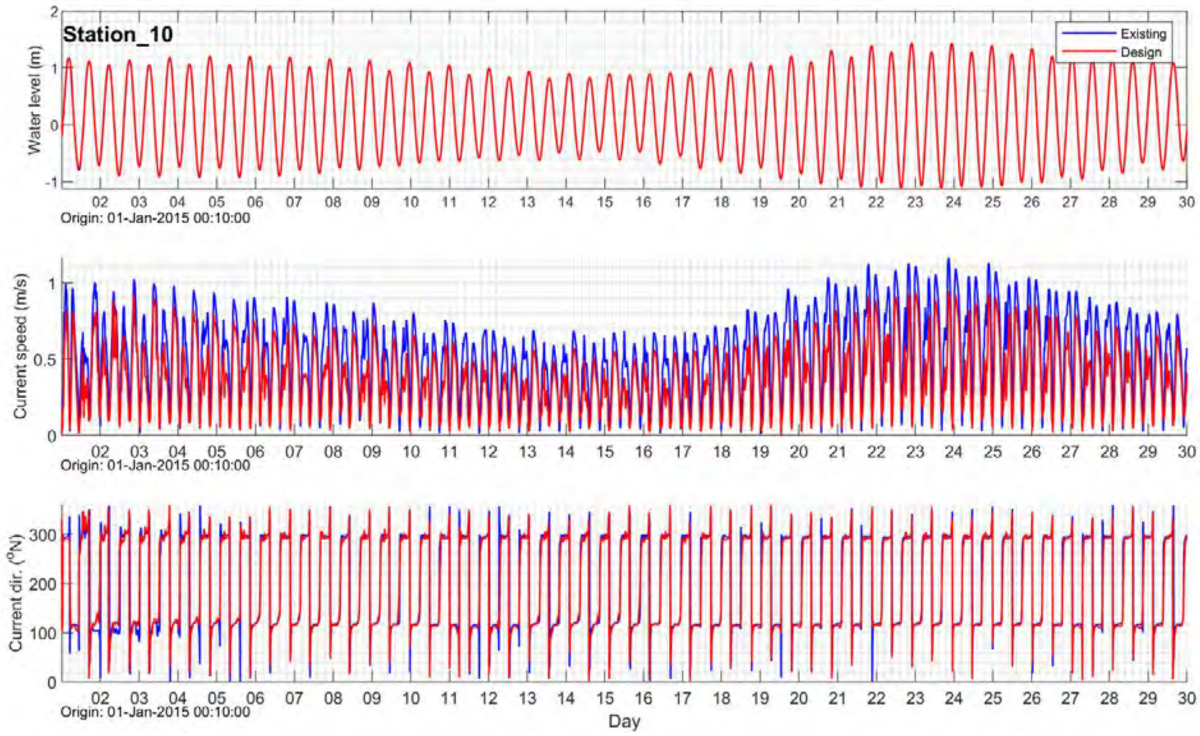

Figure 4-2 Comparison of existing and design (Eastern Reclamation) water levels, current speeds and directions for the full simulation period at station 10.

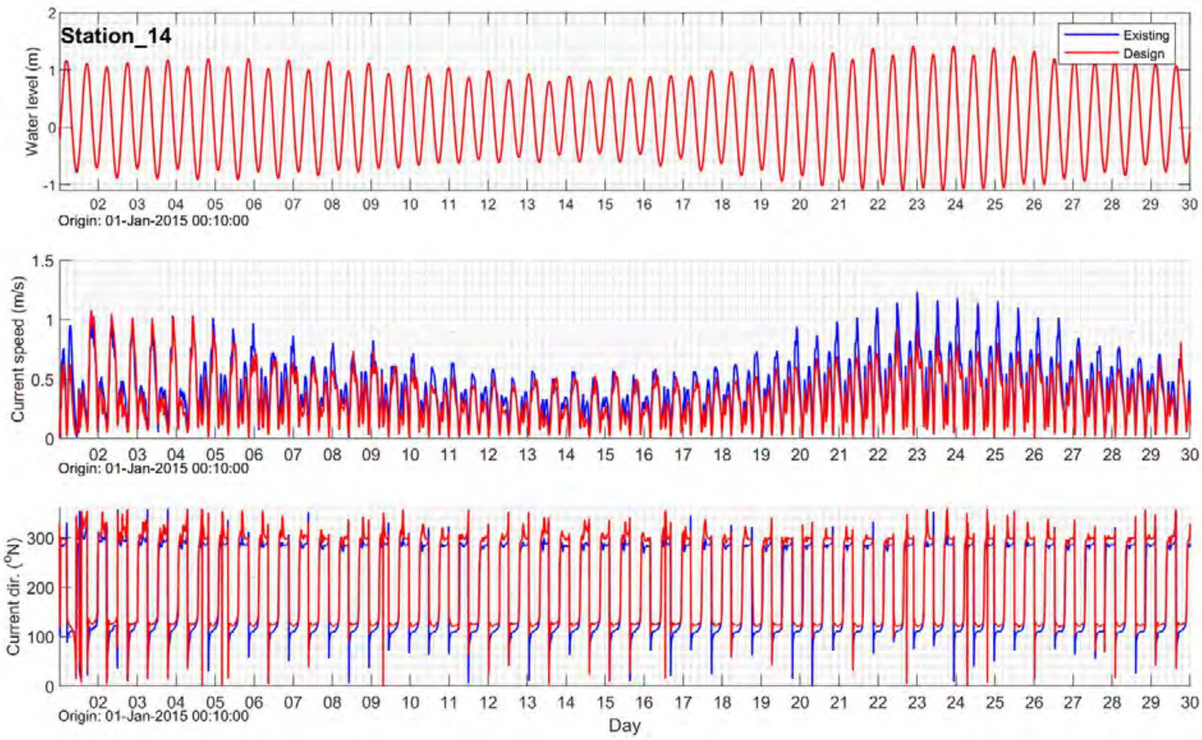

Figure 4-3 Comparison of existing and design (Eastern Reclamation) water levels, current speeds and directions for the full simulation period at station 14.

4.1.1 Spring tidal cycle

Modelled current vectors during a spring tide for the existing and the proposed Eastern Reclamation (design east) layout are displayed at peak flood in Figure 4-4 and at peak ebb in Figure 4-5. The predicted change in current magnitude between the two options (design-existing) is presented in Figure 4-6 and Figure 4-7 for the flood and ebb tide respectively. Potential changes less than 0.05 $m.s^{-1}$ are masked as they are within the magnitude of model error and were not considered as a meaningful change.

In terms of magnitude, the current speed during an ebb tidal cycle is expected to be stronger than during a flood tidal cycle as seen in the subplot timeseries and length of current vectors in both maps. During a peak flood and ebb tide, in the majority of the study area the potential reductions in current speed is predicted to be less than 0.4 $m.s^{-1}$, with localised areas of 0.5$m.s^{-1}$. A decrease in current speeds is within the following areas;;

- A reduction at the western edge of the dredge footprint. Currents speeds decreased in this area due to the increase in depth between the two simulations from 8.4 m to 16.1 m MSL;
- A reduction of 0.5$m.s^{-1}$ at the eastern edge of the proposed reclamation and as the flood tide is diverted further into the main channel around the reclamation and on an ebb tide is in the lee of the reclamation;

- On a flood tide, a decrease of less than 0.2 $m.s^{-1}$ on the northern channel inside the harbour entrance opposite the port due to the deepening of the dredge footprint in front of the reclamation to 17.6 m MSL, directing more of the tidal prism alongside the port rather than through the northern flood channel; and
- On an ebb tide, a reduction in current speed less than 0.2 $m.s^{-1}$ in the area around Blacksmith Creek

Modelled results also show a slight increase in current speeds in some areas during the peak flood and ebb tides. The potential increase in current speeds on a flood and ebb tide in the majority of the study area is predicted to be less than 0.2$m.s^{-1}$, with localised areas with an increase of 0.4 $m.s^{-1}$. An increase in current speeds is within the following areas;

- An increase in front of the reclamation area within the eastern side of the dredge footprint less than 0.2 $m.s^{-1}$;
- Increased current speeds to the west of the dredge footprint less than 0.2 $m.s^{-1}$;
- The largest increase in current speeds is seen alongside the existing berths at 0.4 $m.s^{-1}$change; and
- On a flood tide, there are negligeable increases in current speed less than 0.1 $m.s^{-1}$ in the areas around Blacksmith Creek.

Further, comparisons of current magnitudes for a spring tide over 13 hours at 14 locations in the vicinity of the port are shown in Figure 4-8. In terms of magnitudes, the potential changes within Blacksmith creek can be determined at stations 1-7 which at these points show less than 0.05 $m.s^{-1}$ of change during both a flood (increased speeds) and ebb tide (reduced speeds), this change was too low in magnitude to be displayed within the colour maps in Figure 4-6 and Figure 4-7.

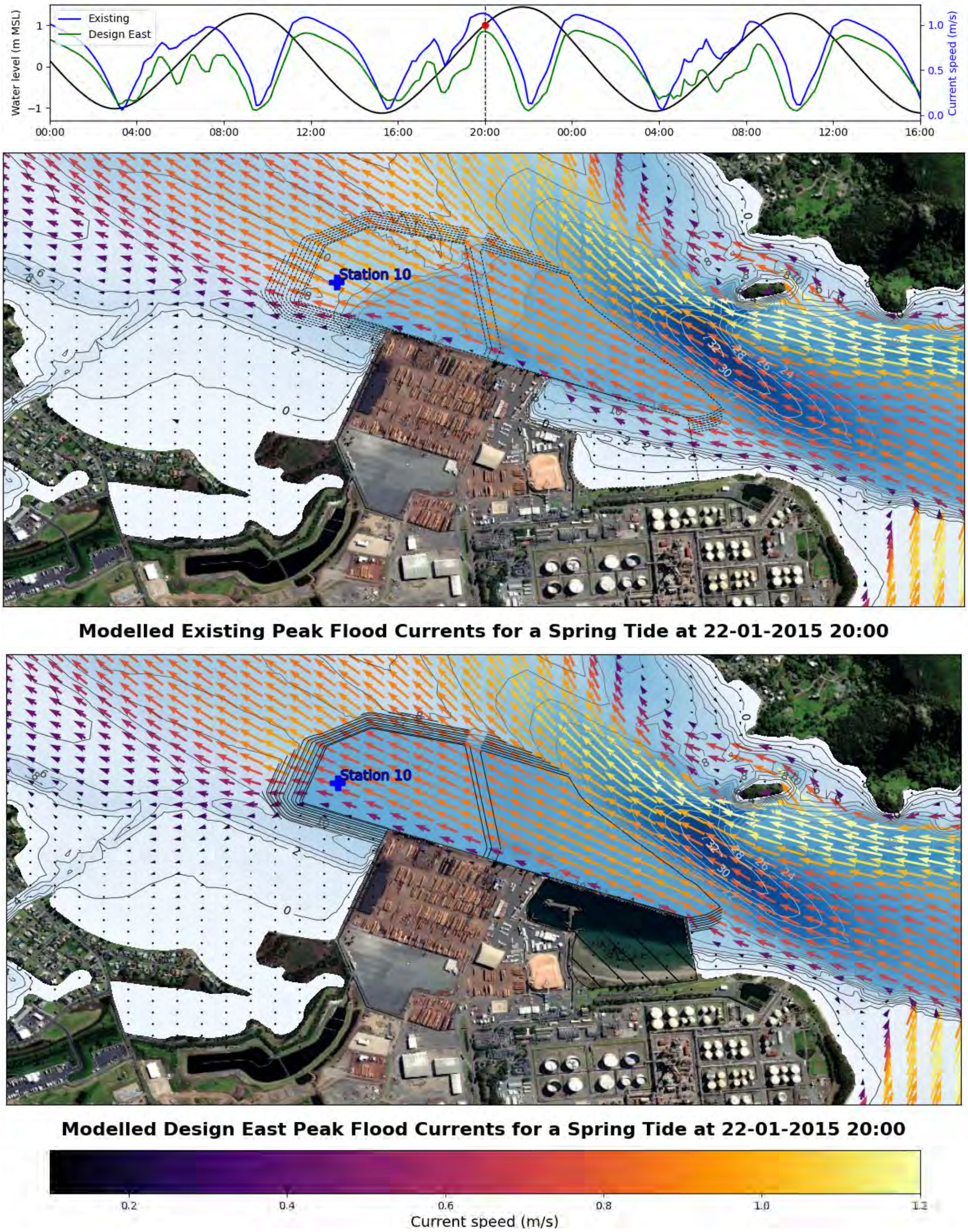

Figure 4-4 Modelled current vectors for the existing (top) and Eastern Reclamation/Design East layout (bottom) during the peak of a flood spring tide and the bathymetry and depth contours used in each simulation. Black design lines display the proposed reclamation and dredging.

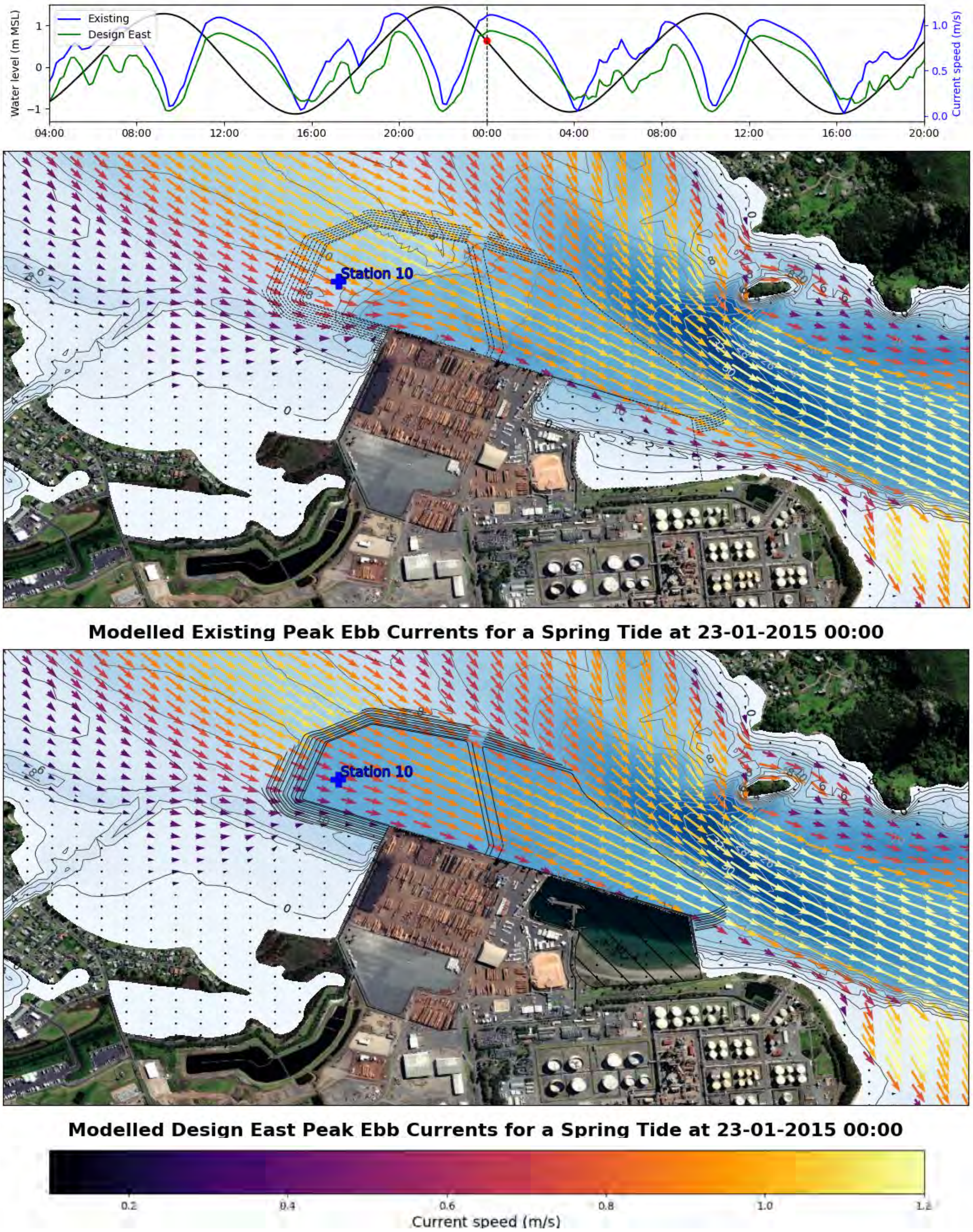

Figure 4-5 Modelled current vectors for the existing (top) and Eastern Reclamation/Design East layout (bottom) during the peak of an ebb spring tide and the bathymetry and depth contours used in each simulation. Black design lines display the proposed reclamation and dredging.

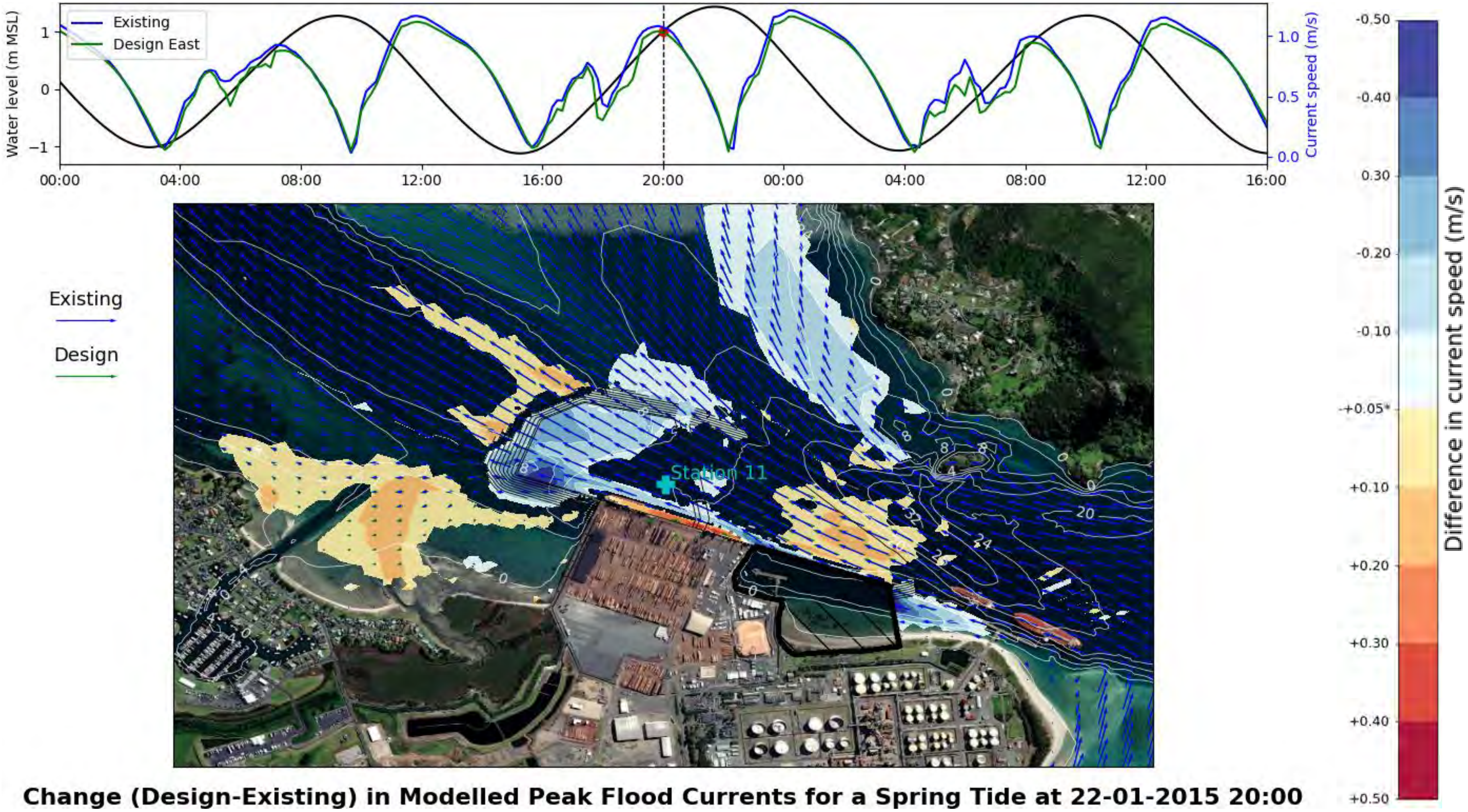

*Figure 4-6 Modelled current vectors for the existing and Eastern Reclamation (Design East) layout and difference in current magnitude during the peak of a flood spring tide. White depth contours are from the existing case and the black design lines display the proposed reclamation and dredging. * Note potential changes less than 0.05 m.s^{-1} are masked as they are within the magnitude of model error and were not considered as a meaningful change.*

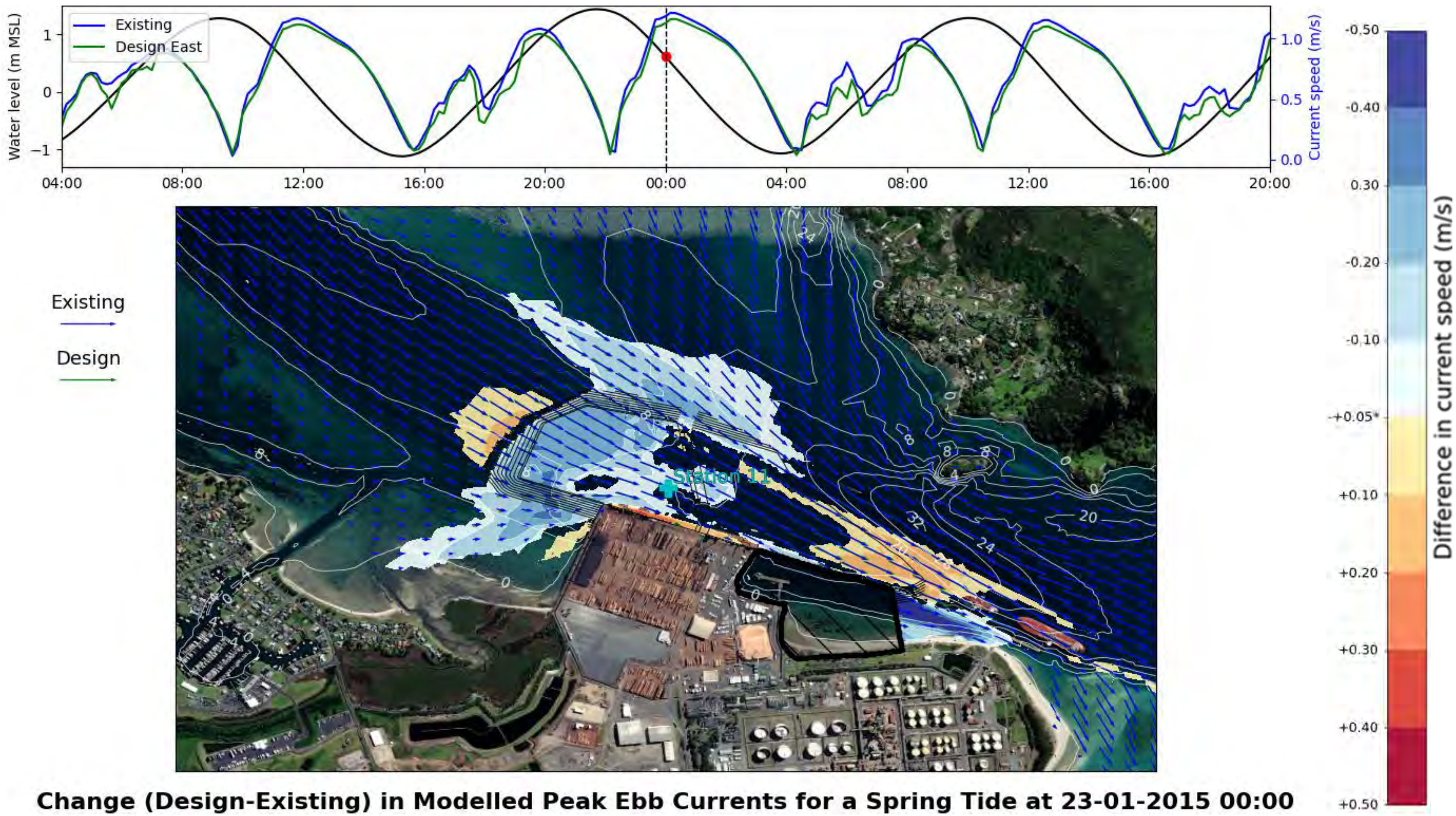

*Figure 4-7 Modelled current vectors for the existing and Eastern Reclamation (Design East) layout and difference in current magnitude during the peak of an ebb spring tide. White depth contours are from the existing case and the black design lines display the proposed reclamation and dredging. * Note potential changes less than 0.05 m.s^{-1} are masked as they are within the magnitude of model error and were not considered as a meaningful change.*

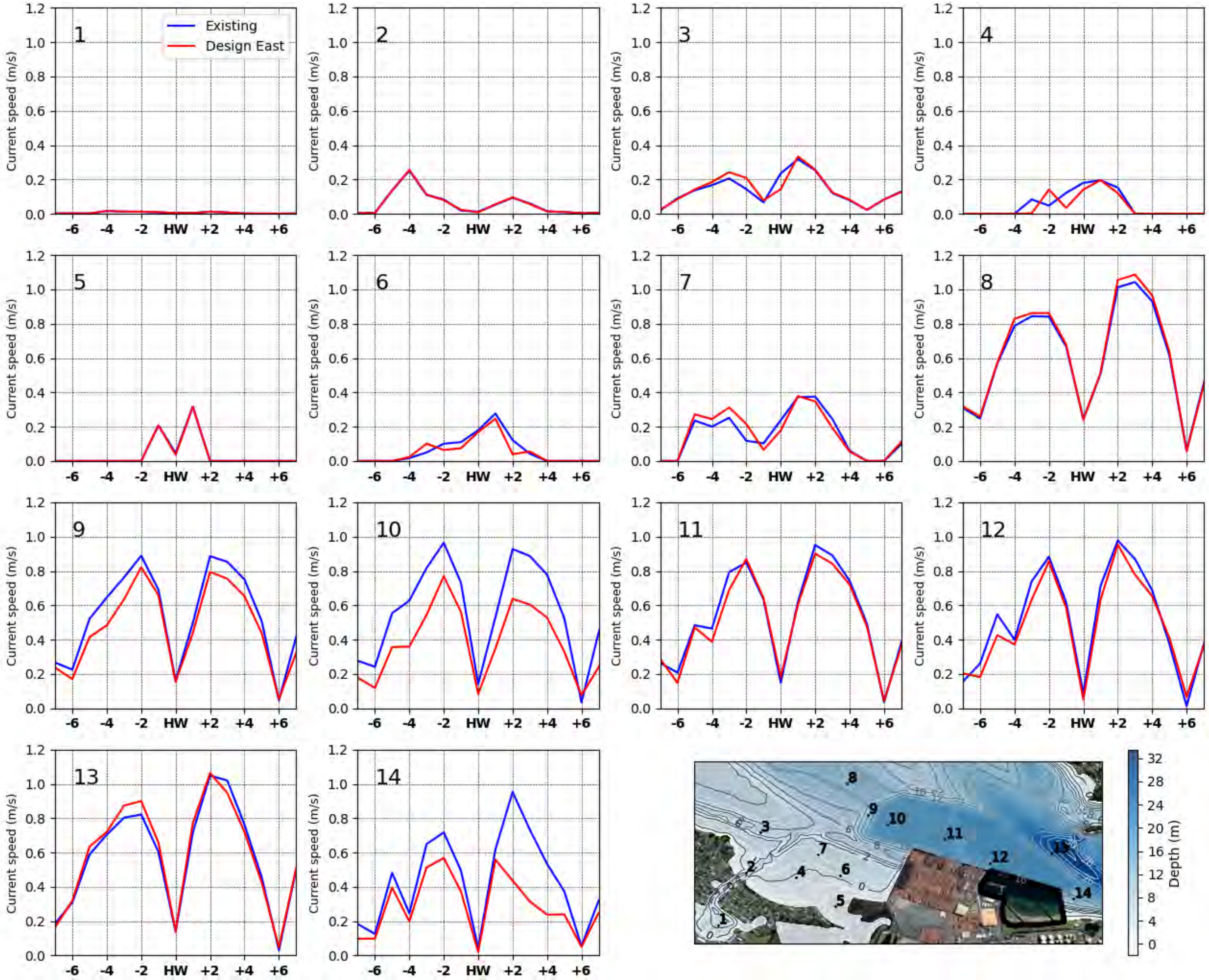

Figure 4-8 Comparisons between modelled current magnitudes for the existing and Eastern Reclamation (Design East) layout for 13 hours of a typical spring tidal cycle.

4.1.2 Neap tidal cycle

Modelled current vectors during a neap tide for the existing and the proposed Eastern Reclamation (design east) layout are displayed at peak flood in Figure 4-9 and at peak ebb in Figure 4-10. The predicted change in current magnitude between the two options (design-existing) is presented in Figure 4-11 and Figure 4-12 for the flood and ebb tide respectively. In terms of magnitude, the current speed near the project site is about 0.5-0.6 $m.s^{-1}$ during a neap tide and about half the speed observed during spring. As a result, the potential changes to current speeds during a neap tide are less than during a spring tide.

Similar patterns are seen, with the reduction occurring at the western edge of the dredge footprint for both a flood and ebb tide, and a slight reduction in the lee of reclamation during an ebb tide. Figure 4-11 and Figure 4-12 also display a potential increase in current speeds to the west of the dredge footprint on a flood tide and alongside the existing berths on an ebb tide.

Further, comparisons of current magnitudes for a neap tide over 13 hours at 14 locations in the vicinity of the port are shown in Figure 4-13.

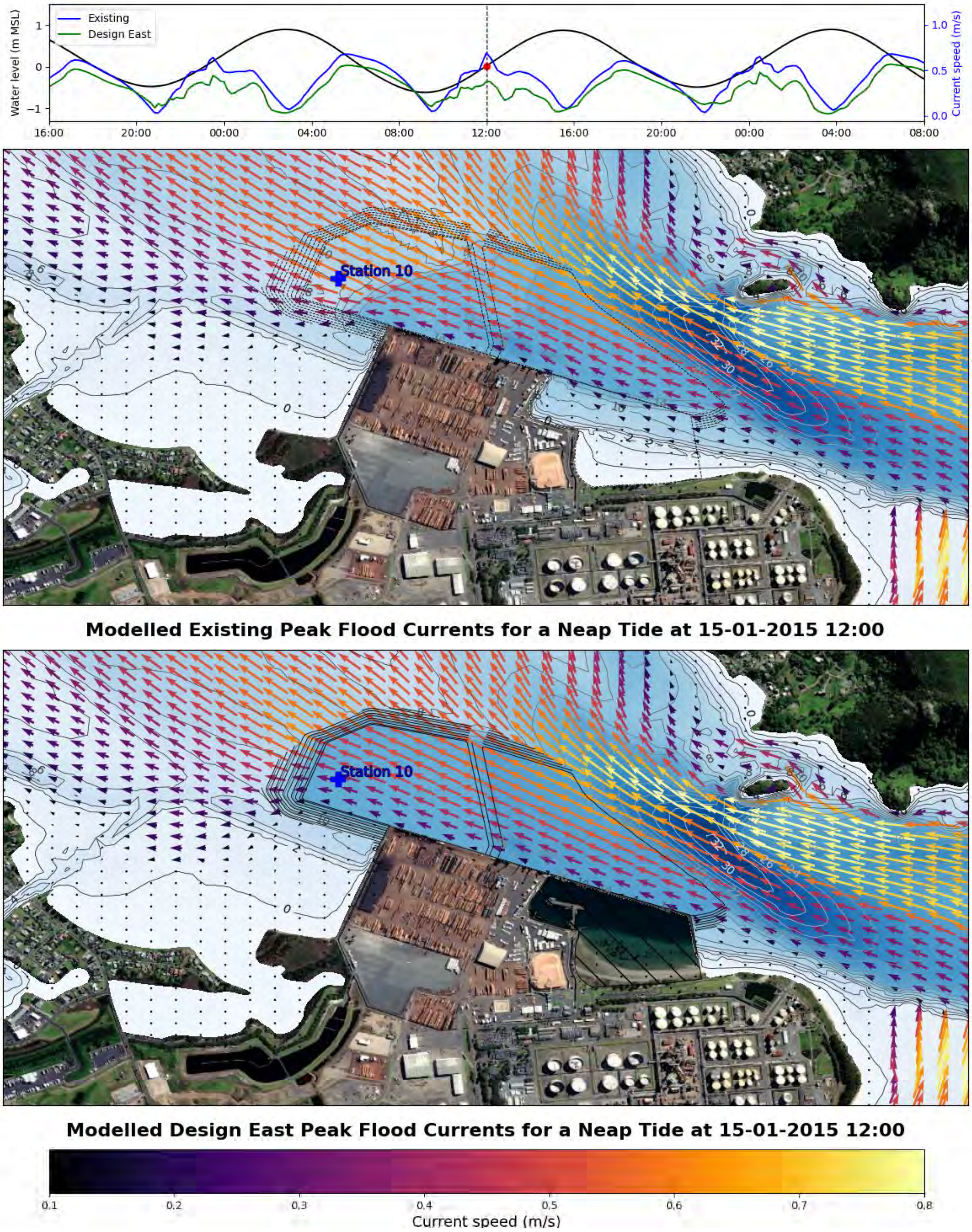

Figure 4-9 Modelled current vectors for the existing (top) and Eastern Reclamation/Design East layout (bottom) during the peak of a flood neap tide and the bathymetry and depth contours used in each simulation. Black design lines display the proposed reclamation and dredging.

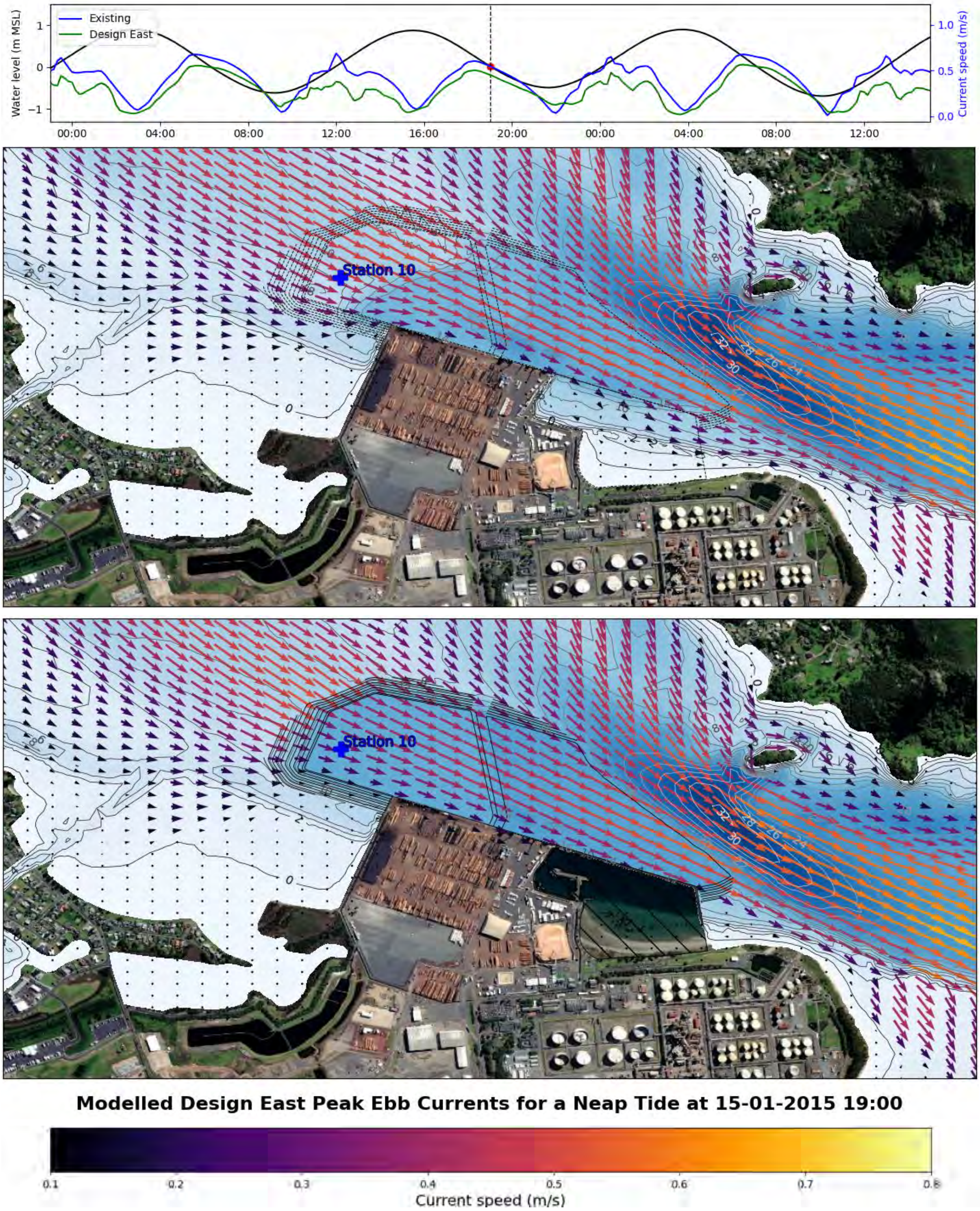

Figure 4-10 Modelled current vectors for the existing (top) and Eastern Reclamation/Design East layout (bottom) during the peak of an ebb neap tide and the bathymetry and depth contours used in each simulation. Black design lines display the proposed reclamation and dredging.

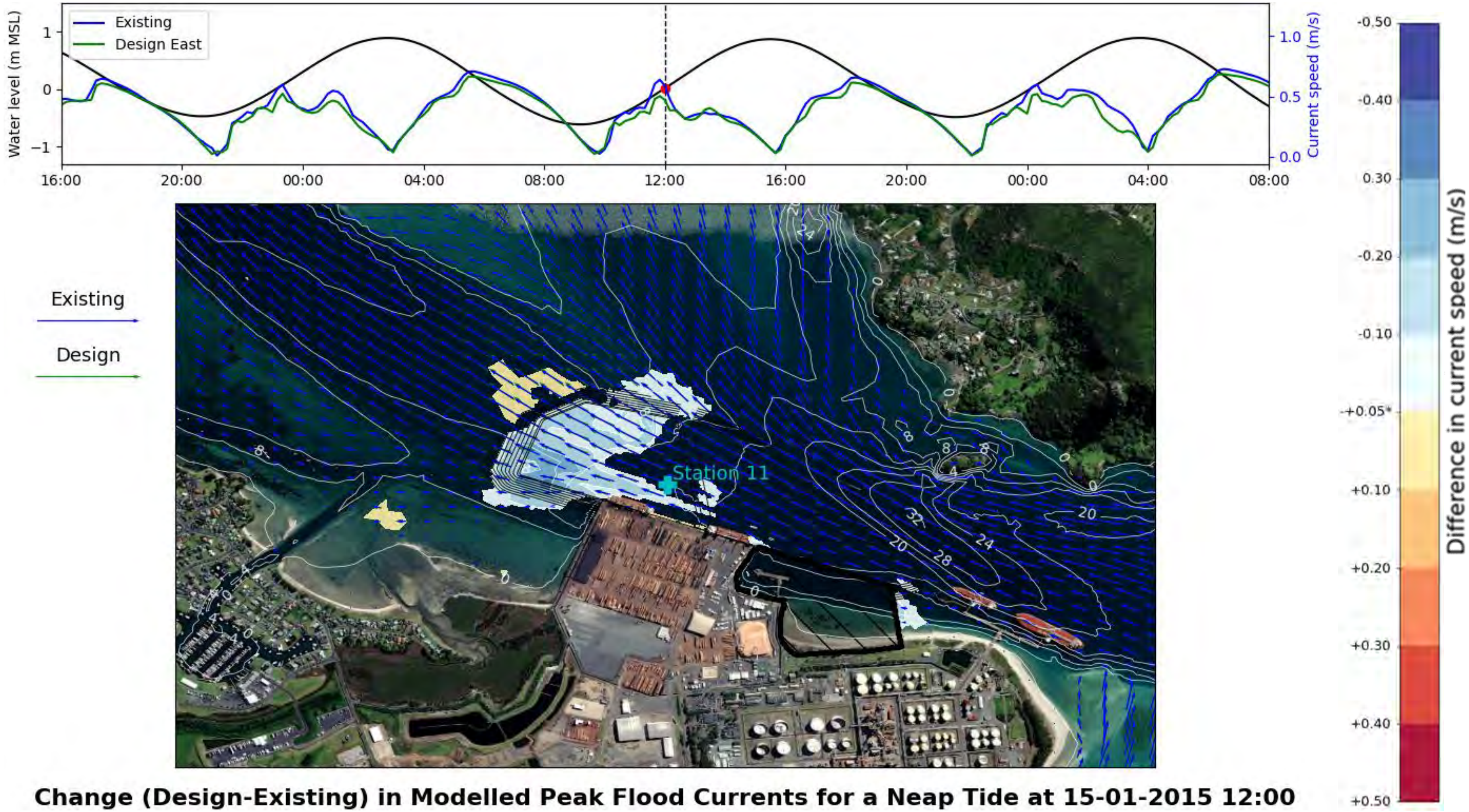

*Figure 4-11 Modelled current vectors for the existing and Eastern Reclamation (Design East) layout and difference in current magnitude during the peak of a flood neap tide. White depth contours are from the existing case and the black design lines display the proposed reclamation and dredging. * Note potential changes less than 0.05 m.s[-1] are masked as they are within the magnitude of model error and were not considered as a meaningful change.*

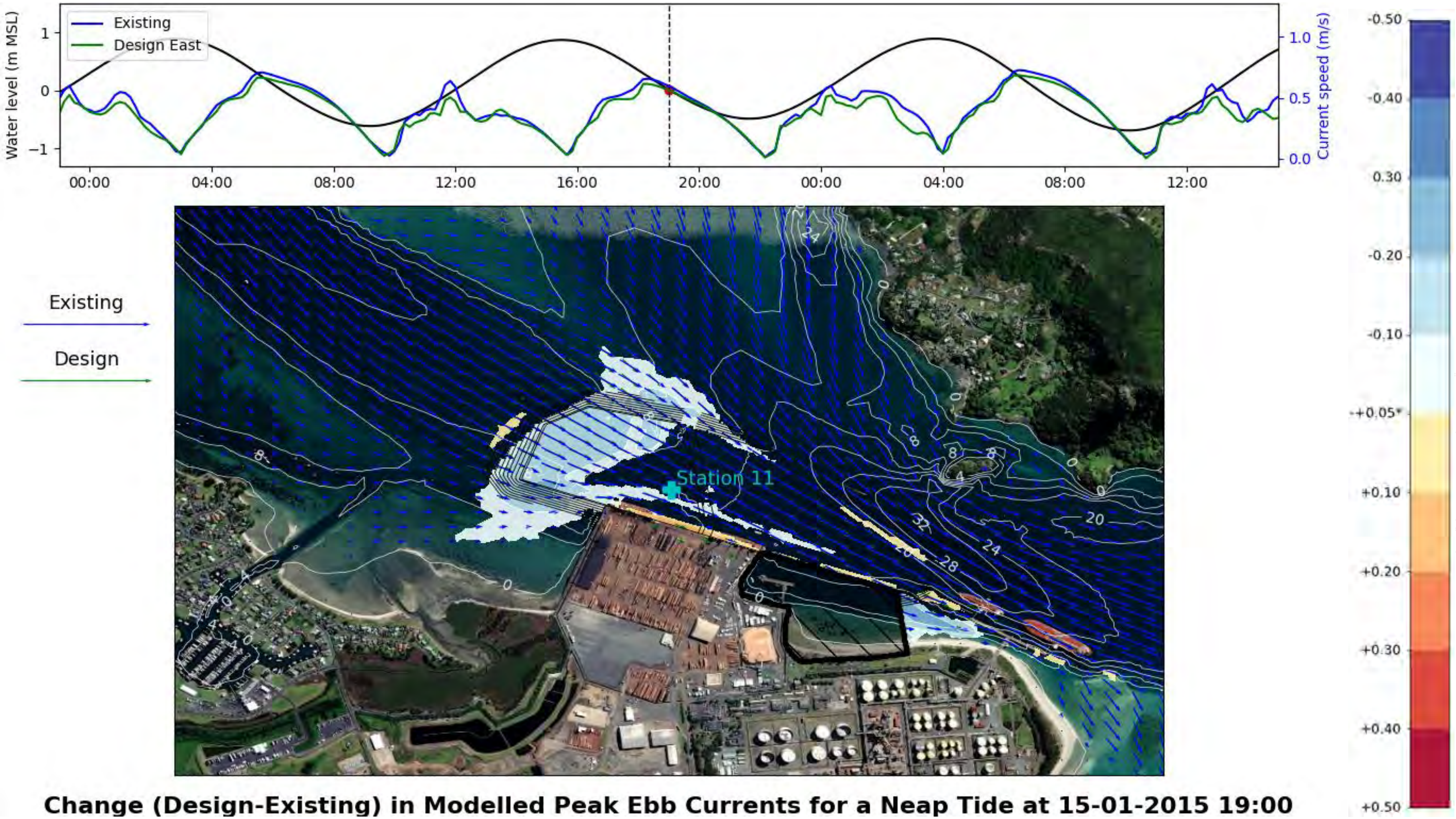

*Figure 4-12 Modelled current vectors for the existing and Eastern Reclamation (Design East) layout and difference in current magnitude during the peak of an ebb neap tide. White depth contours are from the existing case and the black design lines display the proposed reclamation and dredging. * Note potential changes less than 0.05 m.s^{-1} are masked as they are within the magnitude of model error and were not considered as a meaningful change.*

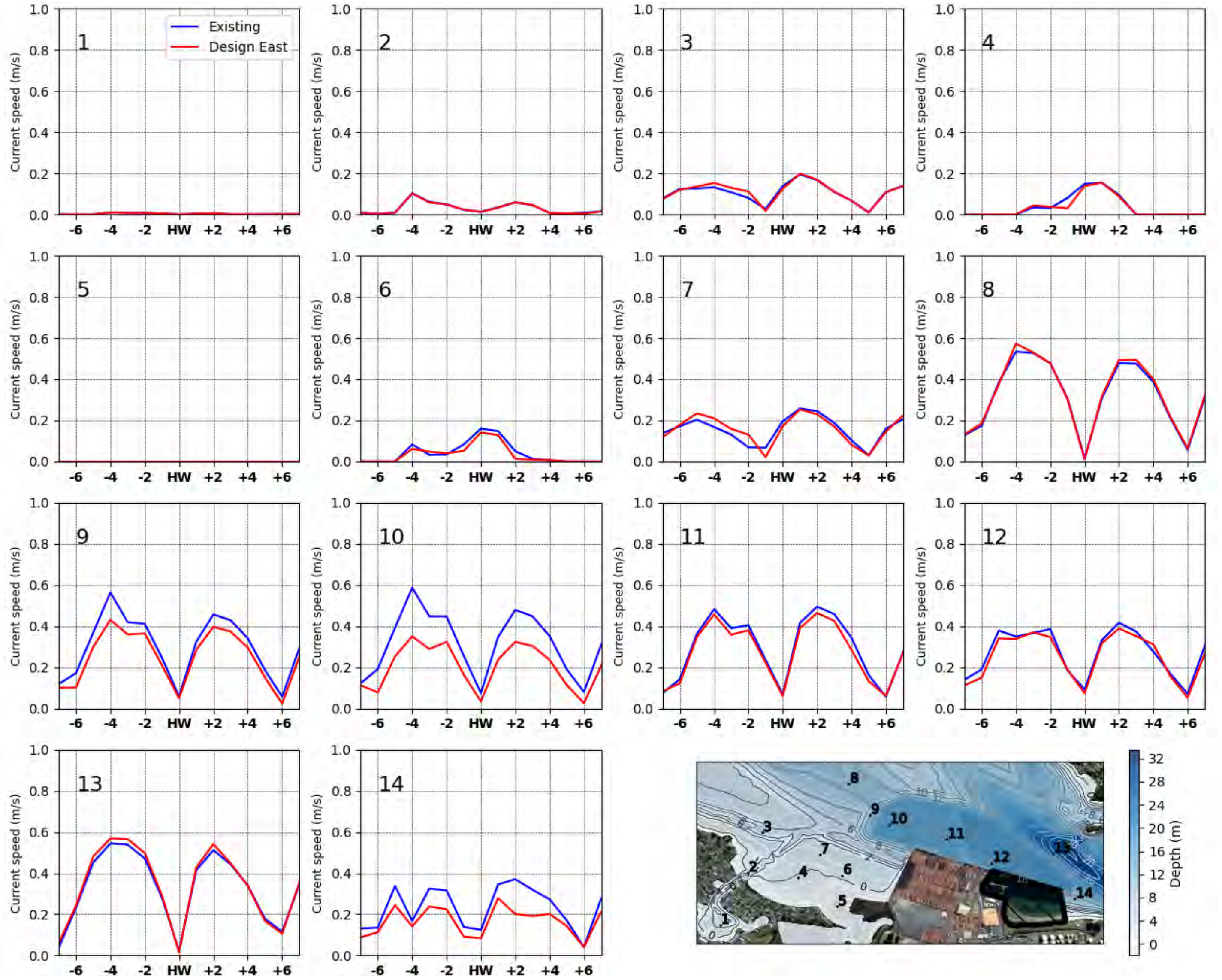

Figure 4-13 Comparisons between modelled current magnitudes for the existing and Eastern Reclamation (Design East) layout for 13 hours of a typical neap tidal cycle

5. Summary

In this study, hydrodynamic modelling was undertaken for both existing and the proposed design configuration (Eastern Reclamation) based on 3D SCHISM modelling framework. Results showed that changes in the current field are confined to the region where the dredging and reclamation works will be undertaken.

In comparison with the existing simulations, current speeds is expected to reduce at the western edge of the dredge footprint and at the eastern end of the reclamation area. Areas with a potential increase in current speeds are in front of the reclamation area within the eastern side of the dredge footprint, to the west of the dredge footprint and alongside the existing berths.

There is only a minor effect of proposed layouts on the current field in the nearshore area surrounding Blacksmith Creek on a spring tide, with an increase of less than 0.2 $m.s^{-1}$ on a flood tide and a decrease of 0.1 $m.s^{-1}$ on an ebb tide. There is also minor decreases in current speeds on the northern channel inside the harbour entrance opposite the port, however this is less than 0.2 $m.s^{-1}$ reduction on a flood tide only. There is no potential changes to the current field in these areas during a neap tide.

The small decrease in currents near the eastern end of the Eastern Reclamation area indicates a potential for increase in sedimentation. The western edge of the dredge footprint may also see an increase for sedimentation, especially during an ebb tide when an increase in current speeds directly upstream of the dredge footprint may increase the sediment mobility to then be deposited in this area.

6. References

Deltares, 2018a. User Manual Delft3D-FLOW, Version: 3.15. ed. Deltares.

Deltares, 2018b. User Manual Delft3D-WAVE, Version: 3.05. ed. Deltares.

Haidvogel, D.B, Arango, H.G., Budgell, W.P., Cornuelle, B.D., Curchitser, E., Di Lorenzo, E., Fennel, K., Geyer, W.R., Hermann, A.J., Lanerolle, L., Levin, J., McWilliams, J.C., Miller, A.J., Moore, A.M., Powell, T.M., Shchepetkin, A.F., Sherwood, C.R., Signell, R.P., Warner, J.C., Wilkin, J., 2008. Ocean forecasting in terrain-following coordinates: Formulation and skill assessment of the Regional Ocean Modeling System. Journal of Computational Physics 227, 3595–3624.

Holthuijsen, L.H., Booij, N., Ris, R.C., Haagsma, I.J., Kieftenburg, A.T.M.M., Kriezi, E.E., Zijlema, M., van der Westhuysen, A.J., 2007. SWAN cycle III version 40.51, Technical Documentation. Delft, 2600 GA Delft The Netherlands.

Liu, Z., Wang, H., Zhang, Y.J., Magnusson, L., Loftis, J.D., Forrest, D., 2020. Cross-scale modeling of storm surge, tide, and inundation in Mid-Atlantic Bight and New York City during Hurricane Sandy, 2012. Estuarine, Coastal and Shelf Science 233, 106544. https://doi.org/10.1016/j.ecss.2019.106544

Lopes, V., Silva, P.A., Bertin, X., Fortunato, A.B., Oliveira, A., 2009. Impact of a Dredged Sandpit on Tidal and Wave Hydrodynamics. Journal of Coastal Research 529–533.

Mendes, D.S., Fortunato, A.B., Pires-Silva, A.A., 2016. Assessment of three dredging plans for a wave-dominated inlet. Proceedings of the Institution of Civil Engineers - Maritime Engineering 169, 64–75. https://doi.org/10.1680/jmaen.2015.7

MetOcean Solutions Ltd, 2021a. Hydrodynamic Modelling - Effect of Proposed Reclamation Layouts on Hydrodynamics (Report prepared for Northport No. Report P0519-01).

MetOcean Solutions Ltd, 2021b. Morphodynamic Modelling for the Northport Environment. Modelling Update . Predicted morphological response to proposed capital dredging and land reclamation (Report prepared for Northport No. Report P0519-02).

MetOcean Solutions Ltd, 2021c. Dredge Plume Modelling . Dredging sediment plume dispersion over existing and proposed port configurations (Report prepared for Northport No. Report P0519-03).

MetOcean Solutions Ltd, 2019. Waste Water Dispersion Modelling (Report prepared for Refining New Zealand (RNZ) No. Report P0460).

MetOcean Solutions Ltd, 2018a. Dredging plumes (Report prepared for Northport No. Report P0367 – 04 Rev B).

MetOcean Solutions Ltd, 2018b. Hydrodynamic Modelling - Methodology, validation and simulations (Report prepared for Northport No. Report P0367 – 02).

MetOcean Solutions Ltd, 2018c. Morphodynamic Evolution Modelling for the Northport Environment - Predicted morphological response to proposed capital dredging and land reclamation (Report prepared for Northport No. Report P0367 – 03).

MetOcean Solutions Ltd, 2018d. Morphodynamic Evolution Modelling for the Northport Environment - Morphological model calibration (Report prepared for Northport No. Report P0367 – 01 Rev B).

MetOcean Solutions Ltd, 2018e. Morphodynamic Evolution Modelling for the Northport Environment - Five year morphological prediction of the swinging basin morphological response (Report prepared for Northport No. Report P0367 – 05).

MetOcean Solutions Ltd, 2018f. Northport Dredging Project - Dredging Plume Modelling (Report prepared for Northport No. Report P0367 – 01).

MetOcean Solutions Ltd, 2016. Characterisation of the physical environment at the Whangarei Harbour entrance and establishment of numerical models of wave, current and sediment dynamics (Report prepared for Refining New Zealand No. Crude Freight Shipping Project Whangarei Harbour).

Northport, 2020. Northport [WWW Document]. Northport - About us. URL https://northport.co.nz/aboutus (accessed 12.9.20).

Saha, S., Moorthi, S., Pan, H.-L., Wu, X., Wang, Jiande, Nadiga, S., Tripp, P., Kistler, R., Woollen, J., Behringer, D., Liu, H., Stokes, D., Grumbine, R., Gayno, G., Wang, Jun, Hou, Y.-T., Chuang, H.-Y., Juang, H.-M.H., Sela, J., Iredell, M., Treadon, R., Kleist, D., Van Delst, P., Keyser, D., Derber, J., Ek, M., Meng, J., Wei, H., Yang, R., Lord, S., Van Den Dool, H., Kumar, A., Wang, W., Long, C., Chelliah, M., Xue, Y., Huang, B., Schemm, J.-K., Ebisuzaki, W., Lin, R., Xie, P., Chen, M., Zhou, S., Higgins, W., Zou, C.-Z., Liu, Q., Chen, Y., Han, Y., Cucurull, L., Reynolds, R.W., Rutledge, G., Goldberg, M., 2010. The NCEP Climate Forecast System Reanalysis. Bull. Amer. Meteor. Soc. 91, 1015–1057. https://doi.org/10.1175/2010BAMS3001.1

Song, Y.T., Hou, T.Y., 2006. Parametric vertical coordinate formulation for multiscale, Boussinesq, and non-Boussinesq ocean modeling. Ocean Modelling 11, 298–332. https://doi.org/10.1016/j.ocemod.2005.01.001

Ye, F., Zhang, Y.J., Friedrichs, M.A.M., Wang, H.V., Irby, I.D., Shen, J., Wang, Z., 2016. A 3D, cross-scale, baroclinic model with implicit vertical transport for the Upper Chesapeake Bay and its tributaries. Ocean Modelling 107, 82–96. https://doi.org/10.1016/j.ocemod.2016.10.004

Ye, F., Zhang, Y.J., Wang, H.V., Friedrichs, M.A.M., Irby, I.D., Alteljevich, E., Valle-Levinson, A., Wang, Z., Huang, H., Shen, J., Du, J., 2018a. A 3D unstructured-grid model for Chesapeake Bay: Importance of bathymetry. Ocean Modelling 127, 16–39. https://doi.org/10.1016/j.ocemod.2018.05.002

Ye, F., Zhang, Y.J., Wang, H.V., Huang, H., Wang, Z., Liu, Z., Li, X., 2018b. Cross-Scale Baroclinic Simulation of the Effect of Channel Dredging in an Estuarine Setting. Water 10. https://doi.org/10.3390/w10020163

Zhang, Y., Ateljevich, E., Yu, H.-C., Wu, C., Yu, J., 2014. A new vertical coordinate system for a 3D unstructured-grid model. Ocean Modelling 85. https://doi.org/10.1016/j.ocemod.2014.10.003

Zhang, Y.J., Gerdts, N., Ateljevich, E., Nam, K., 2020. Simulating vegetation effects on flows in 3D using an unstructured grid model: model development and validation. Ocean Dynamics 70, 213–230. https://doi.org/10.1007/s10236-019-01333-8

Zhang, Y.J., Ye, F., Stanev, E.V., Grashorn, S., 2016. Seamless cross-scale modeling with SCHISM. Ocean Modelling 102, 64–81.

Zhang, Y.L., Baptista, A.M., 2008. A semi-implicit Eulerian-Lagrangian finite element model for cross-scale ocean circulation. Ocean Modelling 21, 71–96.

Morphodynamic Modelling for the Northport Environment

Modelling Update

Predicted morphological response to proposed eastern land reclamation

Report prepared for Northport

August 2022

MetOcean SOLUTIONS

Document History

Versions

Version	Revision Date	Summary	Reviewed by
0.1	11/07/2022	Draft for internal review	Cussioli
0.2	15/07/2022	Draft for internal review	Berthot
0.3	26/08/2022	Updated draft following client review	Cussioli/Berthot

Distribution

Version	Date	Distribution
1.0		

Document ID: P0519-11

Authors

Berthot A., Cussioli M.

Contributors

Gardiner S., Watson, H.

MetOcean Solutions is a Division of Meteorological Services of New Zealand Ltd, MetraWeather (Australia) Pty Ltd [ACN 126 850 904], MetraWeather (UK) Ltd [No. 04833498] and MetraWeather (Thailand) Ltd [No. 0105558115059] are wholly owned subsidiaries of Meteorological Service of New Zealand Ltd (MetService).

Contents

List of Figures

List of Tables

1.Introduction

Northport is a deep-water commercial port strategically situated at Marsden Point near Whangarei in Northland, New Zealand (Figure 1-1). Northport is planning to expand the port's capacity by reclaiming land and building additional berths (Figure 1-2). Northport has decided to proceed with the Eastern Reclamation only (at this stage) and has revised the proposed dredging footprint and depth.

MetOcean Solutions (MOS, a division of the Meteorological Service of New Zealand) has already undertaken a number of numerical hydrodynamic and morphological modelling simulations and dredged plume dispersion simulations related to this project, with results presented in MOS reports P0367-01 to P0367-06 (MetOcean Solutions 2018a,b,c,d,e) and P0519-01 to P0519-03 (MetOcean Solutions 2021a,b,c).

The following investigations are now required to be undertaken with the proposed revised layout:

- Hydrodynamic : update bathy with proposed dredge footprint and rerun of full month of hydrodynamic (2 spring/neap cycles). Assessment of change in currents over a typical spring tidal cycle.
- Morphological modelling: Modelling of predicted seabed morphological change in the vicinity of the proposed dredge footprint over a 5-year period
- Sediment plumes: Modelling of sediment plumes generated during dredging operation , likely a trailer dredge to be confirmed

This report focuses on the morphological modelling. This is achieved through the application of a calibrated and validated morphological model (Delft3D) that has been previously undertaken for the Northport region through the comparison of morphological model outputs against hydrographic survey data (MetOcean Solutions Ltd 2018d). Details of the modelling configuration and application are provided in MetOcean Solutions Ltd. (2018d).

The report is structured as follows; the methodology applied in this study is detailed in Section 2, including a description of the different scenarios simulated. Results are presented in Section 3, while a brief summary is presented in Section 4. References cited in this document are listed in Section 5.

Figure 1-1 Location of Northport within Whangarei Harbour.

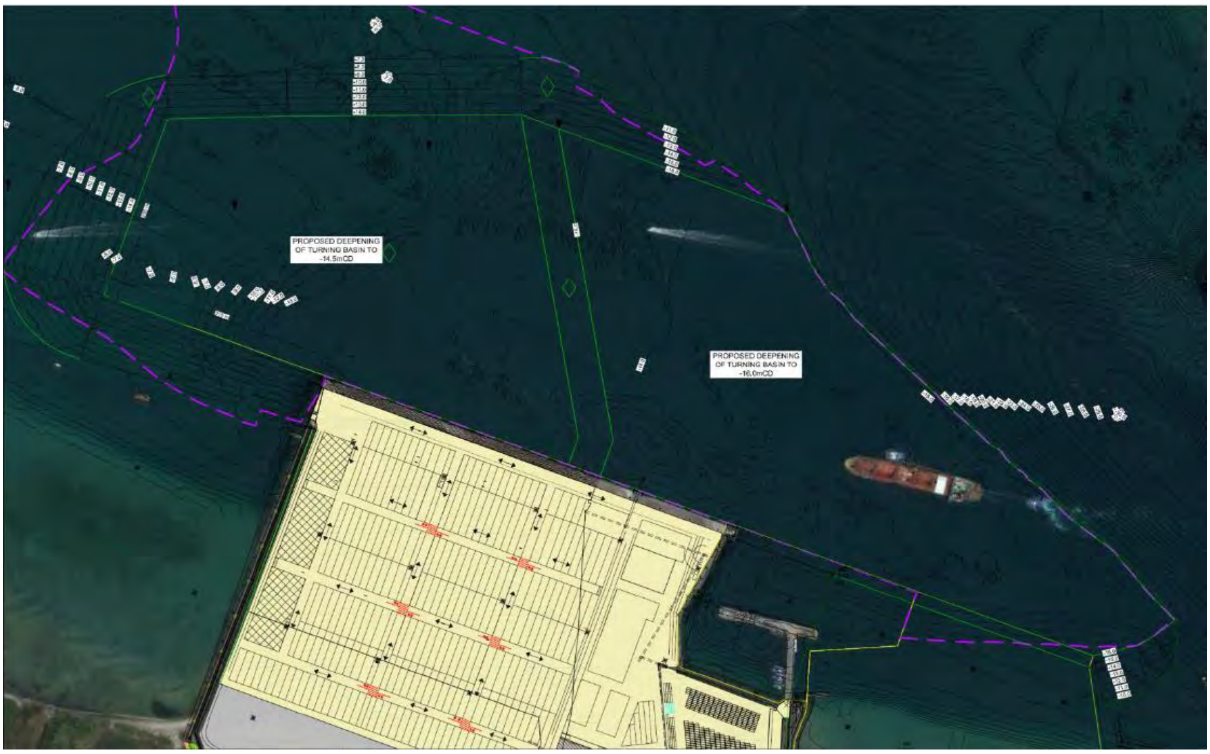

Figure 1-2 Draft concept drawing for the proposed area to be dredged and reclaimed.

2.Methods

The primary objective of the study is to understand the likely morphological response of the existing environment to the proposed dredging and land reclamation. To achieve this, morphological modelling of the existing and proposed design are undertaken using a calibrated and validated Delft3D configuration (MetOcean Solutions Ltd 2018d). The model methodology applies an input reduction technique combined with morphological acceleration factors to examine dynamics and morphological response within the port environs for a period of 5 years.

The following sections detail the methodology used to undertake the morphological modelling.

2.1 Numerical modelling

2.1.1 Initial bathymetry

Northport has undertaken an extensive hydrographic monitoring program of the access channel, turning basing and berths over the last decade to assess the depth changes at the port and surroundings. Hydrographic surveys using single and multi-beam echo-sounders are available for the period 2006 – 2022.

In MetOcean Solutions (2018d), the 2016 and the 2017 multi-beam hydrographic survey datasets were used to setup, calibrate and validate the morphological numerical model. The calibrated and validated model is used in this study to examine the predicted morphological effects of the proposed design by modifying the bathymetry.

The bathymetry for the 2022 design is derived from existing Metocean Solutions numerical model of Northport and updated with two Northport Hydro hydrographic survey data from February 2022 of Portland Channel and Wellington Reach and the Marsden Point Harbour Survey. The reclamation layout as well as the dredging extents for the design scenario bathymetry is derived from drawings provided by Northport (*Eastern ExpansionDredging Design.pdf).* The predicted morphological effects assuming the granting of the Refining New Zealand (RNZ) channel deepening Resource Consent (Royal HaskoningDHV 2016) is not considered hereafter.

The two different scenarios are described below in Table 2-1 and illustrated in Figure 2-1.

Table 2-1 Modelled scenarios.

Scenario	Description
Existing	Existing channel bathymetry and port layout
Design	Existing channel bathymetry and includes eastern reclamation and dredged turning basin

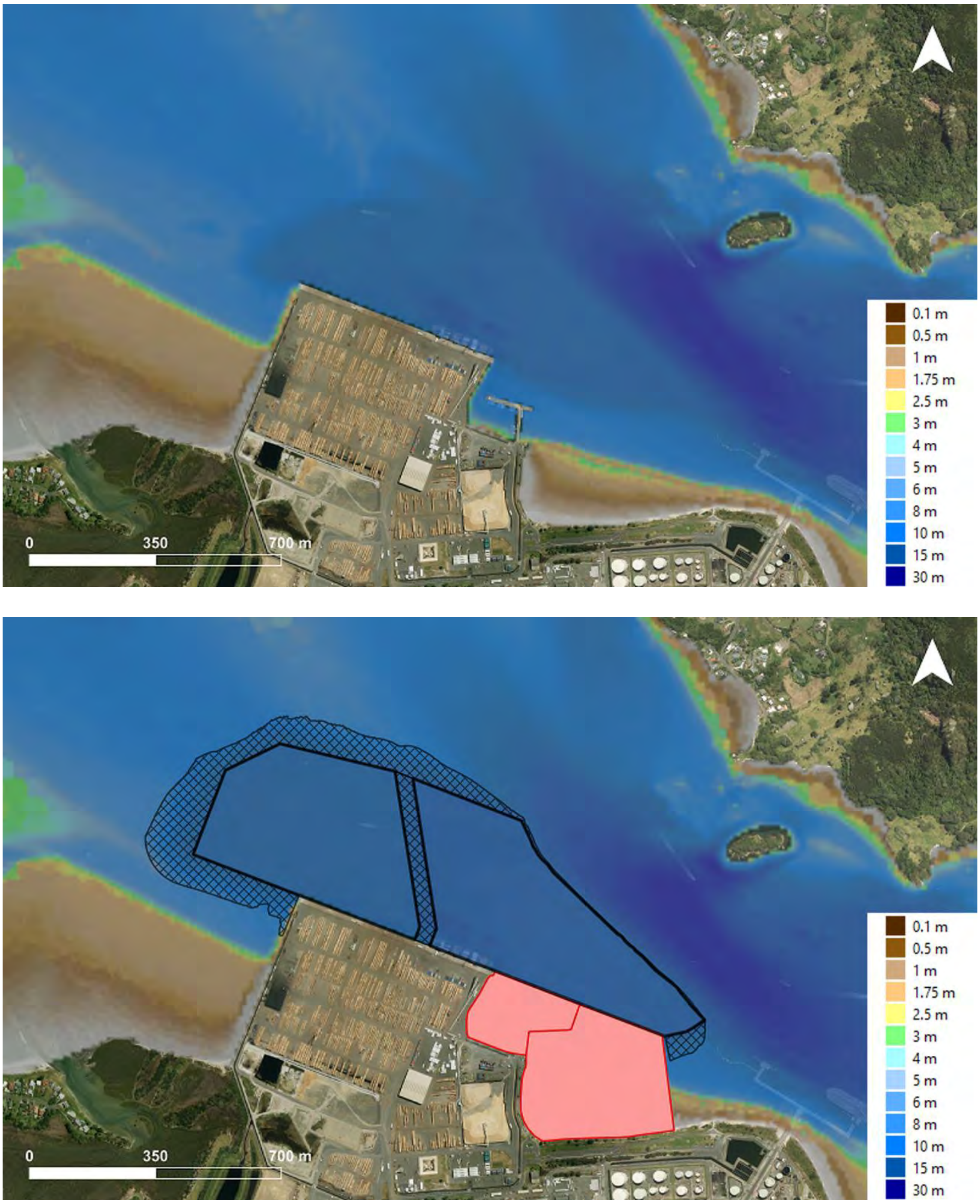

Figure 2-1 Bathymetric maps (MSL datum) of Northport existing (top) and proposed development (bottom). Hatched areas represent batter slopes and solid black line polygons represent dredged areas.

2.1.2 Initial bed composition

An accurate definition of the surficial sediment grain size distribution in the area of interest plays an important role in correctly determining sediment dynamics and morphological response. As such, a sedimentological spin-up following a bed stratigraphy approach was carried out in MetOcean Solutions (2018d), whereby the spatial surficial sediment distribution was allowed to adjust to the *in-situ* bed shear-stresses associated with both hydrodynamics and wave forcing. The derived surficial sediment grain size distributions are applied to the bathymetry defining the proposed development.

2.1.3 Forcing

Winds, waves and tidal currents are defined as in MetOcean Solutions (2018d) for both scenarios to allow the comparison of the effect of the proposed dredging and land reclamation on the existing sediment dynamics and morphological response. Model derived tidal constituents are used to define the Delft3D–FLOW boundary tidal currents as appropriate (MetOcean Solutions Ltd 2018d).

2.1.4 Model settings

The same model configuration derived from the calibration and validation process is used to initiate the modelling. An overview of the parameters and settings used within Delft3D is provided in MetOcean Solutions (2018d). The model grid is presented on Figure 2-2.

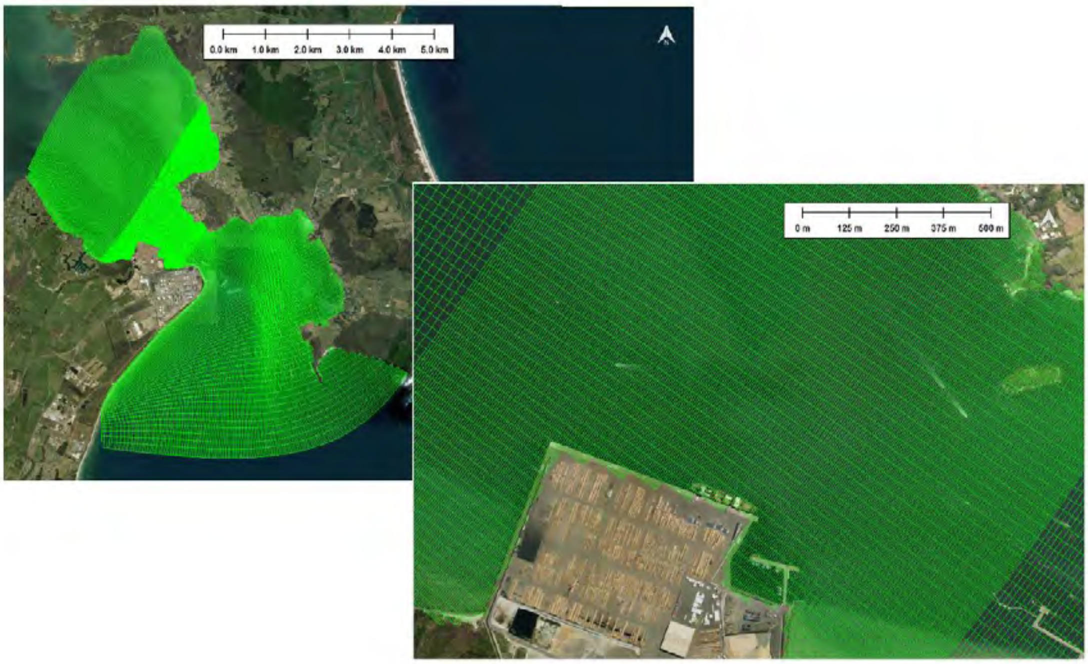

Figure 2-2 Map showing the Delft3D – FLOW and MOR grids used to replicate the hydro- and morpho-dynamics over the entrance to Whangarei Harbour. The resolution of the grid varies from 10 m to 100 m.

3. Results

3.1 Sediment Transport

Averaged sediment transport rates for the existing and design scenarios are presented in Figure 3-1 for the 1st year and Figure 3-2 for the 5th year, together with the difference in transport rates between the existing and design scenarios. Results are presented for transport related to the three most significant and contrasting wave classes simulated (16 classes in total were applied at the boundary of the coarse grid – see more details in MetOcean Solutions Ltd, 2018d). The characteristics for these three wave classes are:

- Wave class 1: Hs = 1.6 m; Tp = 9.3 s; Dir = 34.4 deg; Prob. Occurrence = 15.1%;
- Wave class 12: Hs = 6.6 m; Tp = 12.1 s; Dir = 119.9 deg; Prob. Occurrence = 0.48%;
- Wave class 15: Hs = 3.4 m; Tp = 8.7 s; Dir = 323.4 deg; Prob. Occurrence = 2.0%.

For wave class 1, significant changes in transport rates due to the development are observed along the batter area west of the turning basin, as transport rate is increased due to depth gradient of the batter slope. Within the turning basin, transport rate is reduced throughout, mostly as a result of the deeper design bathymetry and removal of the sand wave located in this area (Figure 3-1 and Figure 3-2 top right panel).

Wave class 12 is the most energetic event simulated and is related to higher transport rates, especially in the main channel and around the intertidal and nearshore areas (e.g., at the sandflat at the entrance of the creek west of the port). Transport rates are more significantly reduced along the batter north of the turning basin. Also, localised areas of reduction in sediment transport are present east of the reclamation area. Based on the comparison of the transport rates from two configurations , the design configuration did not significantly affect the averaged net transport rate (Figure 3-1 and Figure 3-2 middle right panel).

For wave class 15, changes are similar to wave class 1, i.e., more significant in the leeward slope of the turning basin, represented as an increase in transport rate compared to the exiting configuration, and a decrease in transport rate withing the western turning basin polygon (Figure 3-1 and Figure 3-2 bottom right panel). Some localised changes also occur near the sandflat and Blacksmith creek west of the port, as well as for nearshore areas across the main channel.

Over the years, differences tend to reduce following smoothing of the batter slopes and bathymetry.

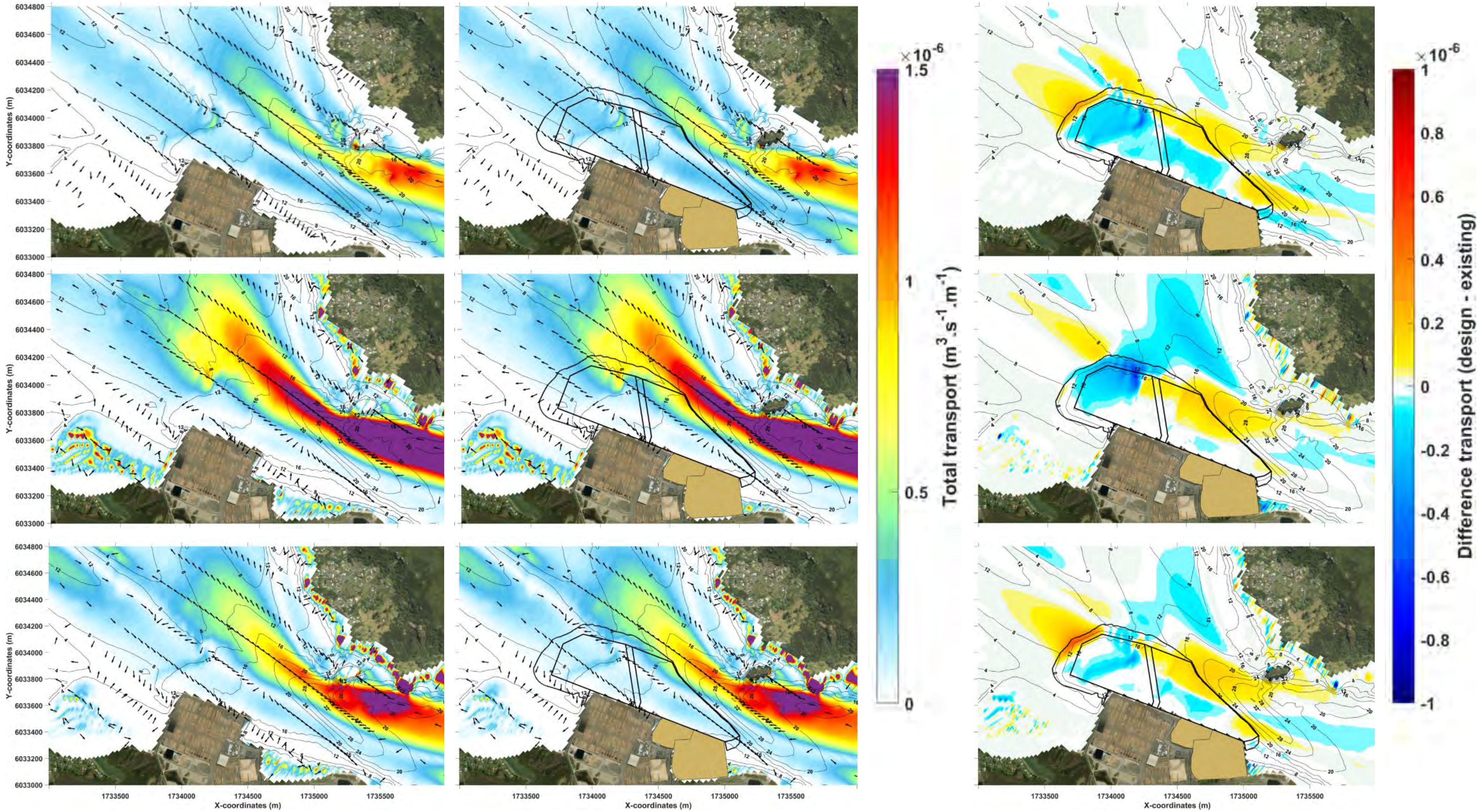

Figure 3-1 Predicted sediment transport rate at Northport averaged over one tidal cycle (~12.25 hours) for the existing (left column) and the design (middle column) configurations for the 1st year simulation for boundaries forced with wave class 1 (top row), wave class 12 (middle row), and wave class 15 (bottom row). The difference in net transport rates between design and existing configuration is provided in the right column.

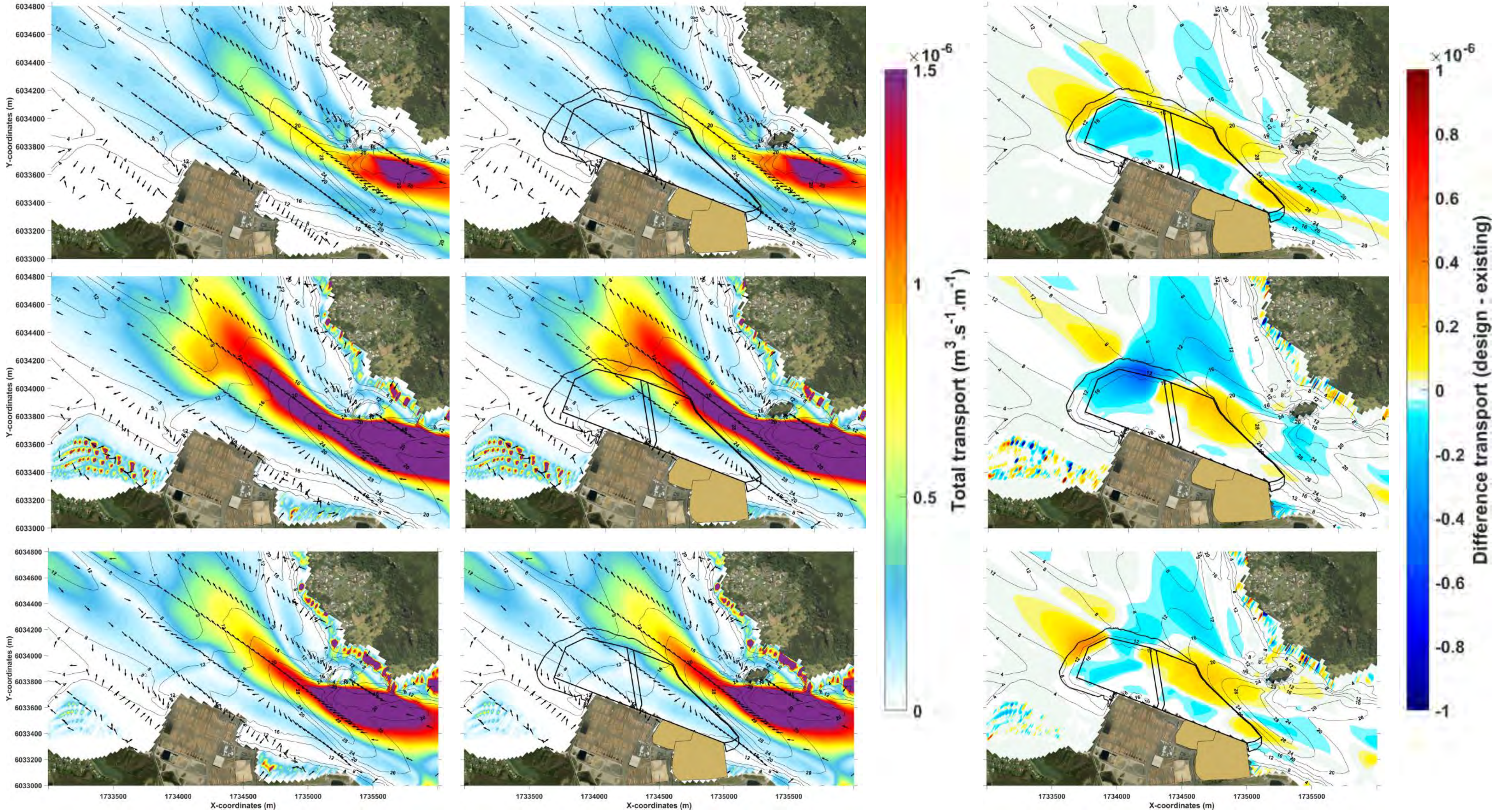

Figure 3-2 Predicted sediment transport rate at Northport averaged over one tidal cycle (~12.25 hours) for the existing (left column) and the design (middle column) configurations for the 5th year simulation for boundaries forced with wave class 1 (top row), wave class 12 (middle row), and wave class 15 (bottom row). The difference in net transport rates between design and existing configuration is provided in the right column.

3.2 Morphological Changes

In order to isolate the morphological response of the proposed design (i.e., the proposed eastern reclamation and dredging), the predicted changes due to the proposed design have been compared to the changes occurring with existing configuration, following the equation:

$$Response = (Design_{end} - Design_{start}) - (Existing_{end} - Existing_{start}) \tag{3.1}$$

where $\boldsymbol{Design_{end}}$ and $\boldsymbol{Design_{start}}$ are the bathymetry at the end and start of the model simulation using the design configuration, and $\boldsymbol{Existing_{end}}$ and $\boldsymbol{Existing_{start}}$ are the existing bathymetry at the start and end of model simulation, respectively.

Depth change is, therefore, the morphological response at the end of the simulation period due to the proposed design only. The results presented here are a combination of the 16 classes simulated to represent the final bathymetry (see report MetOcean Solutions, 2018d for wave classes description). The predicted depth changes after 1 year and 5 years simulation are presented in Figure 3-3.

In general, depth changes associated with the design configuration are expected to be predominantly limited to the immediate port environs, with only subtle modifications to the overall sediment dynamics within the broader region (Figure 3-3 right panel column).

The largest morphological changes are predicted to occur along the batter slopes, mostly northwest of the turning basin. The depth changes for these areas are attributed to the erosion of the batter slope crest and deposition along the slope until it reaches a state of equilibrium. Maximum accretion within the slope area is approximately 0.6 m at the end of 1 year simulation and 1.9 m at the end of 5 years (Figure 3-3, top row and bottom row, respectively). Turning basin and berth pockets may also experience erosion and accretions.

Significant differences observed between the existing and design scenarios are mainly attributed to the combination of dredging (deepening), slope changes, and the transport of sand wave features previously characterized in this region (MetOcean Solutions Ltd 2018d).

Within Marsden Bay, localised changes in sediment transport rate are not expected to change the morphology of the bay, resulting in small, localised adjustments of the water depth (Figure 3-3).

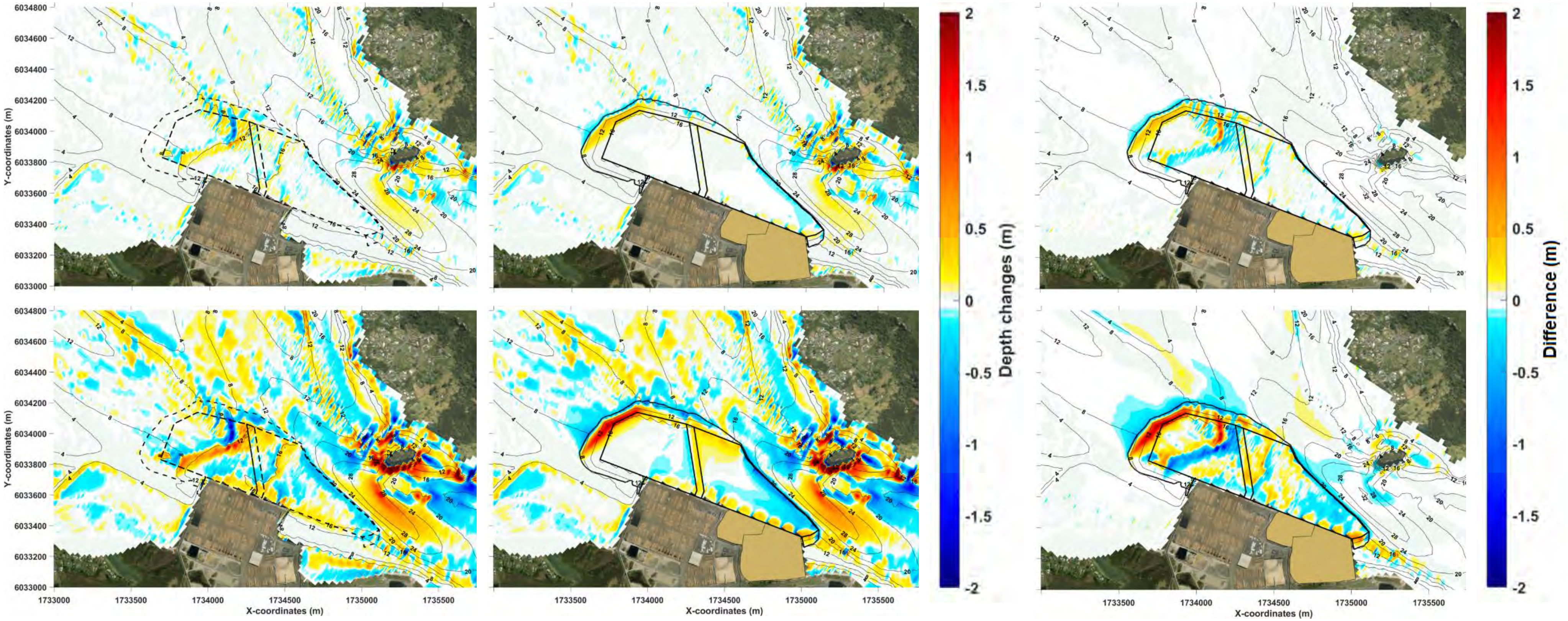

Figure 3-3 Depth change predicted at Northport in 1 year (top) and in 5 years (bottom) simulation considering the existing (left) and design bathymetry (middle). The relative differences between the design and existing scenarios are presented in the right panel. Dashed and solid black lines represent the design footprint.

3.3 Infilling Rates

Approximate infilling and erosion rates, as well as the total change in volume within different areas of the proposed development are provided in Table 3-1. Total infilling of 5,527 m^3 is expected within the new development area, including the batter slopes area (i.e., areas B1 and B2) after 1 year. The expected infill after 5 years is of 24,150 m^3. Batter B1 is the area with greatest infill, as illustrated by the maps of depth changes in the previous section.

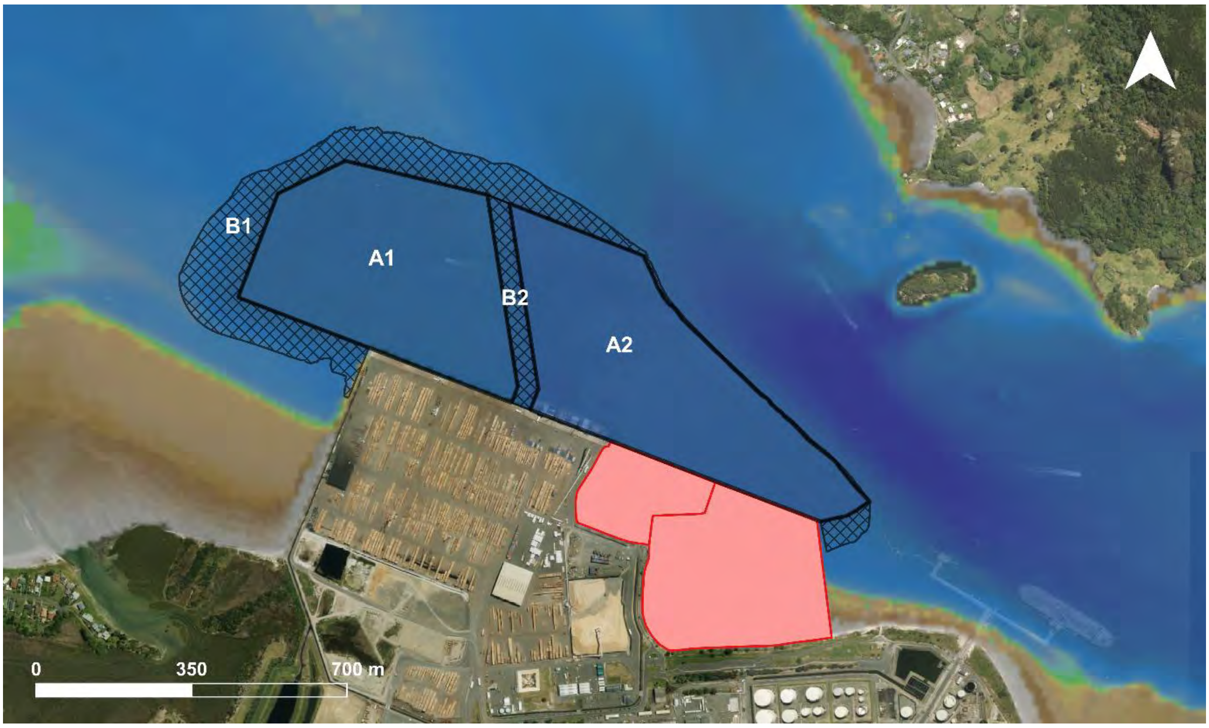

Figure 3-4 Areas used for the calculation of the infilling rates. Red polygons represent reclaimed areas.

Table 3-1 Predicted infill volumes within areas A1 and A2, and batter B1 and B2 after 1 year and 5 years simulation of the design bathymetry.

		Volumetric changes (m^3)				
		Area A1	**Area A2**	**Batter B1**	**Batter B2**	**Total**
1 year	**Infilling**	2,231	3,891	10,264	813	17,199
	Erosion	-1,594	-6,049	-4,002	-27	-11,672
	Total	637	-2,158	6,262	786	5,527
5 years	**Infilling**	12,799	18,315	37,701	3,483	72,298
	Erosion	-6,507	-27,800	-13,767	-74	-48,148
	Total	6,292	-9,485	23,934	3,409	24,150

3.4 Profiles

The morphological response to the design after 1 year and 5 years are presented along six transects across the batter slopes (Figure 3-5). Results are presented in Figure 3-6. Profile P1 presents no changes. Profiles P4 and P6 show small changes, with greater morphological changes located at profiles P2, P3, and P5. The profiles show a pattern of erosion along the crest of the batter, with deposition on the flank and at the toe of the batter, consistent with the batter moving towards an equilibrium profile shape.

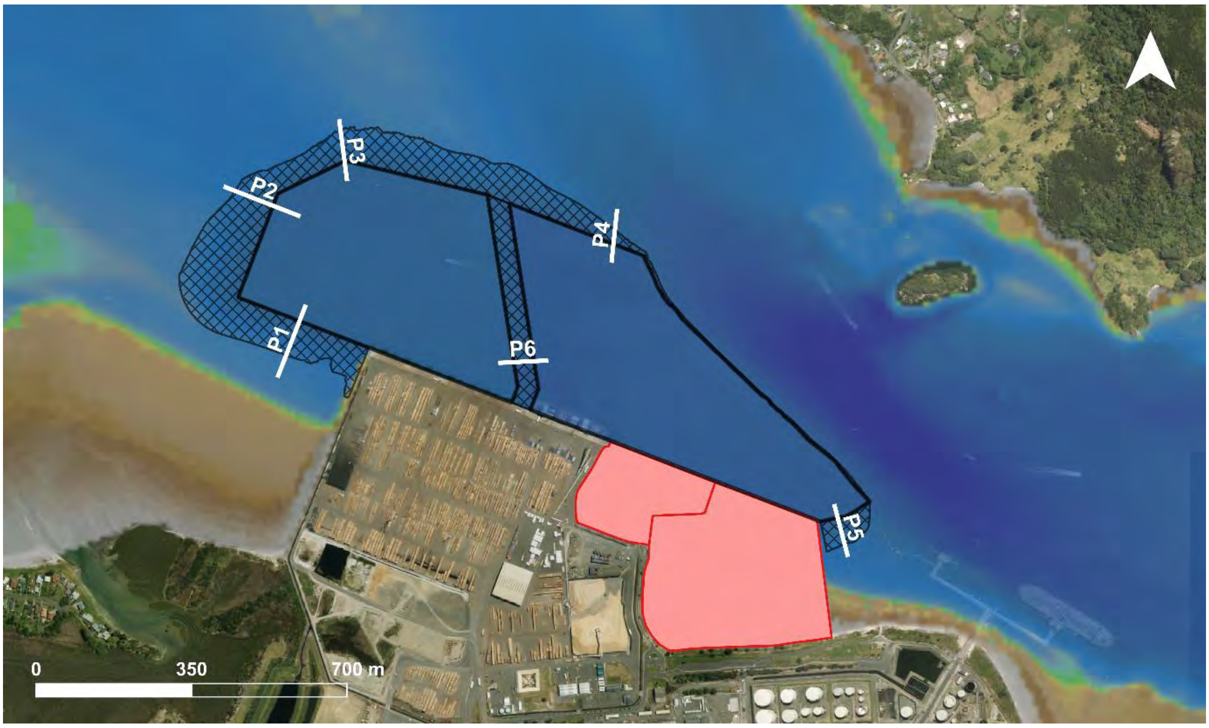

Figure 3-5 Profiles P1 to P6 represented by white lines.

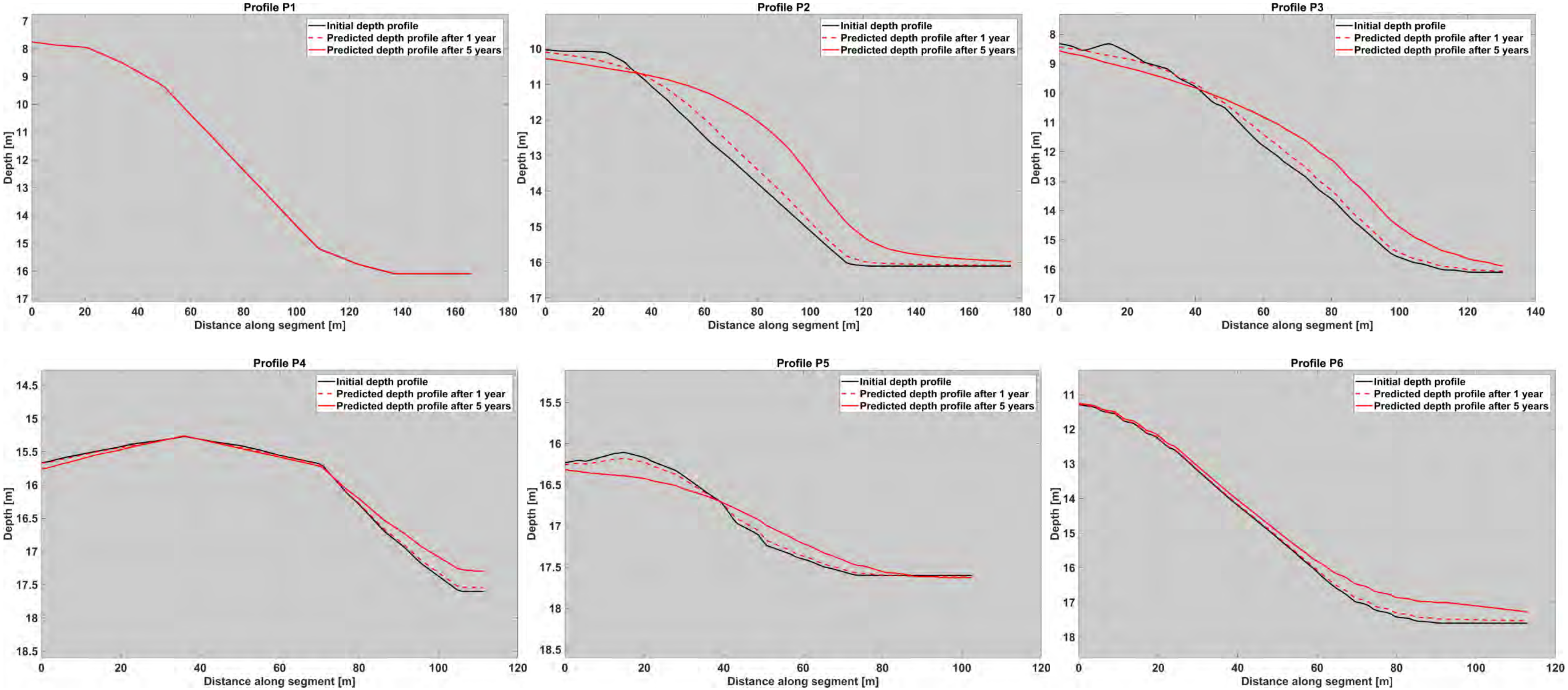

Figure 3-6 Depth profiles of the initial (black) and the predicted bathymetries along segments P1 to P6 at the end of 1 year (dashed red) and 5 years of simulation (solid red).

4. Summary

The calibrated and validated open-source Delft3D system (MetOcean Solutions Ltd 2018d) has been used to run high-resolution process based morphodynamic simulations of the Whangarei Harbour in the vicinity of Northport to understand the likely morphological response of the existing environment to the proposed design development (Figure 1-2). The numerical modelling involved fully coupled wave, current and seabed interactions.

The modelling approach consisted in simulating the sediment dynamics over a 5-year period using the input reduction technique and morphological acceleration factors. Details of the applied approach can be found in MetOcean Solutions Ltd (2018d).

A summary of the main conclusions are as follows:

- The morphological response associated with the combination of land reclamation and dredging is expected to be limited to the immediate port environs.
- Significant differences observed between the existing and design scenarios are mainly attributed to the combination of dredging (deepening), slope changes, and the transport of sand wave features previously characterized in this region.
- The largest depth changes are expected to occur along the batter slopes, mainly northwest of the turning basin. Sediment accretion is expected within these areas (Figure 3-3).
- Maximum accretion along the slopes ranges from approximately 0.6 to 1.9 m at the end of 1 year and 5 years of simulation, respectively. Turning basin and berth pockets also present some small patterns of erosion and accretions.
- The total infill volume within the dredged areas and batter (areas A1, A2, B1 and B2 – Figure 3-4) after 1-year simulation is expected to be 5,527 m^3 and 24,150 m^3 after 5 years (Table 3-1), with the majority of the infill occurring within the batter slope area (area B1).
- While some changes to the sediment transport rate and bathymetry due to the design configuration are predicted within Marsden Bay, morphological modelling suggests these will not alter the bays morphology.

5. References

MetOcean Solutions Ltd. 2018a. 'Dredging Plumes'. Report prepared for Northport Report P0367 – 04 Rev B.

MetOcean Solutions Ltd. 2018b. 'Hydrodynamic Modelling - Methodology, Validation and Simulations'. Report prepared for Northport Report P0367 – 02.

MetOcean Solutions Ltd. 2018c. 'Morphodynamic Evolution Modelling for the Northport Environment - Five Year Morphological Prediction of the Swinging Basin Morphological Response'. Report prepared for Northport Report P0367 – 05.

MetOcean Solutions Ltd. 2018d. 'Morphodynamic Evolution Modelling for the Northport Environment - Morphological Model Calibration'. Report prepared for Northport Report P0367 – 01 Rev B.

MetOcean Solutions Ltd. 2018e. 'Morphodynamic Evolution Modelling for the Northport Environment - Predicted Morphological Response to Proposed Capital Dredging and Land Reclamation'. Report prepared for Northport Report P0367 – 03.

MetOcean Solutions Ltd. 2018f. 'Northport Dredging Project - Dredging Plume Modelling'. Report prepared for Northport Report P0367 – 01.

Northport. 2020. 'Northport'. Northport - About Us. 2020. https://northport.co.nz/aboutus.

Royal HaskoningDHV. 2016. 'Refining NZ Crude Shipping Project - Shipping Channel - Concept Design Report Prepared for Refining NZ.'

Dredge Plume Modelling

Dredging sediment plume dispersion over existing and proposed port configurations

Report prepared for NorthPort

August 2022

MetOcean SOLUTIONS

Document History

Versions

Version	Revision Date	Summary	Reviewed by
0.1	13/08/2022	draft for internal review	Cussioli
0.2	18/08/2022	Updated draft for internal review	Weppe
0.3	18/08/2022	Draft for Client Review	Berthot
0.4	26/08/2022	Updated draft for client review	Weppe/Berthot

Distribution

Version	Date	Distribution
1.0		

Document ID:P0519-12

Authors

Cussioli M., Weppe S., Berthot A.

Contributors

Gardiner S., Watson, H.

MetOcean Solutions is a Division of Meteorological Services of New Zealand Ltd, MetraWeather (Australia) Pty Ltd [ACN 126 850 904], MetraWeather (UK) Ltd [No. 04833498] and MetraWeather (Thailand) Ltd [No. 0105558115059] are wholly owned subsidiaries of Meteorological Service of New Zealand Ltd (MetService).

reserves all legal rights and remedies in relation to any infringement of its rights in respect of this report.

Contents

List of Figures

List of Tables

1. Introduction

Northport is a deep-water commercial port strategically situated at Marsden Point near Whangarei in Northland, New Zealand (Figure 1-1). Northport is planning to expand the port's capacity by reclaiming land, building additional berths and dredging a larger turning basin (Figure 1-2**Error! Reference source not found.**).

MetOcean Solutions (MOS, a division of the Meteorological Service of New Zealand) has already undertaken a number of numerical hydrodynamic and morphological modelling simulations and dredged plume dispersion simulations related to this project, with results presented in MOS reports P0367-01 to P0367-06 (MOS, 2018a, 2018b, 2018c, 2018d, 2018e, 2018f) and P0519-01 to P0519-03 (MOS, 2021a, 2021b, 2021c).

The following investigations are now required to be undertaken for the proposed revised layout:

- Hydrodynamics: update bathymetry with proposed dredge footprint and rerun of full month of hydrodynamic (2 spring/neap cycles). Assessment of change in currents over a typical spring tidal cycle.
- Morphological modelling: Modelling of predicted seabed morphological change in the vicinity of the proposed dredge footprint over a 5-year period
- Sediment plumes: Modelling of sediment plumes generated during dredging operations, including with Trailer Suction Hopper Dredger (TSHD hereafter), Cutter Section Dredger (CSD hereafter) (swing basin), and Backhoe Dredger (BHD hereafter) (berth area).

The present study builds upon the update of the hydrodynamic models of the existing and proposed port configurations (MOS, 2022a) to characterise the dispersion of sediment plumes associated with the required dredging.

The structure of this report is organised as follows. Section 2 describes the methodology and results are presented in Section 3. Section 4 provides a brief summary of the report. References are provided in the final section 5.

Figure 1-1 Location of Northport within Whangarei Harbour.

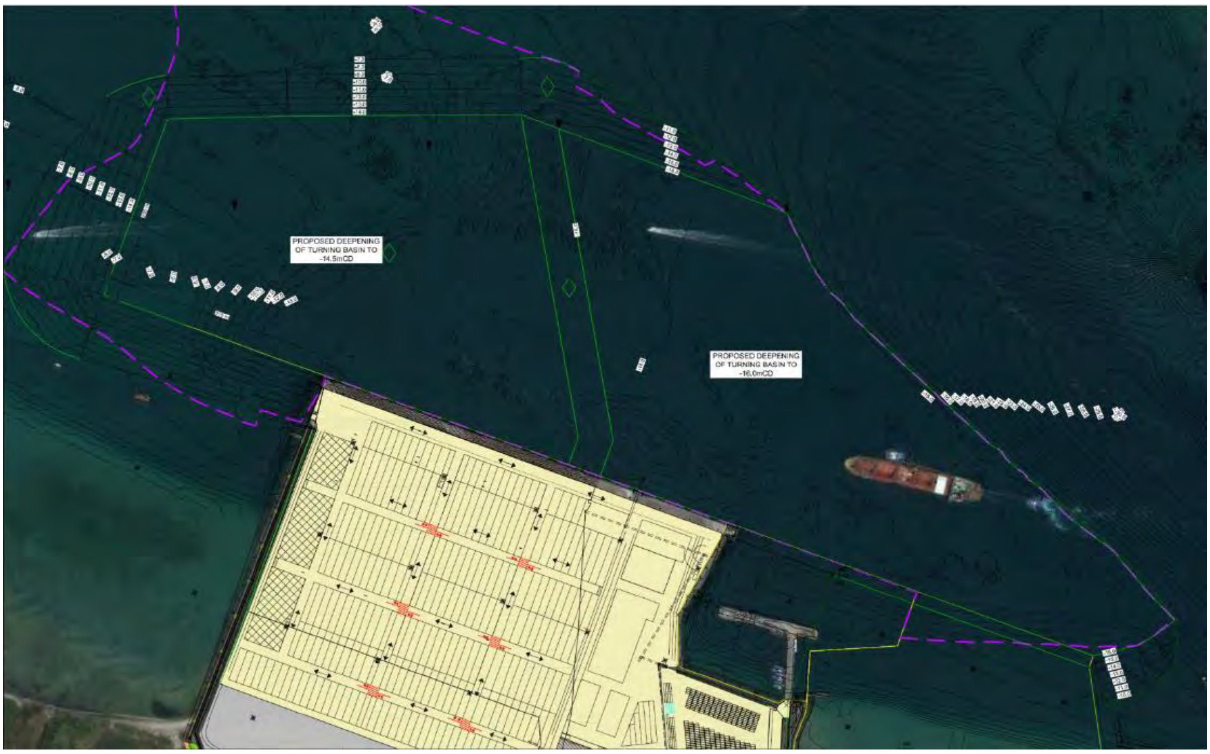

Figure 1-2: Draft concept drawing for the proposed area to be dredged and reclaimed (from NorthPort).

2. Methods

2.1 Approach

An actual release of sediment in the oceanic environment is a process that is finite in time (i.e., occurring at a specific time, over a finite period) and inherently non-deterministic (i.e., controlled by a range of random and unpredictable variables such as currents and turbulences). Since future ocean conditions and exact timing of the dredging works are unknown, it is not possible to predict the actual outcomes of a release before the event occurs. However, the probability of future oceanic conditions can be assessed from the historical conditions, thereby allowing statistical characterisation of the spatial dispersion of the suspended sediment plume patterns.

In the present study, dredging operations were simulated over a 1-month period, including a complete spring/neap tidal cycle, Previous investigations have shown that very little difference in sediment plumes patterns are observed between an El Niño and La Niña years, therefore simulations will consider a single monthly period (September 2010, La Niña episode).

A range of dredging locations (Figure 2-1 and Table 2-1) and dredging methods were considered to assess the dispersion characteristics of the generated plumes.

2.2 Hydrodynamics

Details on the implementation and validation of the hydrodynamic model employed in the sediment plume modelling are provided in MOS (2022a).

2.3 Dredging scenarios

It is expected that the dredging of the turning basin will be undertaken using both a Trailing Suction Hopper Dredge (TSHD) (Figure 2-2) and a Cutter Section Dredge (CSD) (Figure 2-3). A scenario with dredging near the berth pocket using a Backhoe Dredger (BHD) (Figure 2-4) was also considered.

All dredgers were assumed to operate 24h a day, 7 days a week, over the 1-month period. The TSHD simulations assumed a large TSHD with hopper volume of 1860m^3 (Albatros vessel) with dredging cycles according to information provided by Northport and dredging contractors. The cycle times varied depending on the areas to be dredged and therefore on considered sites (Figure 2-1). Cycle times for the dredging with no overflow, dredging with overflow, and sediment pumping to shore are shown in Table 2-2. The CSD and BHD were assumed to operate continuously (i.e. no specific cycles). The TSHD and

CSD simulations were reproduced at 4 different sites within the turning basin. The BHD simulations were run for 1 site within the berth pocket near the proposed eastern reclamation area (see positions in Figure 2-1).

The month-long simulations at the different sites allow capturing a wide range of tidal and residual flows, and their spatial variability within the areas to be dredged.

Table 2-1 Positions and depth of dredging positions. Depths are relative to chart datum.

	Site 1a	Site 1b	Site 2a	Site 2b	Berth Pocket
longitude	174.4831	174.4854	174.4889	174.4914	174.4923
latitude	-35.8292	-35.8311	-35.8310	-35.8327	-35.83385
depth existing	9.0	13.3	14.9	14.7	14.8
depth proposed	14.5	14.5	16.0	16.0	16.0

Table 2-2 TSHD cycle times for sites of interest in turning basin.

	Site 1a	Site 1b	Site 2a	Site 2b
Dredging to overflow [min.]	12	12	12	12
Dredging with overflow [min.]	51	113	59	59
Pumping to shore [min.]	152	100	142	142

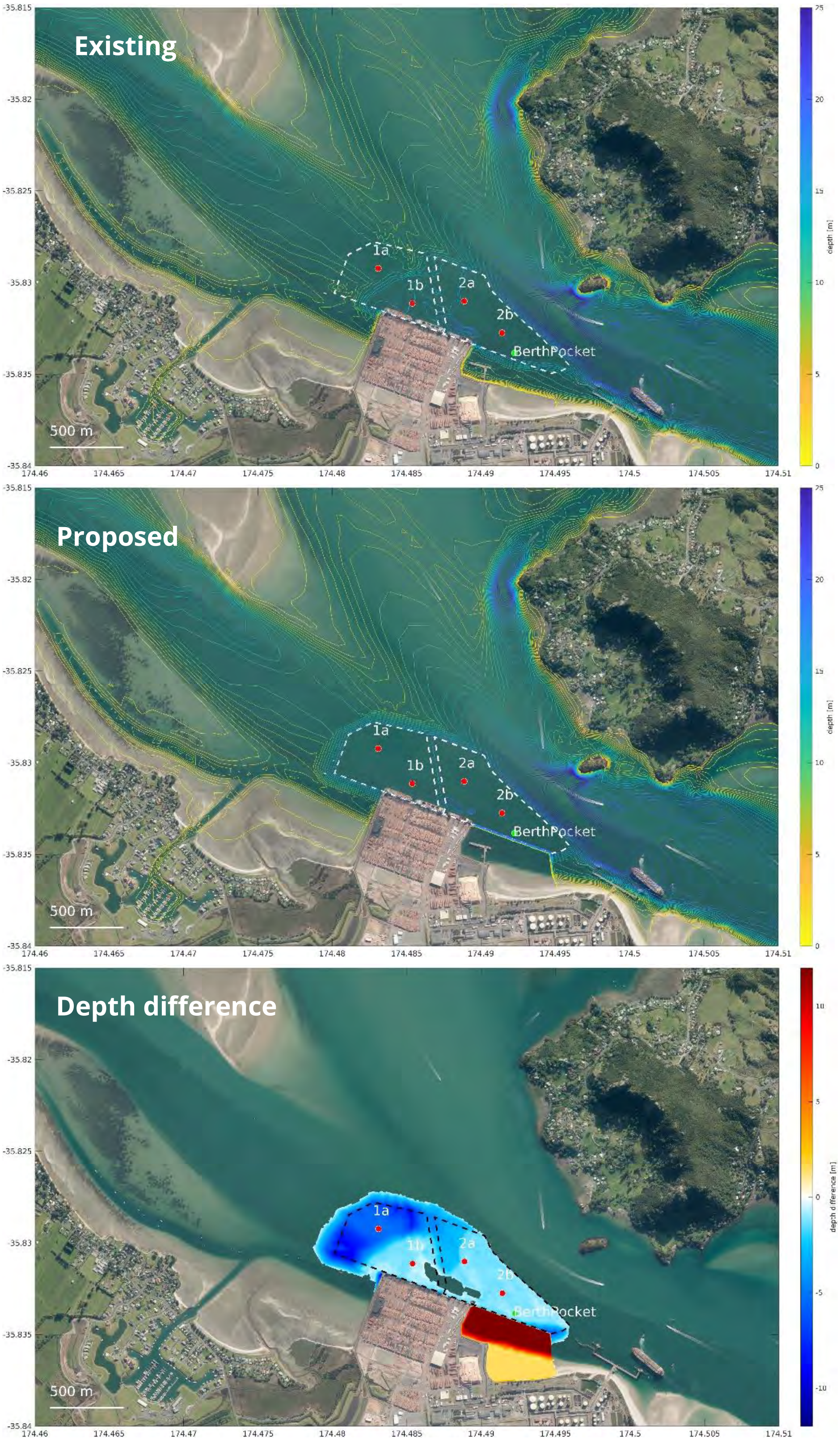

Figure 2-1 Dredging locations considered for the sediment plume modelling over the existing (top) and proposed (middle) port bathymetries. The bottom plot shows the depth difference between the two bathymetries. Site positions and depths are provided in Table 2-1.

2.3.1 Sediment distribution

Information on the particle size distribution of the sediment to be dredged was provided by a range of borehole records (Babbage Geotechnical Laboratory Report numbers: 63009#L/HYD, 63009#L/FINES and 63009#L/PSD) (Table 2-3).

Two representative sediment distributions were assumed in the sediment plume modelling:

- A ***silty sand***, with PSD defined from the average of the samples obtained below 10m (Table 2-4)
- A ***sandy silt***, with PSD defined from the shallower BH2 core (6-6.45m) (Table 2-5)

For the fine and medium sediment classes, we assumed a representative median size d_{50} in middle of the size range to determine the associated settling velocities used in the simulations. For the silt, we used a weighted averaged of the median size d_{50} of the different silt subclasses (i.e., 60-20, 20-6, 6-2 microns) using the PSD of sample BH2 (6-6.4m). For clay we used the upper limit of the size range at 2 µm. Settling velocities were computed equations by Van Rijn (1993). The slowest settling velocity was limited to 0.2 $mm.s^{-1}$ for the clay fraction to account for the expected flocculation of the fine cohesive sediment. The coarse sand and gravel classes were not included in the simulation due to their fast settling and very low proportion.

Note the *sandy silt* case includes a larger fraction of small particles (<63 microns), which will settle slower thus remaining in suspension for longer times.

Table 2-3 Summary of PSD available from the borehole records

	Gravel			Sand			Silt / Clay			
	60-20	**20 – 6**	**6 – 2**	**2.0 – 0.6**	**0.6 – 0.2**	**0.2 – 0.06**	**< 0.06mm**	**SUM FRACTION**		
BH1										
8.2-8.65 m	0.0	0.0	0.0	2.0	26.0	61.0	11.0	100.0		
14.2 – 14.65 m	0.0	0.0	0.0	0.0	14.0	73.0	13.0	100.0		
% per class	**0.0**			**88.0**			**12.0**	100.0		
BH2							Silt – 0.06-0.02	Silt – 0.02-0.006	0.006-0.002	Clay < 0.002
6 – 6.45	0.0	0.0	0.0	1.0	3.0	48.0	**14.0**	**9.0**	**8**	**17**
12 – 12.39	0.0	0.0	0.0	1.0	47.0	47.0	5.0	100.0		
15 – 15.45	0.0	1.0	4.0	6.0	29.0	53.0	7.0	100.0		
% per class	**1.7**			**78.3**			**20.0**	100.0		
BH3										
2.7 – 3.15	0.0	0.0	0.0	2.0	4.0	72.0	22.0	100.0		
8.7 – 9.15	0.0	1.0	1.0	1.0	15.0	64.0	18.0	100.0		
13.2 – 13.65	0.0	0.0	1.0	1.0	38.0	55.0	5.0	100.0		
% per class	**1.0**			**84.0**			**15.0**	100.0		
BH4										
4.5 – 4.95	0.0	0.0	0.0	1.0	4.0	64.0	31.0	100.0		
12.00-12.45	0.0	0.0	0.0	0.0	26.0	66.0	8.0	100.0		
13.5-13.95	0.0	0.0	0.0	0.0	34.0	62.0	4.0	100.0		
% per class	**0.0**			**85.7**			**14.3**	100.0		
BH5										
2.7 – 3.15	0.0	0.0	2.0	9.0	77.0	10.0	2.0	100.0		
16.2 – 16.65	0.0	0.0	2.0	1.0	8.0	70.0	19.0	100.0		
% per class	**2.0**			**87.5**			**10.5**	100.0		
BH6										
3.00 – 3.45	0.0	0.0	0.0	0.0	4.0	84.0	12.0	100.0		
7.5 -7.95	0.0	0.0	0.0	0.0	3.0	68.0	29.0	100.0		
9-9.45	0.0	0.0	0.0	0.0	2.0	51.0	47.0	100.0		
% per class	**0.0**			**70.7**			**29.3**			
Overall Average [mm]	0.0	0.1	0.6	1.6	**20.9**	**59.3**	**17.6**	100.0		
	0.8			**81.7**						
< 10 m	0.0	0.1	0.4	2.0	17.0	58.9	**21.6**	100.0		
	0.5			**77.9**						
> 10 m	0.0	0.1	0.9	1.1	24.8	59.6	**13.5**	100.0		
	1			**85.5**						

Table 2-4 Sediment distribution for the ***silty sand*** *and associated settling velocities. The relative fractions were defined by averaging the PSD of all samples below 10m. The relative fraction silt/clay was assumed to be similar to that of the BH2 shallowest sample (6-6.45m), which is the only sample that defined the PSD for grain sizes smaller than 63 microns.*

Silty Sand	**Medium sand (0.2-0.6 mm)**	**Fine Sand (0.06-0.2 mm)**	**Silt (2-60 µm)**	**Clay (<2 µm)**
Representative d50 [µm]	450	130	22.8	2
Proportion	25	60	9	5
Settling velocity (Van Rijn) [m/s]	51.7e-3	9.2e-3	0.33e-3	0.2e-3

Table 2-5 Sediment distribution for the ***sandy silt*** *consistent with the shallowest sample of BH2 borehole (6-6.45m) and associated settling velocities.*

Sandy Silt	**Medium sand (0.2-0.6 mm)**	**Fine Sand (0.06-0.2 mm)**	**Silt (2-60 µm)**	**Clay (<2 µm)**
Representative d50 [µm]	450	130	22.8	2
Proportion	3	48	31	17
Settling velocity (Van Rijn) [m/s]	51.7e-3	9.2e-3	0.33e-3	0.2e-3

2.3.2 Dredging source terms

The processes by which sediment is released and suspended in the water column during dredging operations vary with the type of dredger used. As a result, the different dredging methods results in different source terms for the dispersion modelling.

During the TSHD dredging operations, sediment is sucked into the vessel hopper using a drag head; a fraction of the sediment disturbed by the drag head is not pumped into the hopper and remains suspended in the water column. Sediment suspension is also expected due to the action of propeller wash on the seabed sediment. These two sources of sediment suspension are identified as sources 1 and 3 in Figure 2-2. In the present study the following sediment releases were used for these sources:

- Drag head source: bottom 3 meters of water column.
- Propeller wash source: bottom 3 m of the water column.

After the initial hopper infilling, the actual content of the hopper is a sediment/water mixture which is expected to contain ~20% solids by volume (Spearman et al., 2007). To maximise the amount of sediment in the hopper, it can be decided to continue to pump sediment and water from the seabed; this will result in the hopper "overflowing" and thereby releasing some sediment in the water column. The overflow releases generally occur through pipes in larger TSHD but can be simply released on deck and overboard on smaller vessels. This phase will be referred to as "overflow phase" and is shown as the source 2 in Figure 2-2.

The overflow load consists of a highly concentrated mixture of sediment and water and the bulk behaviour of that sediment mixture may become dominant over the individual particle settling processes (Winterwerp, J.C., 2002). When the overflow mixture is released through pipes, it is expected that the overflow release will be followed by a dynamic plume phase where the sediment mixture descends to bottom as a jet-like feature and impacts the seabed, suspending sediment and forming an initial density driven near-bed plume. A fraction of the sediment load will be de-entrained from the dynamic plume during descent and become suspended in the water column. This is comparable to processes involved during the offshore disposal i.e., 1) Convective descent, 2) Dynamic Collapse, and 3) Passive plume dispersion (Figure 2-5). The general length scales expected for the overflow process are an order of magnitude smaller than the discharge of sediment at the offshore disposal ground. Additionally, the overflow sediment mixture is less concentrated than in offshore sediment disposal context.

In the present simulations, this overflow phase was modelled considering two sources of sediment to the passive plume:

- Suspension of sediment de-entrained from the dynamic plume descent uniform release within the entire water column, and
- Passive plume generated following the dynamic plume impact: release within a cylinder of 2 m height and 60 m radius on the seabed.

For conservatism, an additional source reproducing possible small sediment surface losses was also included in the TSHD simulations (1% of production rate).

- Surface losses : surface 2 meters of water column.

Cutter section dredging (CSD) works by diluting the sediment to be dredged with water via a rotating cutter head (Figure 2-3). The sources of sediment suspension when using a CSD include:

- Near seabed disturbance when diluting the sediment with rotating cutter head.

Backhoe dredging (BHD) consists in mechanically removing seabed sediment using a backhoe mounted on a barge (Figure 2-4). The sources of sediment suspension when using a BHD include:

- Near seabed disturbance when loading the bucket, and
- Across the water column as the bucket is lifted to the barge.

The magnitude of the various source terms was defined using methods described by Becker et al. (2015) . In their approach, source term magnitudes are based on the *expected* dredger production rate which is the amount of *in-situ* sediment removed per unit of time [$m^3.s^{-1}$] (Table 2-6). Depending on the dredging methodology, fraction(s) of that production rate are transferred into the passive sediment plume that will be then advected and dispersed by ambient currents. The different source terms, release depths and fraction of production rate for the TSHD, CSD and BHD dredgers are provided in Table 2-7. These were defined in consultation with NorthPort and dredging contractors. The TSHD production rates were based on recent dredging works undertaken at the site. Corresponding source term magnitudes are provided in Table 2-8 to Table 2-10 for each dredging methods. These sources of sediment were further broken into different sediment classes according to PSD provided in Table 2-4 and Table 2-5 for the *silty sand* and *sandy silt* scenarios.

Note, for conservatism, we applied this approach to both the cohesive and sand fractions, whilst Becker et al. (2015) only consider the cohesive fractions, given the high settling rate of sand. Here, the sandy fractions are indeed included in the computations though with appropriate faster-settling rates (see Table 2-4 and Table 2-5).

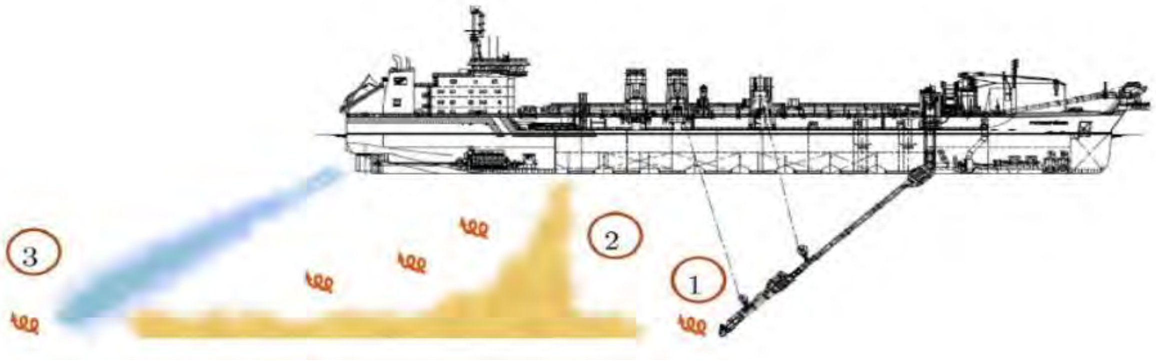

Figure 2-2 Sediment suspension sources for a Trailing Suction Hopper Dredger: 1-Drag Head, 2-Overflow, including de-entrainment during plume descent through the water column and density current on the seabed, 3-Propeller wash (from Becker J. et al., 2015).

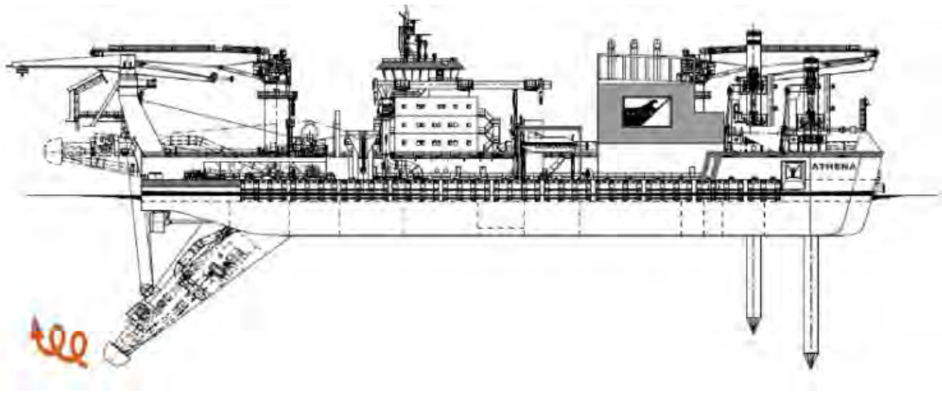

Figure 2-3 Sediment suspension sources for a Cutter Section Dredger (after Becker J. et al., 2015).

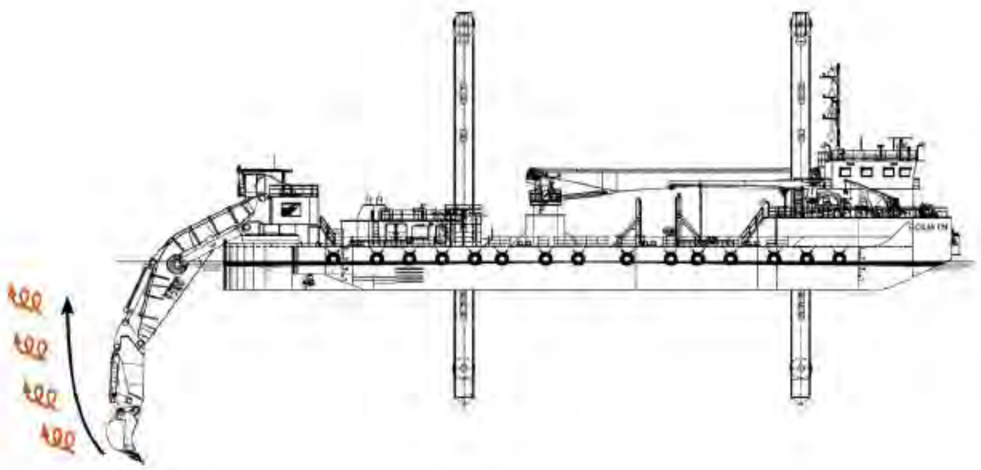

Figure 2-4 Sediment suspension sources for a Backhoe Dredger (after Becker J. et al., 2015).

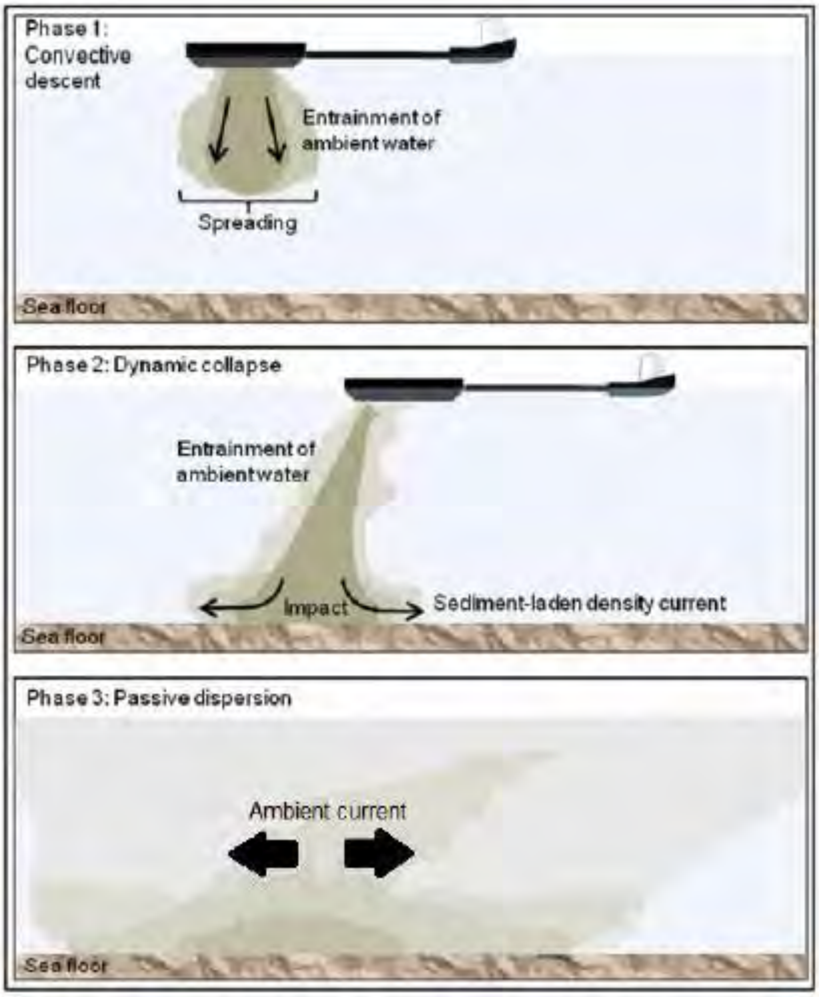

Figure 2-5 Three main phases occurring during the disposal of dredged material: 1) Convective descent, 2) Dynamic Collapse, and 3) Passive plume dispersion. Similar processes are expected when dense overflow sediment mixture is released during dredging.

Table 2-6 Reasonable ranges for (empirical) source term fractions (from Becker et al., 2015)

Plume source	Symbol	Fraction
Draghead	σ_d	0–0.03
Overflow ratio	R_o	0–1
In-hopper settlement	f_{sett}	0–1
In-matrix fixation	f_{trap}	0.01–0.05
Overflow	σ_o	0–0.2
Cutterhead	σ_c	0.01–0.05
Bucket drip	σ_b	0–0.04
Bottom door (hydraulic)	σ_p	0–0.1
Bottom door (mechanic)	σ_p	0.0–0.05

Table 2-7 Summary of source terms and scaling fractions simulated

Source terms	Release depth	Radius [m]	Fraction of production rate
TSHD			
Drag head disturbance	Bottom 3 m	20	0.03
Propeller wash	Bottom 3 m	20	0.03
Surface losses	Surface 2 m	20	0.01
Overflow (sediment de-entrained during descent)	Water column	point	0.2
Overflow (density current at the bottom)	Bottom 3 m	60	0.8
CSD			
Cutterhead disturbance	Bottom 3 m	10	0.05
BHD			
Bucket - near bed disturbance	Bottom 2 m	10	0.04
Bucket losses de-entrainment	Water column	25	0.04

Table 2-8 Magnitude of source terms for the TSHD dredger. This is assuming a daily production rate of 9200 m^3. day^{-1}. Details of computation accounting for TSHD cycle times can be found in Appendix B.

		Magnitude		
TSHD	**Units**	**Site 1a**	**Site 1b**	**Site 2a, 2b**
Daily production rate	m^3.day	9200	9200	9200
dry volumic mass	kg.m^{-3}	1600.0	1600.0	1600.0
Propeller wash(3%)	kg.s^{-1}	17.4	9.2	15.3
Drag head (3%)	kg.s^{-1}	17.4	9.2	15.3
Surface losses (1%)	kg.s^{-1}	5.8	3.1	5.1
Overflow passive plume (fac0 = 20%)	kg.s^{-1}	79.1	41.7	69.5
Overflow density current (1-fac0 = 80%)	kg.s^{-1}	316.3	166.8	278.1

Table 2-9 Magnitude of source terms for the CSD dredger

CSD	Units	Magnitude (all sites)
Production rate	$m^3.s^{-1}$	0.44
dry volumic mass	$kg.m^{-3}$	1600.0
Production rate	$kg.s^{-1}$	704.0
Near bed source (5% of production rate)	$kg.s^{-1}$	35.2

Table 2-10 Magnitude of source terms for the BHD dredger

BHD	Units	Magnitude
Production rate	$m^3.s^{-1}$	0.138
dry volumic mass	$kg.m^{-3}$	1600.0
Production rate	$kg.s^{-1}$	220.8
Nearbed source (4% of production rate)	$kg.s^{-1}$	8.83
Watercolumn source (4% of production rate)	$kg.s^{-1}$	8.83

2.4 Sediment Plume Modelling

2.4.1 OpenDrift Model description

The dispersion of sediment discharged in the harbour during the dredging operations was simulated using the harbour trajectory modelling framework OpenDrift[1] (Dagestad K.F et al., 2018). OpenDrift is an open-source Python-based framework for Lagrangian particle tracking developed by the Norwegian Meteorological Institute, where it is notably used operationally for emergency response for oil spill and search and rescue events. The framework is highly modular and can be used for any type of drift calculations in the ocean or atmosphere. A number of modules have already been developed, including an oil drift module (Röhrs et al., 2019), a stochastic search-and-rescue module, a pelagic egg module, a plastic drift module.

The sediment dispersion simulations described in the study were undertaken using a modified version of the generic OceanDrift[2] module that allows specification of settling velocities.

The sediment dispersion modelling consists of a trajectory tracking scheme applied to discrete particles in time and space-varying 3D oceanic currents.

$$\frac{dx_p}{dt} = \tilde{u}(x, y, z, t) + u_t$$

$$\frac{dy_p}{dt} = \tilde{v}(x, y, z, t) + v_t$$

$$\frac{dz_p}{dt} = w_t + w_s$$

(2.1 a,b,c)

where (x_p, y_p, z_p) are particle 3D coordinates, $\tilde{u}_{(x,y,z,t)}$, $\tilde{v}_{(x,y,z,t)}$ are horizontal ocean currents, (u_t, v_t, w_t) are the diffusion components representing turbulent motions, and w_s is the sediment settling velocity.

In the horizontal plane, particles were advected by ocean currents using a 4th order Runge-Kutta tracking scheme, and subject to additional displacement by horizontal diffusion.

[1] https://github.com/OpenDrift/opendrift

[2] https://github.com/OpenDrift/opendrift/blob/master/opendrift/models/oceandrift.py

In the OpenDrift framework, the horizontal diffusion is included by applying an uncertainty to the horizontal current magnitudes. The magnitude of the current uncertainty was estimated using the general diffusion equation (eqn 2.2)

$$\int_t^{t+\Delta t} u_t.dt = \sqrt{2.K_{u,v}.\Delta t}\ .\theta(-1,1) \quad (2.2)$$

where $\theta(-1,1)$ is a random number from a uniform distribution between -1 and 1, Δt is the time-step of the model in seconds (900 sec. used here) and $K_{u,v}$ is the *horizontal* eddy diffusivity coefficient in $m^2 \cdot s^{-1}$.

In the vertical plane, particles are subject to both vertical settling (w_s) and diffusive displacement (w_t) due to vertical turbulent motion through the water column. In OpenDrift, the vertical mixing process is parameterised in using a numerical scheme described in Visser (1997) which is similar to equation 2.2 when using a constant vertical diffusion coefficient K_z (as employed here).

The horizontal and vertical diffusion are included in the dispersion modelling account for the mixing and diffusion caused by sub grid scale turbulent processes, such as eddies, that are not explicitly resolved by the hydrodynamic models.

For dispersion at oceanic scales, (Okubo, 1974; Okubo, 1971) proposed that $k_{u,v}$ varies approximately as equation 2.3, which is close to the general 4/3 power law often considered for atmospheric (Richardson, L.F, 1962) and oceanic diffusions (Batchelor (1952), Stommel, 1949)) (equation 2.4).

$$k_{u,v} = 0.103.L^{1.15} \quad (2.3)$$

$$k_{u,v} = \alpha.L^{4/3} \quad (2.4)$$

where *L* is the horizontal scale of the mixing phenomena and *α* indicates proportionality.

These equations relate the magnitude of the eddy diffusivity $k_{u,v}$ to the length scale of the phenomena and this 4/3 power relationship was found to be relevant over a large range of scale (10m to 1000km) (Okubo, 1974; Okubo, 1971). A similar relationship was found by List et al. (1990) in coastal waters.

In the present study, since high resolution flows are available (Section 3), the amount of added diffusion should be limited. A generic horizontal coefficient of 0.02 m^2/s was applied which is consistent with a length scale of order 20-40 m. The spatial scales of the vertical turbulent motions within the water column are one or several orders of magnitude smaller than horizontal ones. The vertical diffusion coefficient was set to a value of 1 cm^2/s.

2.4.2 Particle release

Depending on the dredging scenarios modelled (i.e. TSHD, CSD, or BHD), particles were released according to source terms of Table 2-7. Individual simulations were undertaken for each sediment class (Table 2-4, Table 2-5) and results were then combined to obtain the total suspended sediment (TSS) plumes and deposition fields. The total number of particles released per simulation, and per sediment class, was ~ 200,000. This amounts to a total of ~800,000 particles when combining all the different sediment classes.

2.4.3 Post-processing

The total suspended sediment concentration and cumulative deposition fields were reconstructed from the particle clouds on a ~6 km by 4 km frame centred on the dredging locations, with a grid cell resolution of 25 m. Suspended sediment concentration were computed at three levels in the water column, i.e., surface, mid depth and near bed.

Gridded fields of TSS and deposition were reconstructed from the particle clouds using a kernel density estimator (Silverman, 1986). In the kernel density approach, individual particles are assumed to represent the centre of mass of a "cloud"; the density profile of the cloud is described by the *kernel function*, while the spreading of the particle's equivalent mass is defined by the *bandwidths* associated with a given particle or receptor (Bellasio, et al., 2017; Vitali et al., 2006). These two components are then used to derive a *particle density field*, also referred to as a *probability density function*. Here, the kernel density estimation is undertaken following the approach proposed by Botev, et al. (2010). The proposed method uses an adaptive kernel density estimation method based on the smoothing properties of linear diffusion processes. The key idea is to view the kernel from which the estimator is constructed as the transition density of a diffusion process (Botev, et al., 2010). This method limits the amount of guessing, notably to defining bandwidths, as well as possible excessive smoothing of the density fields (e.g., as obtained with Gaussian kernel density estimators).

Based on a given cloud of particles (X_{part}, Y_{part}), the method yields a *probability density function PDF(x,y)*, derived from the *kernel density estimator* describing the density of particles throughout the domain. The spatial integration of the *probability density function PDF(x,y)* over the entire domain equals one.

The *PDF(x,y)* values can be converted to particle density when multiplied by the total number of particles in the domain i.e., with units [particles.m^{-2}]. The particle density can in turn be converted to mass density, or mass distribution, based on the equivalent mass carried by individual particles i.e., with units [kg.m^{-2}]. Mass concentration (i.e. TSS) is obtained by dividing the mass density by the correct vertical depth band i.e., with units [kg.m^{-3}].

TSS concentrations were converted to [$mg.L^{-1}$] which is a more common unit in a dredging context. Note these predicted dredging TSS concentrations would add to any ambient TSS concentration levels. TSS statistics were derived from the obtained time varying TSS fields. The report presents the mean and 90^{th} percentile TSS at each level in the water column.

A similar approach is followed for estimating the depositional thickness. The probability density function of the deposited particles is computed and converted to a (dry) sediment mass density field in [$mass.m^{-2}$]. The sediment mass is converted to a volume using its dry volumic mass (assumed to be 1600 $kg.m^{-3}$) which effectively yields a deposition thickness in meters i.e. [$m^3.m^{-2} = m$]. The deposition thickness fields were masked below 5mm which is the order of magnitude of natural variations at the site (NorthPort, 2022, pers. comm.)

The newly deposited sediment is expected to be less compact that *in-situ* sediment due to incorporation of water between deposited grains. A generic bulking coefficient of 1.5 was applied to predicted deposition thicknesses. This means $1m^3$ of dredged *in-situ* sediment would create a 1.5 m^3 deposition volume. There are uncertainties on the effective bulking coefficient depending on the sediment distribution (e.g. proportion of silt/clay) as well as dredging methods. The influence of the bulking ratio on predicted results is illustrated in section 3.2.2.

3.Results

3.1 Main plume dispersion features

Dispersion of dredging plumes within the harbour were simulated for a wide range of scenarios including :

- 3 different dredgers (TSHD, BHD and CSD, Figure 2-2 to Figure 2-4) 5 different sites (see and Table 2-1)
- 1 month period (September 2010 - La Niña episode)
- *existing* versus *proposed* bathymetries (Figure 2-1)
- *sandy silt* versus *silty sand* (PSD in Table 2-4 and Table 2-5)

Main features from the full set of results are described below. All corresponding mean and 90th percentile Total Suspended Solid (TSS) concentration maps and final cumulative deposition fields are provided in Appendix B (as digital image files). Note we present mean rather than median (i.e. TSS levels exceeded 50% of the time) values since the discontinuous dredging TSHD cycles (see Table 2-2) typically result in null or very small median values which complicates the plume pattern description.

In general, dredging plume and deposition footprints are elliptical, typically centred on the release sites, with a clear northwest-southeast-axis consistent with the channel morphology and ambient hydrodynamics dominated by tides. Dispersion footprints are contained within the main harbour channel, with no significant branching towards secondary northward channel arm (towards Shoal Bay).

The new eastern reclamation has a limited impact on general dispersion patterns with a slight flow deflection in its vicinity. The dredge plume footprints are comparatively more extended for the *sandy silt* scenario relative to the *silty sand* due to the larger fraction of slow settling sediment, which can thus travel further away from the release location. However, the silty sand plumes are typically more concentrated closer to release due to the larger fractions of fast-settling material staying within the release location vicinity.

The TSHD dredging results in significantly larger TSS levels compared to CSD and BHD which is expected given the larger amount of sediment transferred to the passive plume, particularly during the overflow phase (see Figure 2-2, and Table 2-8). In general, TSS plumes are visible across the entire water column with similar footprints. However, TSS levels are smaller at the surface and increase with depth, due to the larger sediment disturbance near the seabed for all dredging techniques.

We note that some of the vertical bands considered for the TSS computations (surface 3m, middle 2m, bottom 2 m) can effectivity overlap for shallower areas. Further, the actual depths at which are provided the TSS can be different in results for the existing and proposed port configurations due to the bathymetric changes associated with the dredging Figure 2-1).

3.2 Additional analysis on a primary scenario

To facilitate the description of results and provide additional quantification, we focus on a primary scenario where a TSHD dredger is used at Site 1a, with a production rate of 9200 $m^3.day^{-1}$. Results for other dredging methods and/or sites can then interpreted relative to this primary scenario.

The complete set of figures results is provided in Appendix B.

3.2.1 Mean and 90th percentile TSS and final deposition of primary scenario

The mean surface, mid-depth, and nearbed TSS fields as well as final deposition after the 1-month dredging period are shown in Figure 3-1 and Figure 3-2 for the *existing* and *proposed* configurations respectively. These mean TSS maps inform on the average TSS levels experienced over a 1-month dredging period. Guidance on the largest TSS levels that can be experienced within the harbour during a 1-month dredging period is provided by maps of the gridded 90th percentile TSS (Figure 3-3 and Figure 3-4). These 90th percentile TSS levels are levels exceeded only 10% of the time over the 1-month simulation.

Overall, plume patterns and magnitudes are similar for both *existing* and *proposed* configurations. For the site 1a shown as reference, we note a change of the distribution of the TSS across the water column which is due to the larger depth change pre/post dredging (9.5 versus 14.5 m, see Table 2-1). The surface and mid depth TSS become smaller, while the nearbed TSS increase post dredging. This feature is less evident at other sites where depth changes are smaller pre/post dredging (see Appendix B).

Statistical maps considering the full 1-month period are supplemented by snapshots of instantaneous TSS during ebb and flood flows in Figure 3-5 and Figure 3-6 to illustrate possible TSS plumes patterns at different stage of the tide.

Cumulative deposition fields are shown in Figure 3-7 and Figure 3-8. We note the deposition maps assume 1 month of continuous dredging at site 1a. In practice, the dredger will move throughout the turning basin over time and, depending on production rate and volume to be removed. In that sense the magnitude and patterns of deposition should be interpreted as worst case scenario and compared relatively with other dredging sites considered.

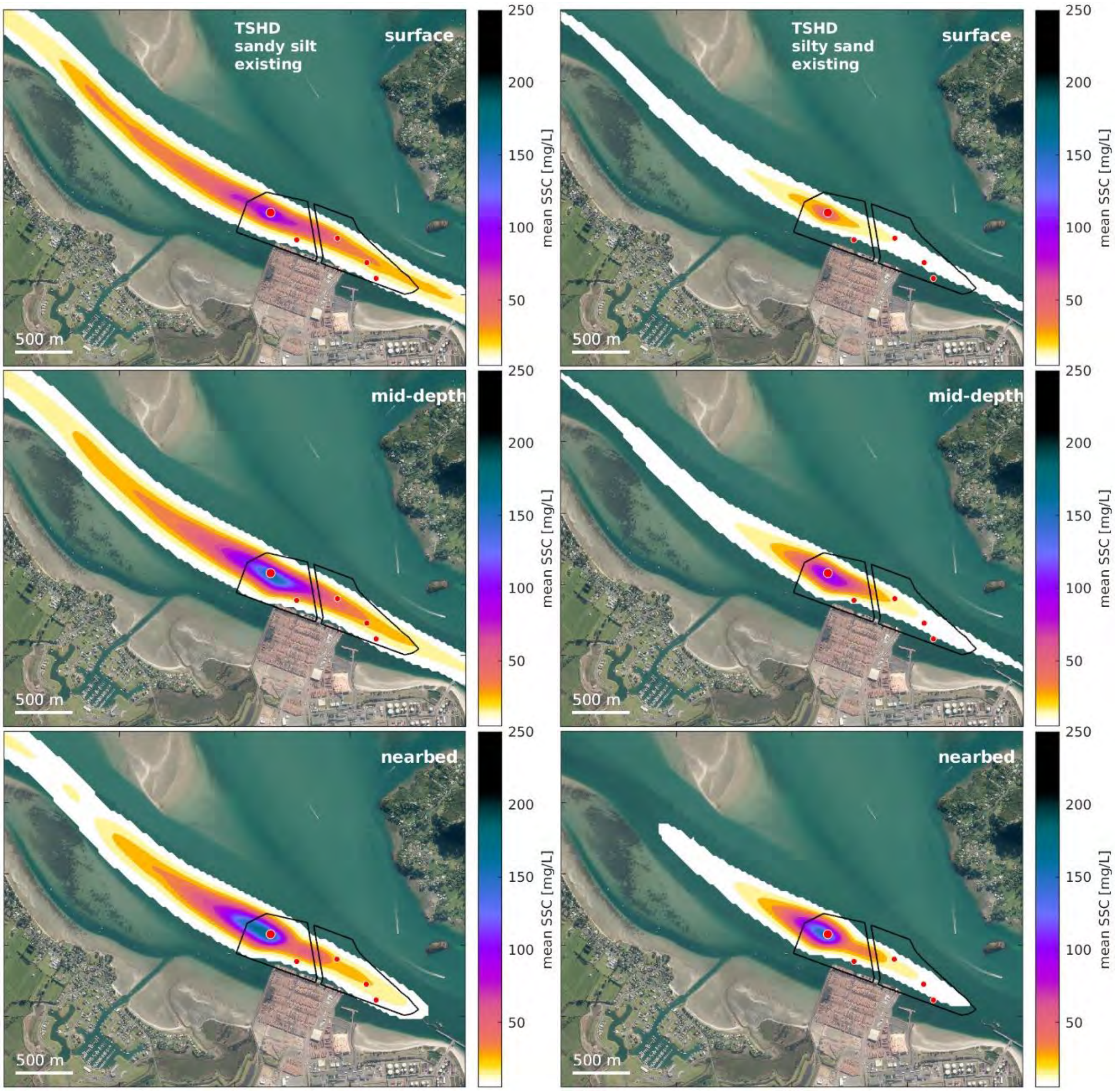

Figure 3-1 ***Mean*** *total suspended sediment concentrations [mg.L*$^{-1}$*] at surface, mid water and nearbed levels (top to bottom) for* ***TSHD*** *dredging at* ***site 1a,*** *over the* ***existing bathymetry****. Results are shown for the* ***sandy silt*** *on the left panel and* ***silty sand*** *on the right panel. The dredger is assumed to dredge continuously over the 1-month simulation period. TSS were masked below 5 mg.L*$^{-1}$*.*

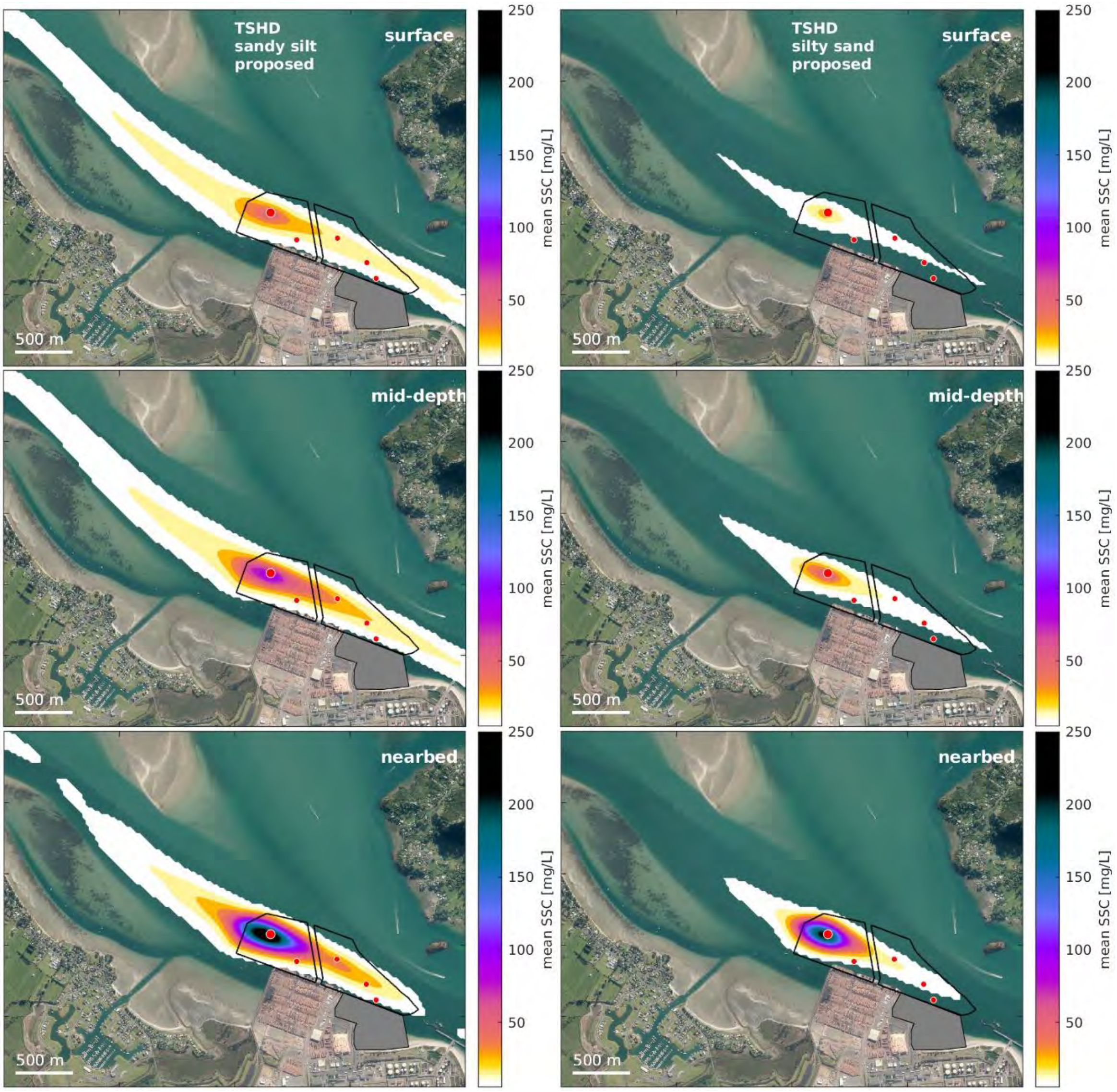

Figure 3-2 ***Mean** total suspended sediment concentrations [mg.L^{-1}] at surface, mid water and nearbed levels (top to bottom) for **TSHD** dredging at **site 1a,** over the **proposed bathymetry**. Results are shown for the **sandy silt** on the left panel and **silty sand** on the right panel. The dredger is assumed to dredge continuously over the 1-month simulation period. TSS were masked below 5 mg.L^{-1}.*

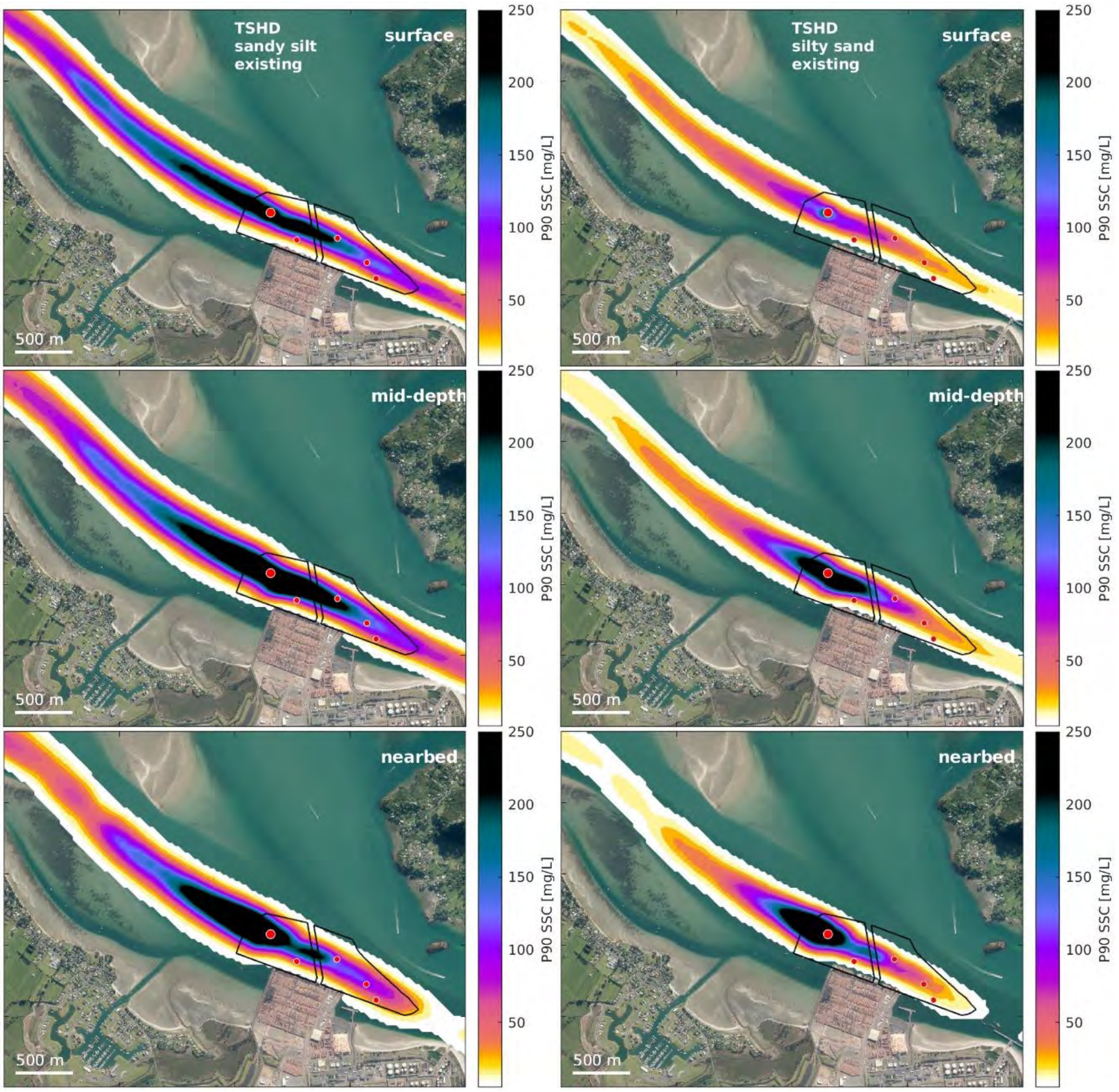

Figure 3-3 ***90th percentile*** *total suspended sediment concentrations [mg.L^{-1}] at surface, mid water and nearbed levels (top to bottom) for* ***TSHD*** *dredging at* ***site 1a,*** *over the* ***existing bathymetry****. Results are shown for the* ***sandy silt*** *on the left panel and* ***silty sand*** *on the right panel. The dredger is assumed to dredge continuously over the 1-month simulation period. TSS were masked below 5 mg.L^{-1}.*

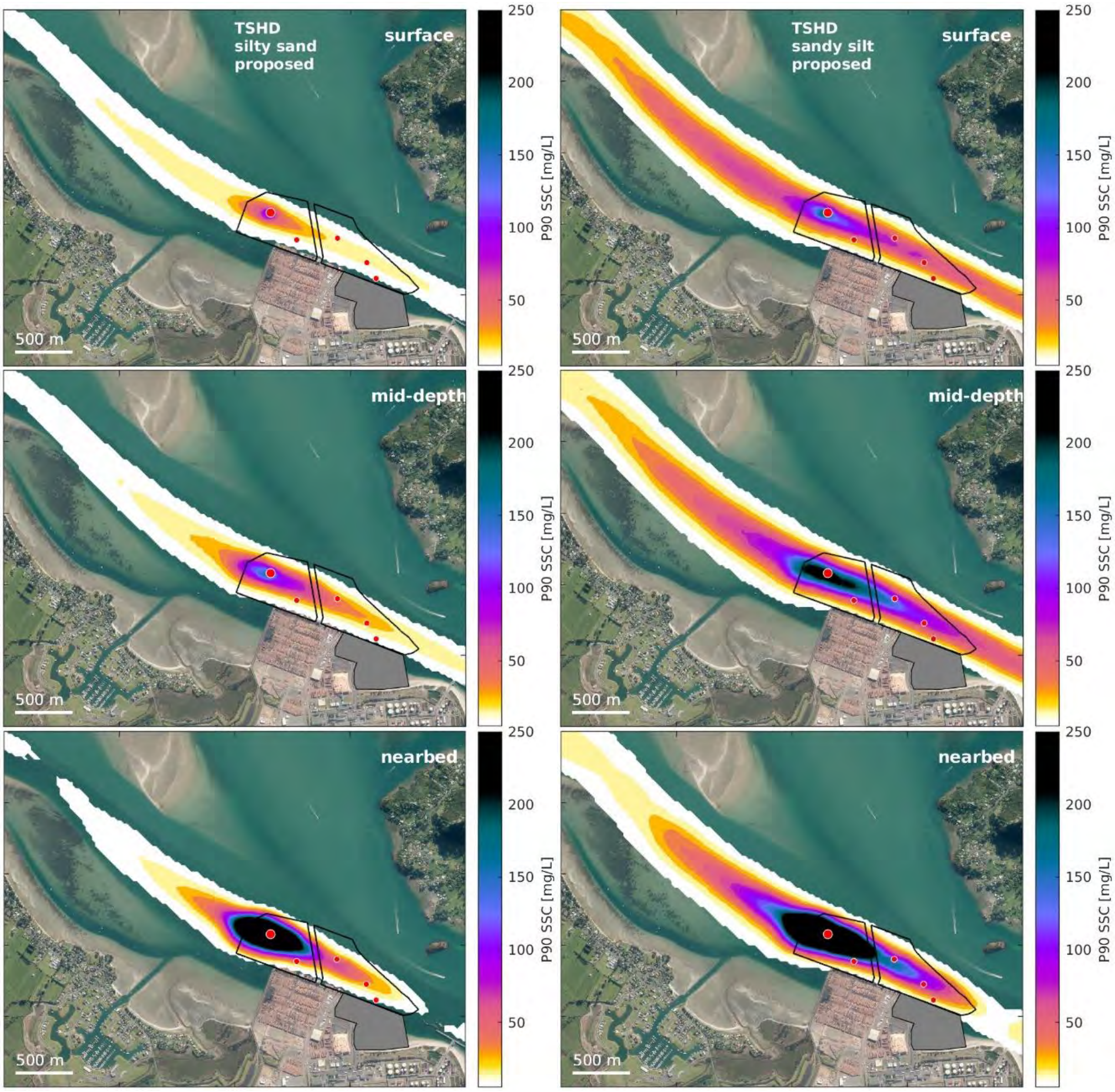

Figure 3-4 ***90th percentile*** *total suspended sediment concentrations [mg.L-1] at surface, mid water and nearbed levels (top to bottom) for* ***TSHD*** *dredging at* ***site 1a,*** *over the* ***proposed bathymetry.*** *Results are shown for the* ***sandy silt*** *on the left panel and* ***silty sand*** *on the right panel. The dredger is assumed to dredge continuously over the 1-month simulation period. TSS were masked below 5 mg.L-1.*

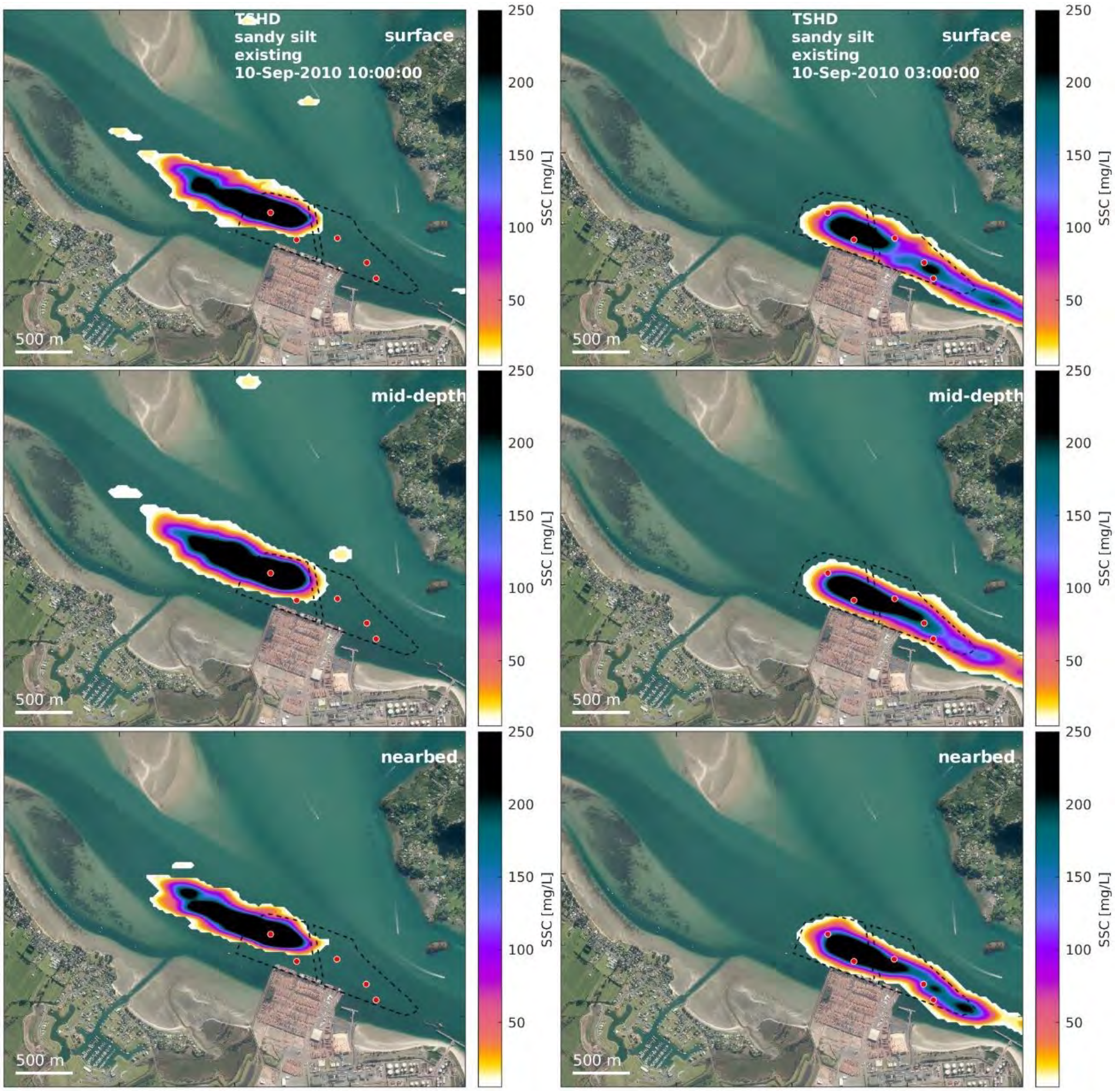

*Figure 3-5 Snapshots of total suspended sediment concentrations [mg.L^{-1}] at surface, mid water and nearbed levels (top to bottom) for **TSHD** dredging at **site 1a,** over the **existing bathymetry**, at **flood** (left) and **ebb** (right) flows. The dredger is assumed to dredge continuously over the 1-month simulation period. TSS were masked below 5 mg.L^{-1}.*

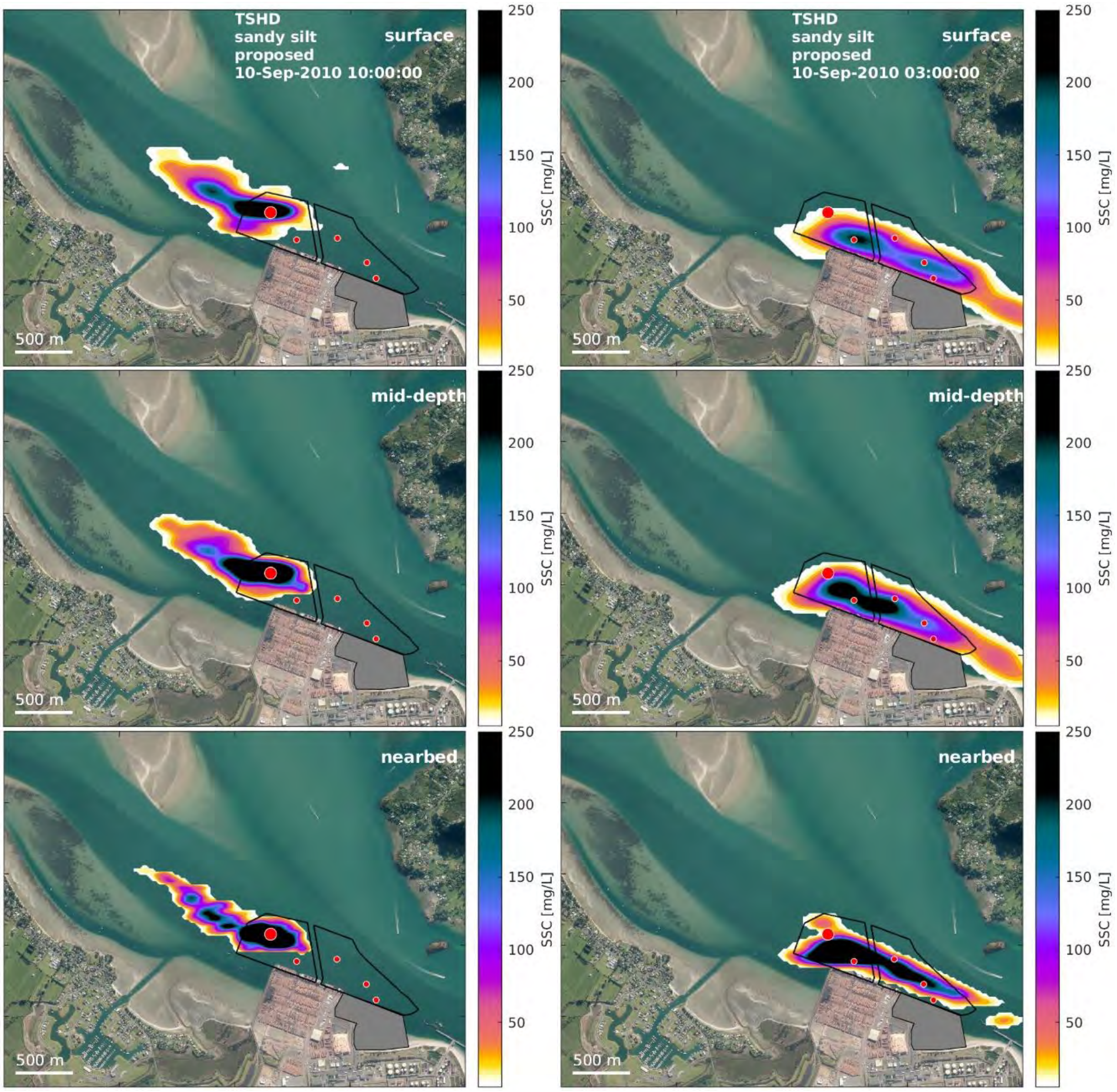

*Figure 3-6 Snapshots of total suspended sediment concentrations [mg.L^{-1}] at surface, mid water and nearbed levels (top to bottom) for **TSHD** dredging at **site 1a,** over the **proposed bathymetry**, at **flood** (left) and **ebb** (right) flows. The dredger is assumed to dredge continuously over the 1-month simulation period. TSS were masked below 5 mg.L^{-1}.*

Existing - Sandy Silt

Existing - Silty Sand

Figure 3-7 Final cumulative sediment deposition thickness [m] for ***TSHD*** *dredging at* ***site 1a,*** *over the* ***existing*** bathymetry, *Results are shown for the* ***sandy silt*** *on the left panel and* ***silty sand*** *on the right panel . Deposition thickness was masked below 5 mm and the 1 and 10 cm contours are shown in grey (dashed and solid lines respectively).*

Proposed - Sandy Silt

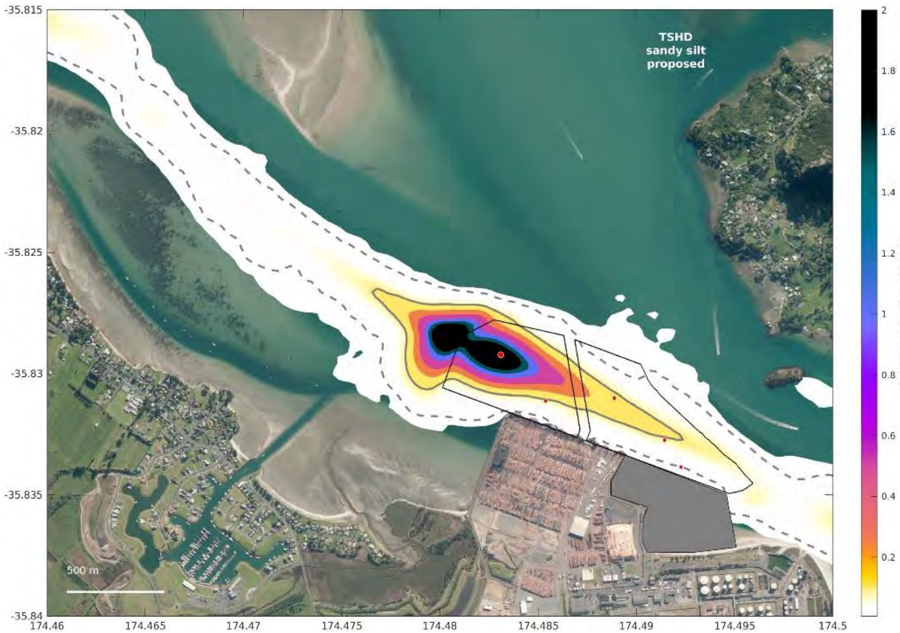

Proposed - Silty Sand

Figure 3-8 Final cumulative sediment deposition thickness [m] for ***TSHD*** *dredging at* ***site 1a,*** *over the* ***proposed*** bathymetry, Results *are shown for the* ***sandy silt*** *on the left panel and* ***silty sand*** *on the right panel . Deposition thickness was masked below 5 mm and the 1 and 10 cm contours are shown in grey (dashed and solid lines respectively).*

3.2.2 Comparison of TSS and final deposition at different dredging locations, for different dredging methods.

A comparison of the TSS plumes for TSHD dredging at different sites are shown in Figure 3-9 (existing) and Figure 3-10 (proposed) (results are shown for the *sandy silt* scenario). As noted in section 3.1, TSS footprints have a clear northwest-southeast-axis for all sites, in both *existing* and *proposed* bathymetries. This indicates a strong influence of the tidal flows in the harbour. We note the mean TSS concentrations are larger at site 1a than at other sites for the *existing* bathymetry due to the shallower water depth (hence reduced initial dilution across the water column) (see Table 2-1). This feature disappears in the *proposed* bathymetry in which all sites all have larger depths (14.5m or 16.0m CD). TSS levels are the largest in the nearbed layer, notably due to the nearbed density current generated during the overflow release (see Figure 2-2 and Figure 2-5).

Corresponding deposition fields are shown in Figure 3-11 (*sandy silt* scenario). Deposition footprints are elongated in a northwest-southeast axis, consistent with the TSS plumes, with largest deposition in the vicinity of the release site. We note that absolute magnitudes of deposition should be interpreted carefully and in a relative sense since, in reality, the dredging will not occur at fixed locations for an entire month but rather move throughout the area to be dredged. In the *proposed* bathymetry, we note some local sediment accumulation near the northwest edge of the turning basin, where most of the dredging will occur (see Figure 2-1. This is reproduced for all sites considered, with reduced deposition magnitudes as the dredging site moves eastwards. We note that actual deposition patterns should be interpreted with care given the absence of feedback between flow and morphology in the simulations, which would most likely redistribute the sediment. However, this general depositional trend should be acknowledged as it may incur additional dredging time over the area in order to reach the required depths. A similar deposition pattern is visible near the southeast edge of the turning basin for sites 1b, 2a,2b as well, though with smaller deposition magnitudes relative to the northwest edge.

Mean TSS plumes and deposition fields predicted for both the TSHD and CSD at *site 1a* and BHD at site *BerthPocket* are compared in Figure 3-12 to Figure 3-14. TSS plume footprints predicted for the TSHD method are larger and wider than for the CSD, notably due to the overflow phase which intermittently release large amounts of sediment across the entire water column, and near the seabed. TSS plumes for the CSD methods are narrower with TSS levels decreasing rapidly with distance from release. For the BHD method near the berth, the mean TSS plumes remain comparatively very compact and are contained in the close vicinity of the release site.

The magnitude differences for the different methods are reproduced in the deposition fields. We note a similar sediment accumulation near the northwest edge of the turning basin for the CSD and BHD dredgers, as identified in the TSHD results.

We note the deposition thickness results presented so far assumed a generic bulking coefficient of 1.5, meaning 1m^3 of dredged *in-situ* sediment would create a 1.5 m^3 deposition volume. There are uncertainties on the effective bulking factor that depends on the sediment distribution (e.g. proportion of silt/clay) as well as dredging methods. Burt (1996) suggests bulking factors in the range 1.1-1.4 for sand, silt, clay or mixed materials. Van Rijn (2019) provides a similar range (1.1-1.5) for cases when mechanical dredging is used (e.g. BHD, CSD) but notes an increase range when hydraulic dredging is used due to the addition of water in the sediment mixture. Bulking remains limited of sand material (1.15) but increases up to 2.5 for soft mud or firm clay. Note these bulking factors were estimated considering the deposition of the dredging vessel content to disposal sites rather than the deposition of the sediment lost in the passive plume resulting from dredging however it is expected that they would remain relevant, especially for the TSHD where most of the deposition is related to the dense overflow mixture release, which is similar to a disposal process.

Here, it is expected that the considered *silty sand* material *(*Table 2-4*)* will have a smaller bulking factors given the high sandy content (1-1.5), however more significant bulking could be observed for the *sandy silt* muddy material (Table 2-5), particularly for TSHD (hydraulic) dredging.

To illustrate the influence of the bulking factors on the predictions, footprints of the 5mm deposition contours resulting from TSHD dredging for the *sandy silt* material are compared for bulking factors from 1 to 2 in Figure 3-15 and Figure 3-16 for *existing* and *proposed* bathymetries. Footprints of the 5mm deposition contours resulting from TSHD dredging for the *silty sand* material are compared in Figure 3-17 for smaller bulking factors given the high sand content (1-1.5). (Site 1a shown only, all maps available in Appendix B). The 5mm deposition footprints are compared for different dredging methods in Figure 3-18 for bulking factors in range 1-2 for the *sandy silt* material, subject to more potential bulking. We note that the bulking factor is expected to remain in the range 1-1.5 for the mechanical dredging methods (BHD, CSD) but footprints with larger factors 1.5-2.0 are still included for comparison.

General deposition patterns are conserved with no new “significant” (i.e. > 5mm) depositional feature appearing, even with the largest bulking factor of 2.0. Considering results for bulking factors of 1 (no bulking) versus 2 (important bulking), we note however relative enlargements of the 5mm contour footprints of up to ~250m in places, notably off the existing berths and towards the north-northwest.

Site 1a *Site 1b* *Site 2a* *Site 2b*

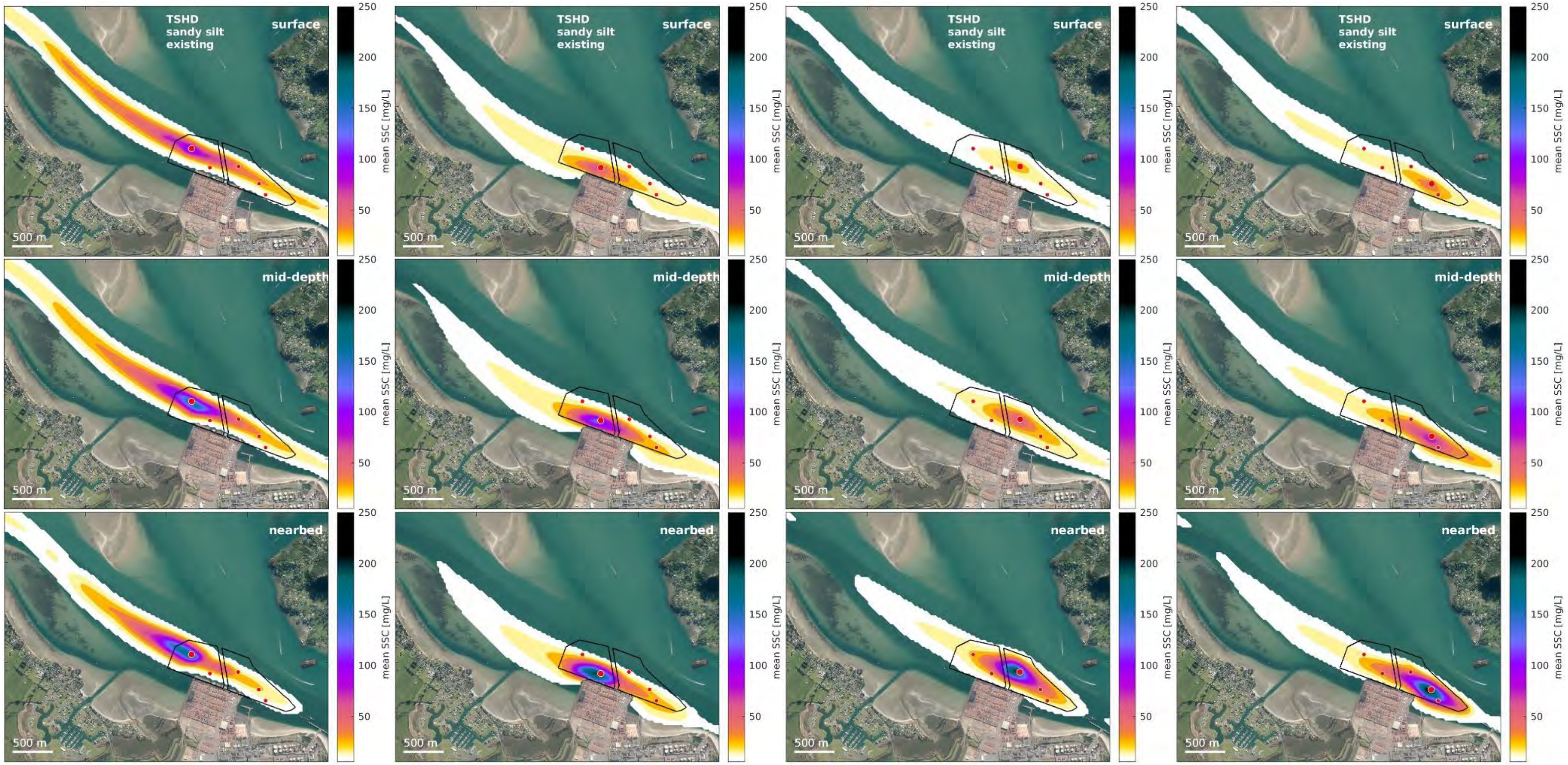

*Figure 3-9 Comparison of **mean** total suspended sediment concentrations [mg.L^{-1}] at surface, mid water and nearbed levels (top to bottom) for **TSHD** dredging at **sites 1a, 1b, 2a and 2b,** over the **existing bathymetry,** for the **sandy silt**. The dredger is assumed to dredge continuously over the 1-month simulation period. TSS were masked below 5 mg.L^{-1}.*

Site 1a ***Site 1b*** ***Site 2a*** ***Site 2b***

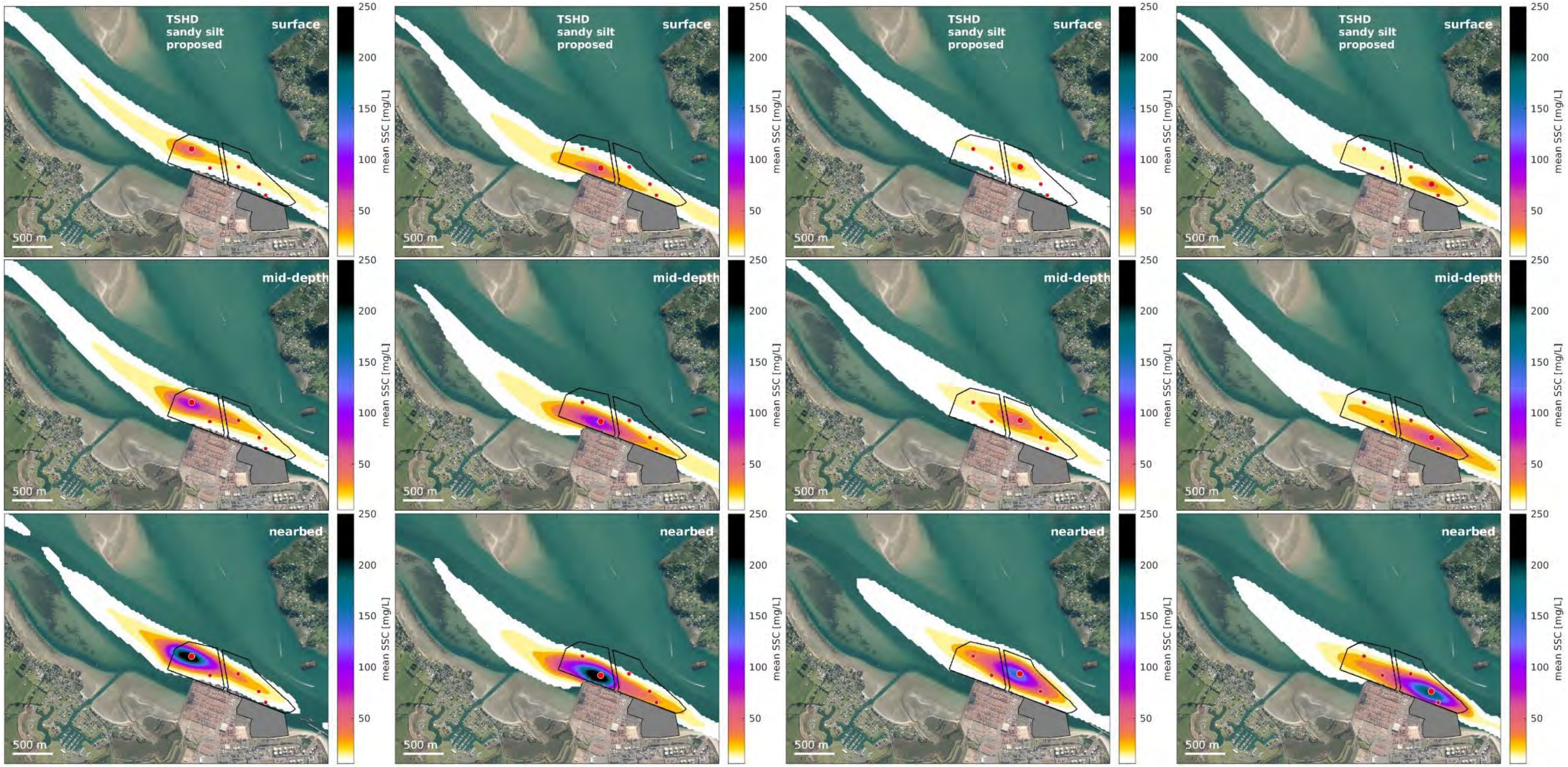

*Figure 3-10 Comparison of **mean** total suspended sediment concentrations [mg.L^{-1}] at surface, mid water and nearbed levels (top to bottom) for **TSHD** dredging at **sites 1a, 1b, 2a and 2b,** over the **proposed bathymetry,** for the **sandy silt**. The dredger is assumed to dredge continuously over the 1-month simulation period. TSS were masked below 5 mg.L^{-1}.*

Site 1a ***Site 1b*** ***Site 2a*** ***Site 2b***

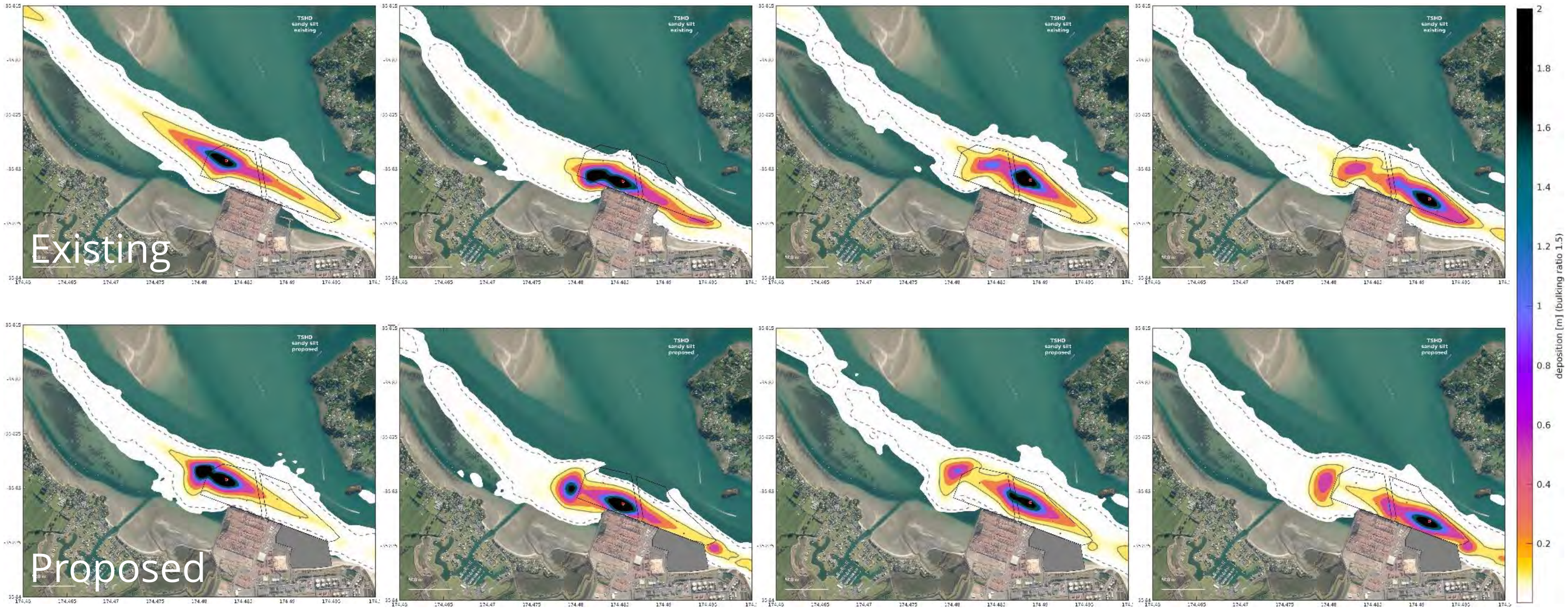

*Figure 3-11 Comparison of final cumulative sediment deposition thickness [m] for **TSHD** dredging at **sites 1a, 1b, 2a and 2b**, over the **existing** (top) and **proposed** (bottom) bathymetries, Results are shown for the **sandy silt**. Deposition thickness was masked below 5 mm and the 1 and 10 cm contours are shown in grey (dashed and solid lines respectively).*

TSHD (Site 1a) **CSD (Site 1a)** **BHD (Site Berth Pocket)**

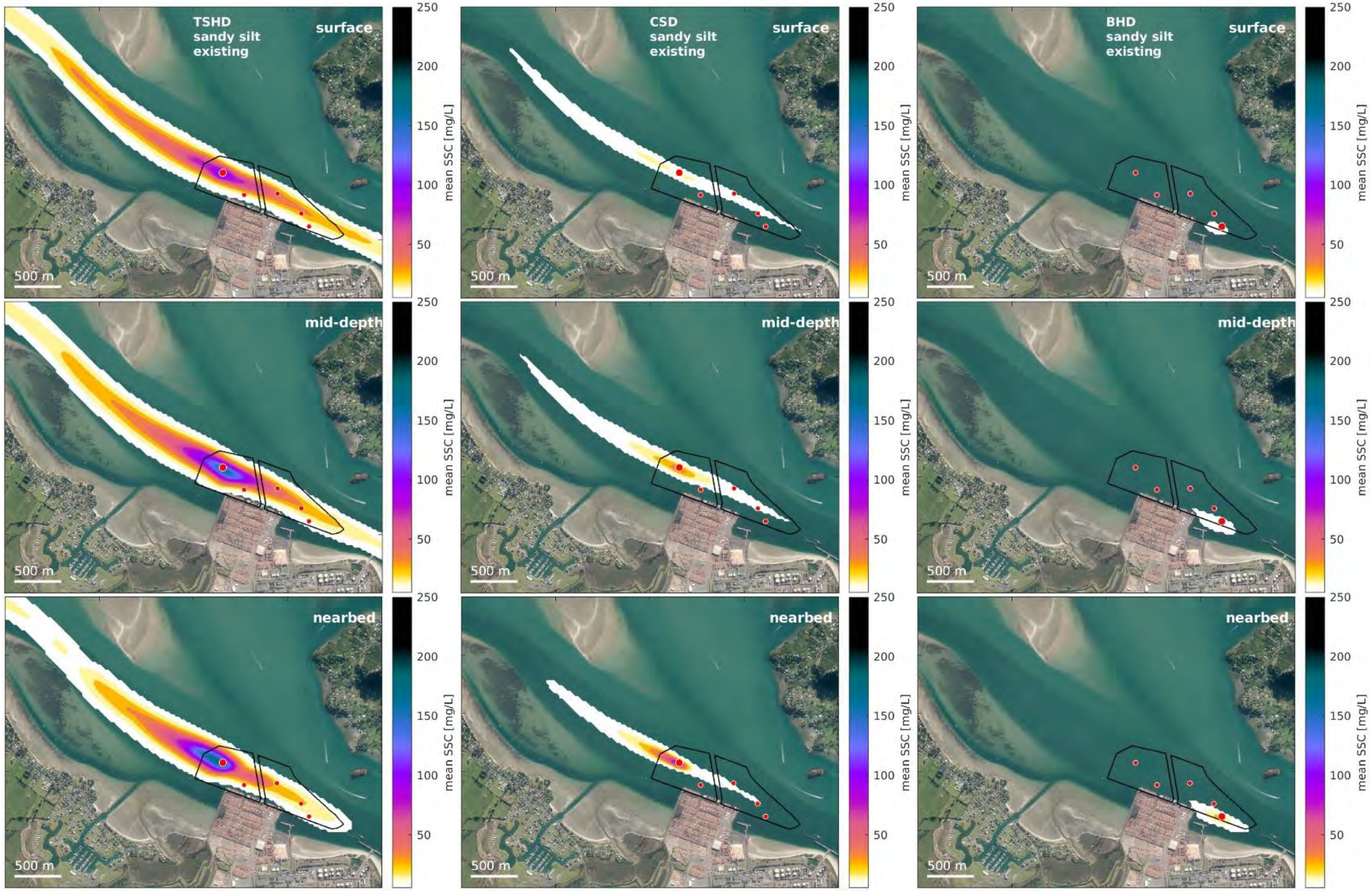

*Figure 3-12 Comparison of **mean** total suspended sediment concentrations [mg.L^{-1}] at surface, mid water and nearbed levels (top to bottom) for **TSHD** (left) and **CSD** (middle) dredging at **site 1a** and for **BHD** dredging at site **Berth Pocket** (right), over the **existing bathymetry**. Results are shown for the **sandy silt**. The dredger is assumed to dredge continuously over the 1-month simulation period. TSS were masked below 5 mg.L^{-1}.*

TSHD (Site 1a) ***CSD (Site 1a)*** ***BHD (Site Berth Pocket)***

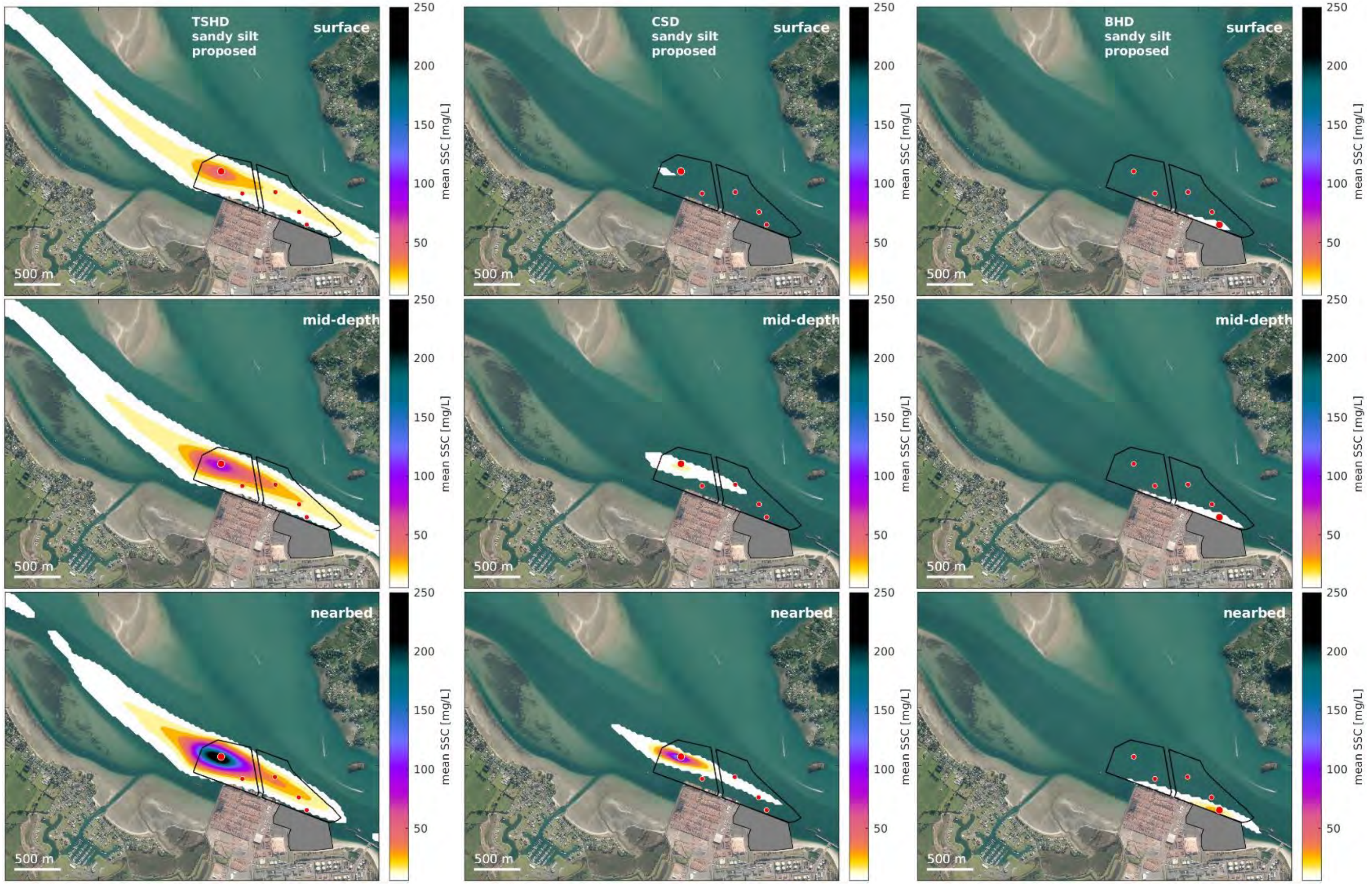

*Figure 3-13 Comparison of **mean** total suspended sediment concentrations [mg.L^{-1}] at surface, mid water and nearbed levels (top to bottom) for **TSHD** (left) and **CSD** (middle) dredging at **site 1a** and for **BHD** dredging at site **Berth Pocket** (right), over the **proposed bathymetry**. Results are shown for the **sandy silt**. The dredger is assumed to dredge continuously over the 1-month simulation period. TSS were masked below 5 mg.L^{-1}.*

TSHD (Site 1a) ***CSD (Site 1a)*** ***BHD (Site Berth Pocket)***

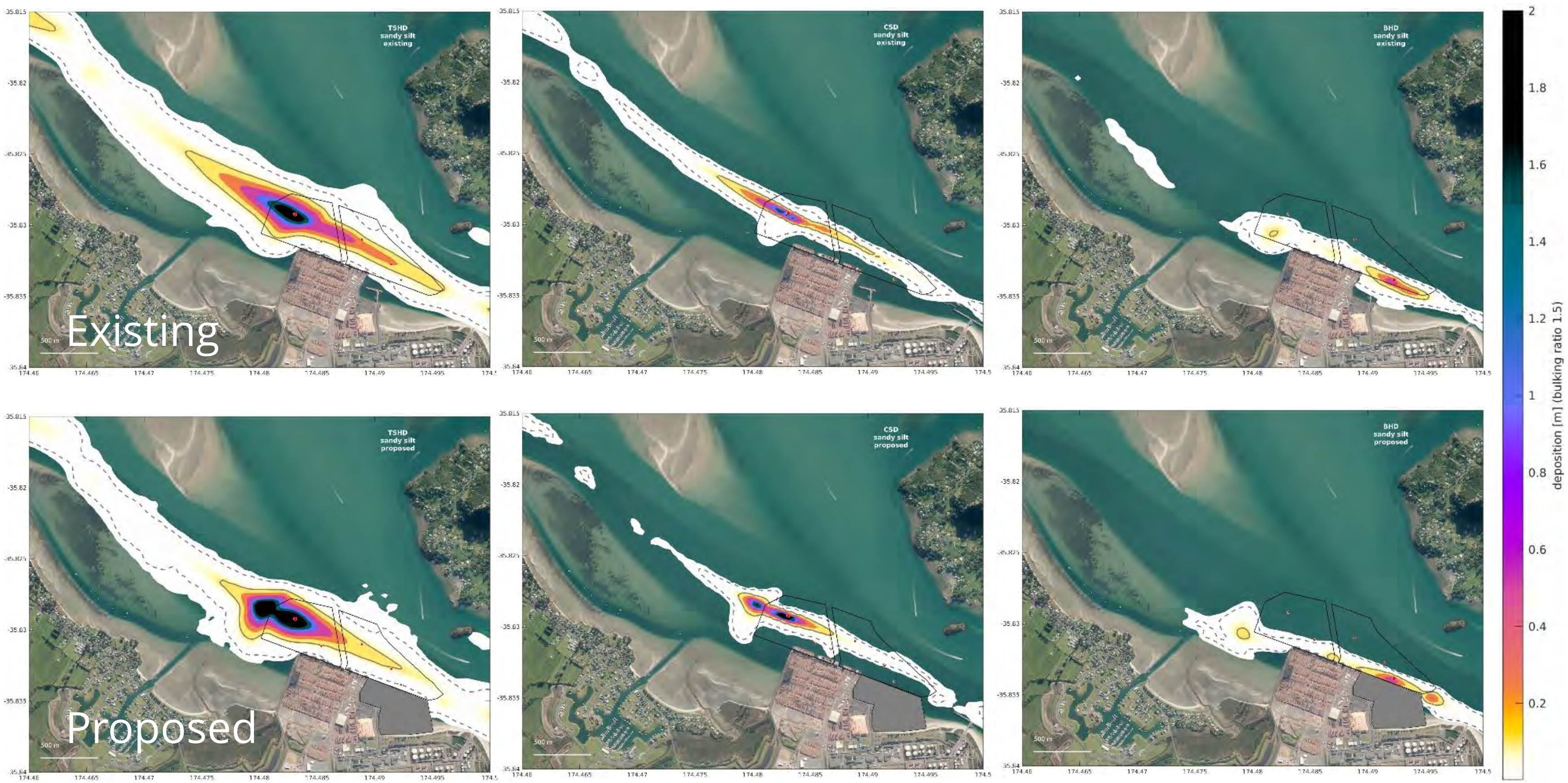

*Figure 3-14 Comparison of final cumulative sediment deposition thickness [m] for **TSHD** (left) and **CSD** (middle) dredging at **site 1a** and for **BHD** (right) dredging at site **Berth Pocket (right),** over the **existing** (top) and **proposed** (bottom) bathymetries. Results are shown for the **sandy silt**. Deposition thickness was masked below 5 mm and the 1 and 10 cm contours are shown in grey (dashed and solid lines respectively).*

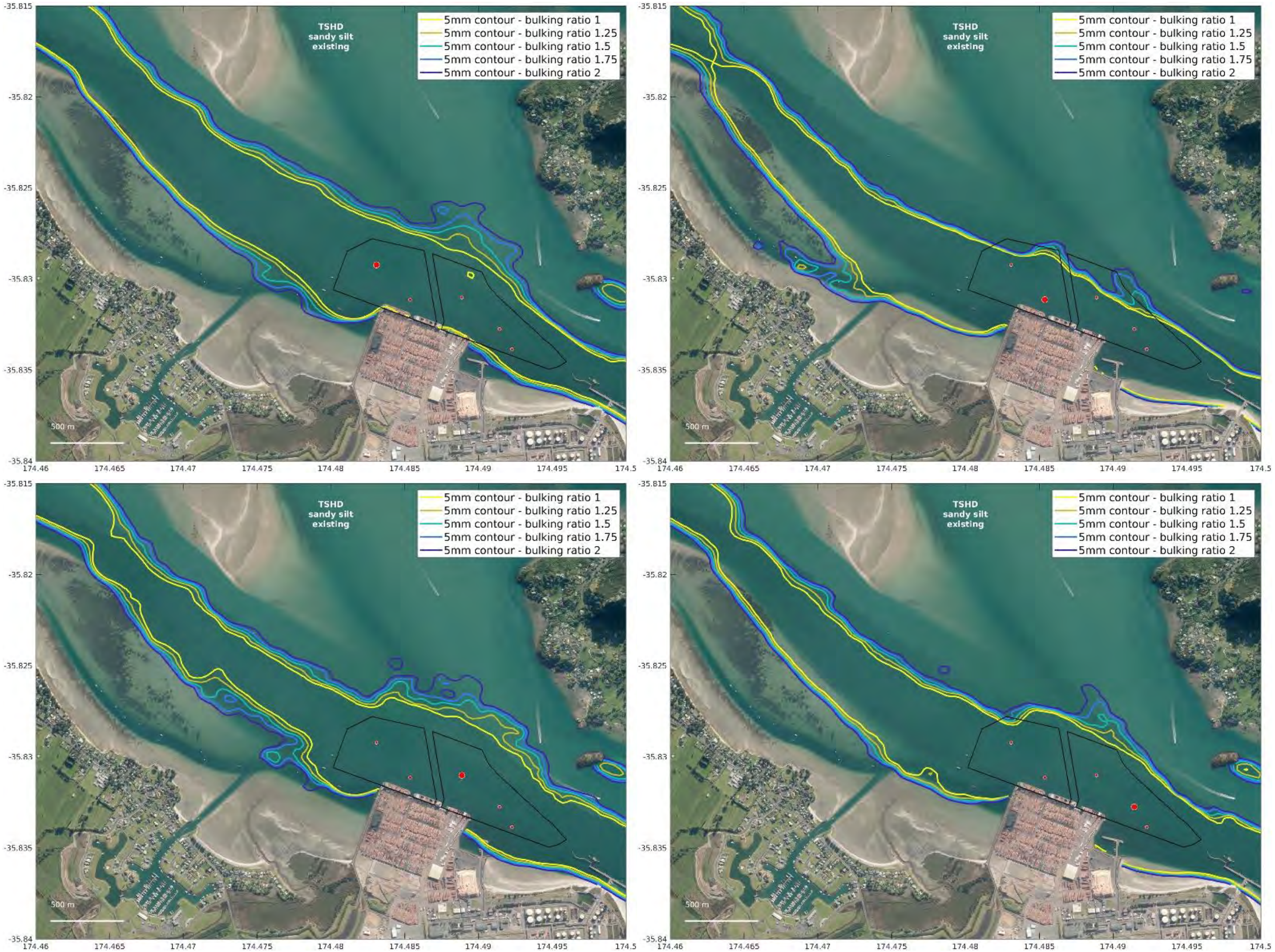

*Figure 3-15 Comparison of 5mm deposition footprints [m] for **TSHD** dredging at **sites 1a, 1b, 2a and 2b**, over the **existing** bathymetry for different bulking factors of the **sandy silt** material, in range 1.0-2.0.*

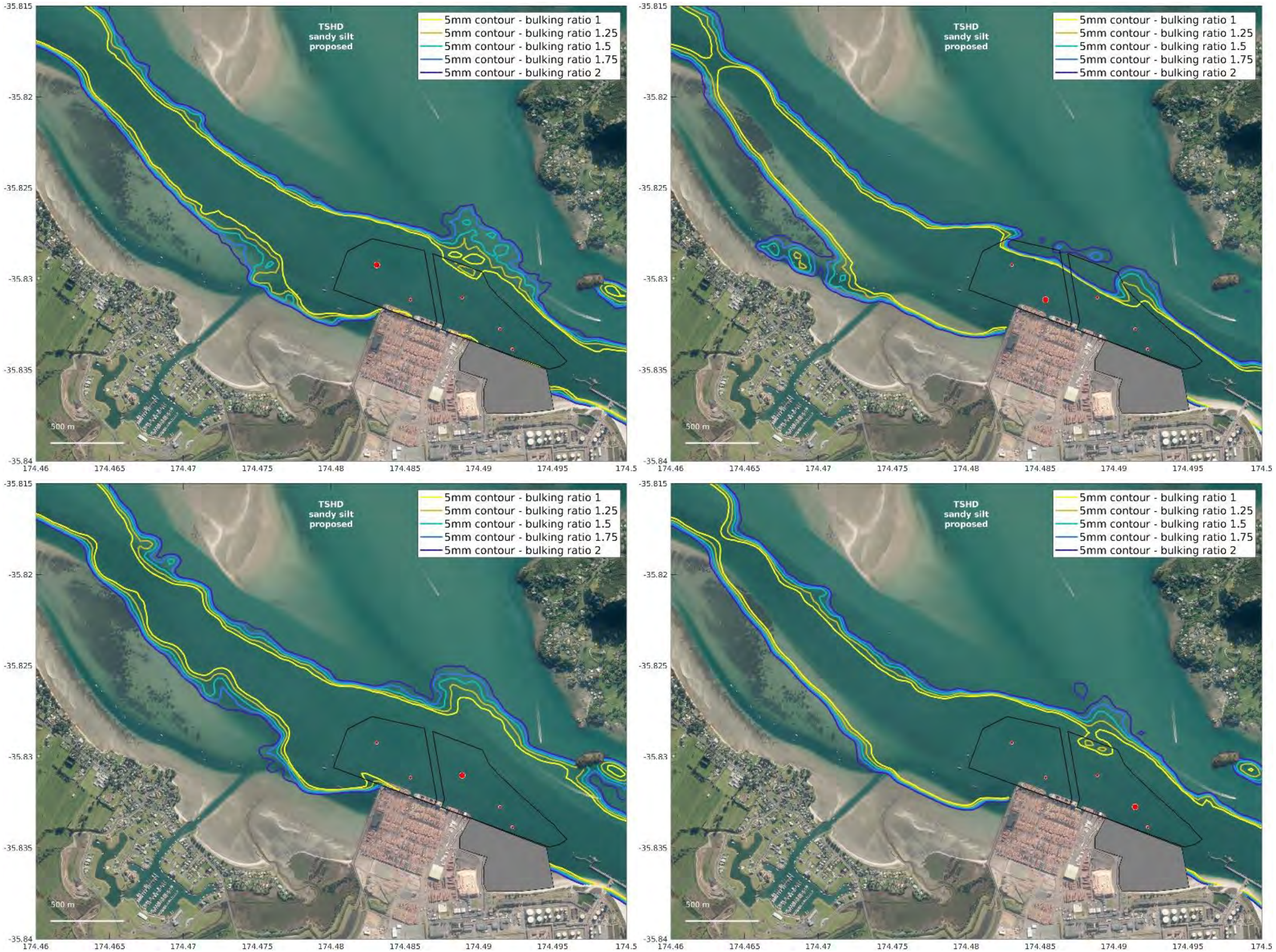

Figure 3-16 Comparison of 5mm deposition footprints [m] for ***TSHD*** *dredging at* ***sites 1a, 1b, 2a and 2b****, over the* ***proposed*** *bathymetry for different bulking factors of the* ***sandy silt*** *material, in range 1.0-2.0.*

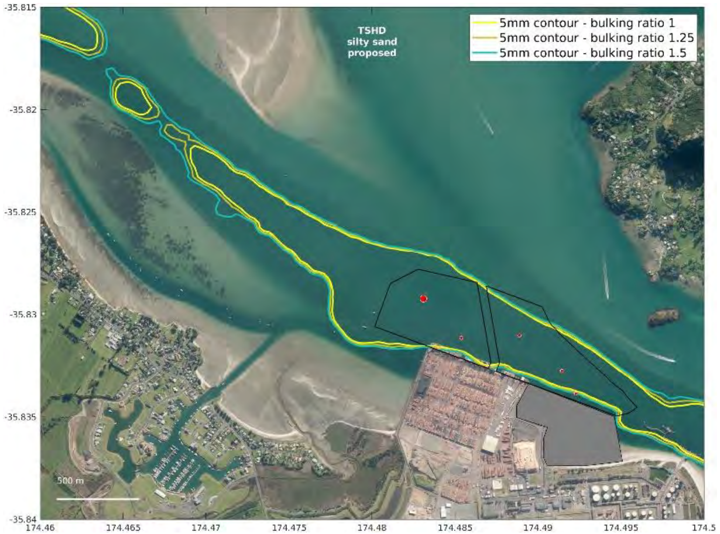

Figure 3-17 Comparison of 5mm deposition footprints [m] for ***TSHD*** *dredging at* ***sites 1a*** *over the* ***existing*** *(top) and* ***proposed*** *(bottom) bathymetries for different bulking factors of the* ***silty sand*** *material, in range 1.0-1.5.*

TSHD (Site 1a) ***CSD (Site 1a)*** ***BHD (Site Berth Pocket)***

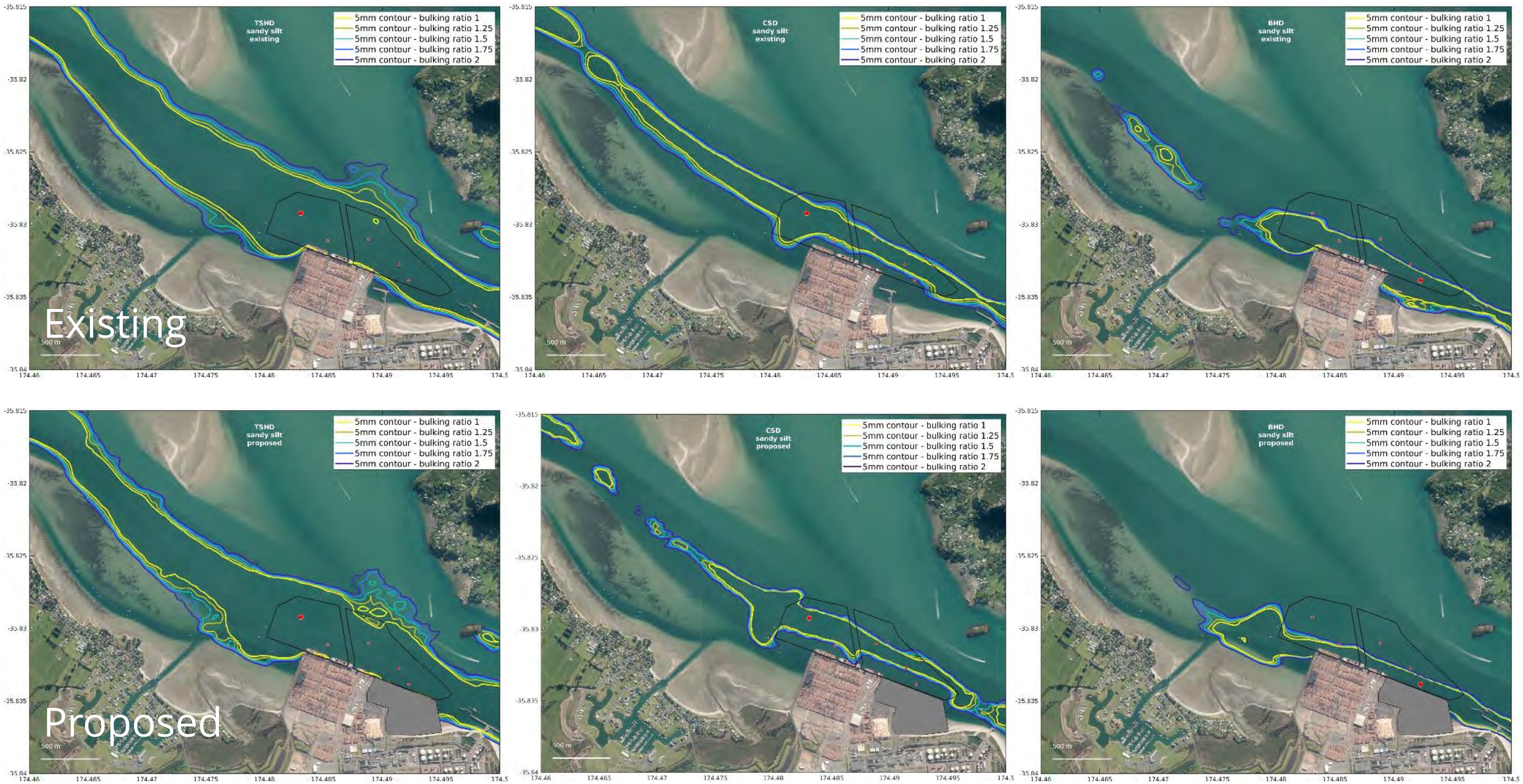

*Figure 3-18 Comparison of 5mm deposition footprints [m] for **TSHD** (left) and **CSD** (middle) dredging at **site 1a** and for **BHD** (right) dredging at site **Berth Pocket (right),** over the **existing** (top) and **proposed** (bottom) bathymetries, obtained with different bulking factors of the **sandy silt** material in range 1.0-2.0.*

3.2.3 TSS threshold exceedance

In an ecological assessment context, it is useful to quantify more precisely the percentage of time certain TSS thresholds would be exceeded. Maps quantifying the percentage of time TSS threshold of 20, 40, 80 and 160 mg.L^{-1} are exceeded are provided in Figure 3-19 and Figure 3-21 for the existing configuration for the *sandy silt* and *silty sand*, respectively. Corresponding maps for the proposed configuration are provided in Figure 3-21 and Figure 3-22.

Overall footprints are contained within the main harbour channel, with no significant branching towards secondary northward channel arm. The effective percentage of time expectedly reduce for increasing TSS thresholds. We clearly observe larger percentage of time for the *sandy silt* relative to the *silty sand*. This can be explained by a larger fraction of slow-settling sediment which will remain in the TSS plume for longer before eventually settling. In contrast, the larger fraction of faster-settling sediment in the silty sand scenario may result in larger absolute TSS magnitudes, though over more compact areas around releases due to the reduced dispersion times.

General footprint extents obtained for *existing* and *proposed* port configurations are similar. However, we note smaller percentage values for the *proposed* scenario in general. The reduction can be explained by the larger depth at release site which comparatively dilutes more the released sediment across the water column and reduce initial TSS.

A comparison of TSS exceedance for TSHD and CSD dredging at *site 1a* and BHD dredging at site *BerthPocket* is shown Figure 3-23 (TSS>40 mg.L^{-1}, *existing* bathymetry). We note that CSD footprints are narrower than TSHD ones, and mostly contained to the deeper channel. We note that larger percentage of time above TSS threshold are more extended for CSD than for TSHD (i.e. dark purple footprints) but this also due to the assumption of non-stop CSD dredging whereas dredging cycles are considered for the TSHD (i.e. including period of no dredging occur). The footprints are expectedly less extended for the BHD dredger near the berth, with reduced percentage of time the TSS threshold is exceeded across the water column, except in the immediate dredging site vicinity.

TSS > 20mg.L^{-1} **_TSS > 40mg.L^{-1}_** **_TSS > 80mg.L^{-1}_** **_TSS > 160mg.L^{-1}_**

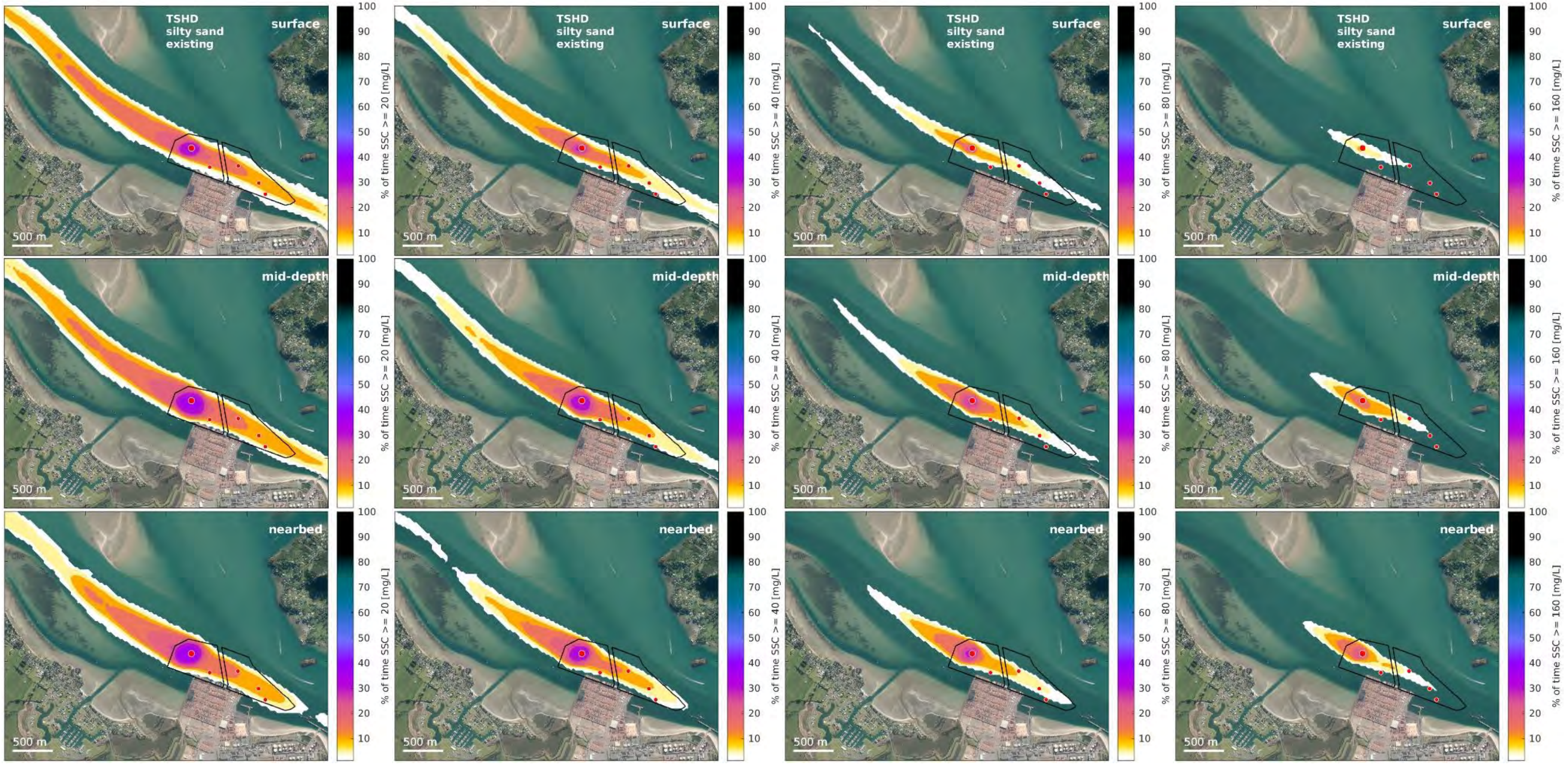

Figure 3-19 ***Percentage of time*** *total suspended sediment concentrations [mg.L^{-1}] are above thresholds of* ***20, 40, 80 and 160 mg.L^{-1}****(left to right), at surface, mid water and nearbed levels (top to bottom) for* ***TSHD*** *dredging at* ***site 1a,*** *over the* ***existing bathymetry.*** *Results are shown for the* ***silty sand****. The dredger is assumed to dredge continuously over the 1-month simulation period. Results were masked below 1%.*

TSS > 20mg.L $^{-1}$ ***TSS > 40mg.L*** $^{-1}$ ***TSS > 80mg.L*** $^{-1}$ ***TSS > 160mg.L*** $^{-1}$

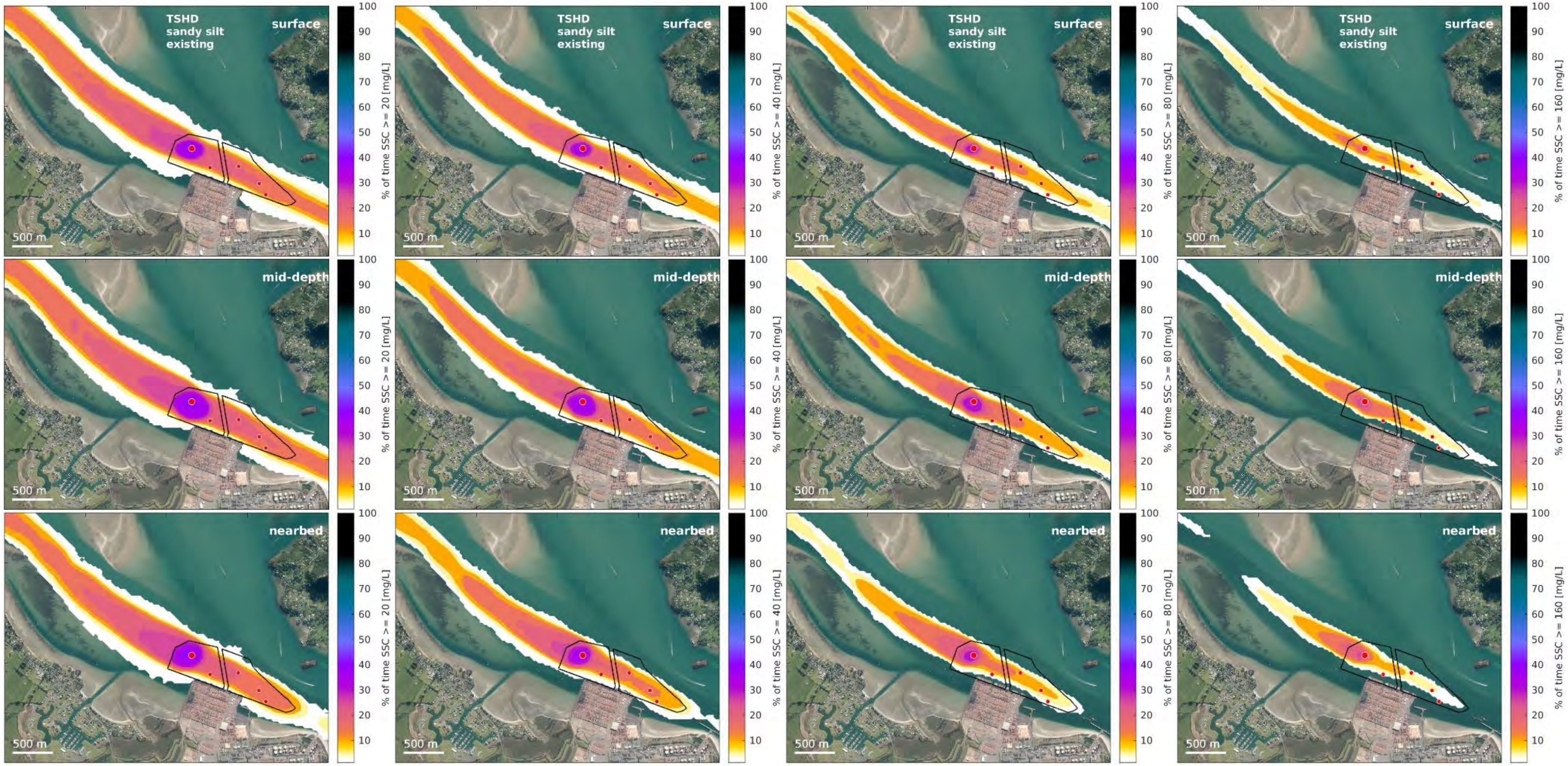

Figure 3-20 ***Percentage of time*** *total suspended sediment concentrations [mg.L*$^{-1}$*] are above thresholds of 20, 40, 80 and 160 mg.L*$^{-1}$*(left to right), at surface, mid water and nearbed levels (top to bottom) for* ***TSHD*** *dredging at* ***site 1a,*** *over the* ***existing bathymetry.*** *Results are shown for the* ***sandy silt****. The dredger is assumed to dredge continuously over the 1-month simulation period. Results were masked below 1%.*

TSS > 20mg.L^{-1} **TSS > 40mg.L^{-1}** **TSS > 80mg.L^{-1}** **TSS > 160mg.L^{-1}**

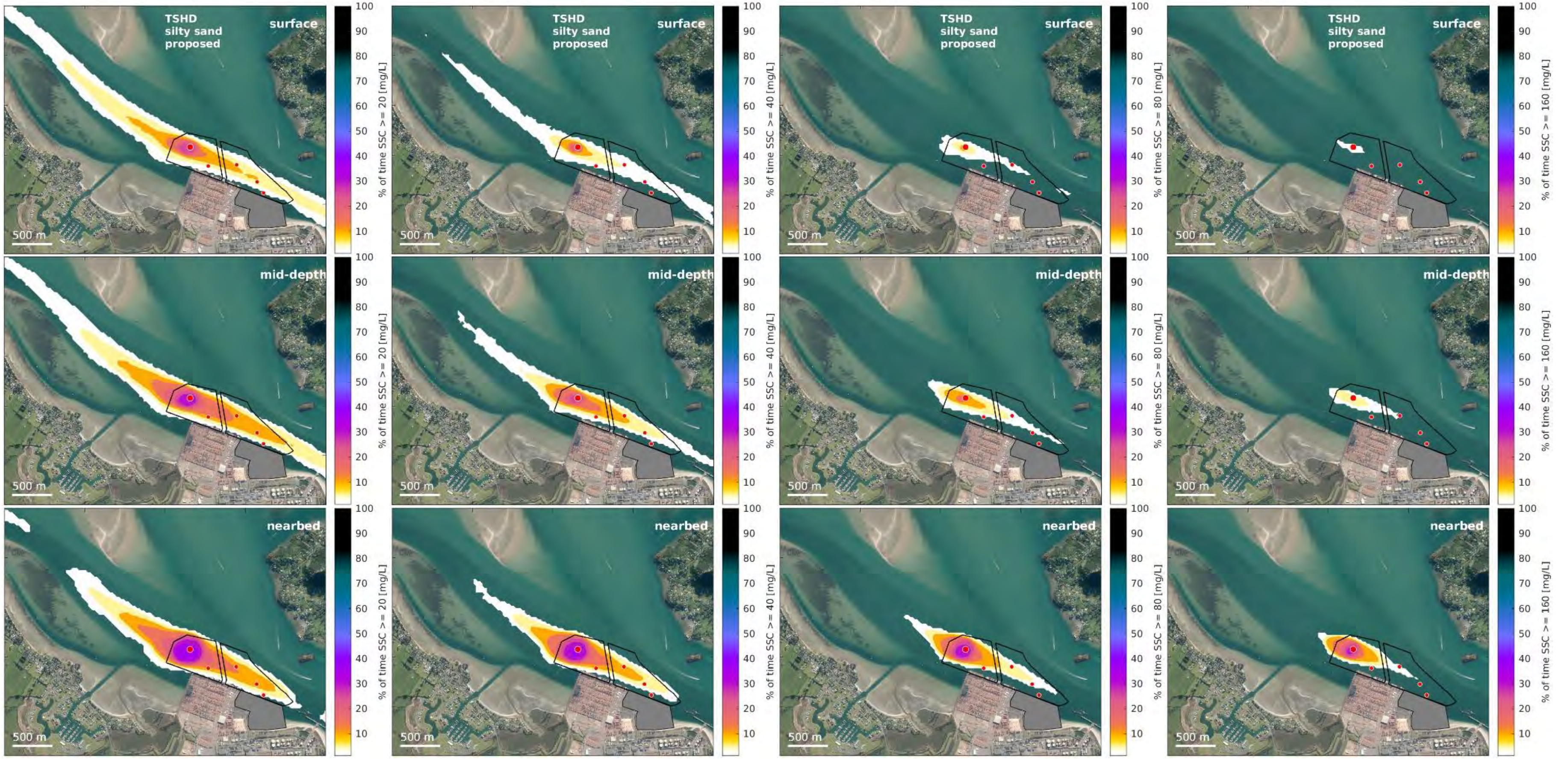

Figure 3-21 ***Percentage of time*** *total suspended sediment concentrations [mg.L^{-1}] are above thresholds of 20, 40, 80 and 160 mg.L^{-1}(left to right), at surface, mid water and nearbed levels (top to bottom) for* ***TSHD*** *dredging at* ***site 1a,*** *over the* ***proposed bathymetry.*** *Results are shown for the* ***silty sand****. The dredger is assumed to dredge continuously over the 1-month simulation period. Results were masked below 1%.*

TSS > 20mg.L^{-1} ***TSS > 40mg.L^{-1}*** ***TSS > 80mg.L^{-1}*** ***TSS > 160mg.L^{-1}***

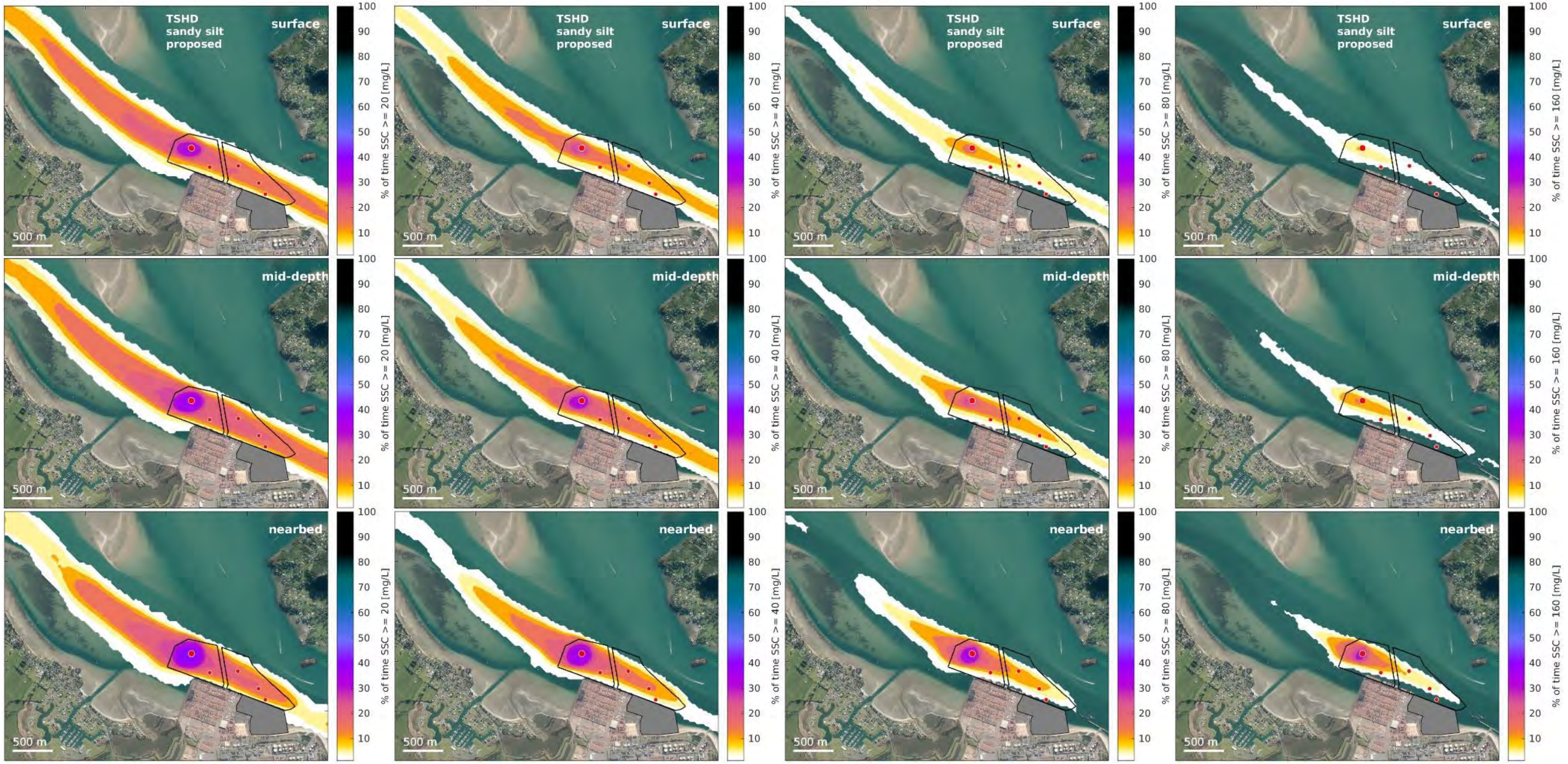

Figure 3-22 ***Percentage of time*** *total suspended sediment concentrations [mg.L^{-1}] are above thresholds of 20, 40, 80 and 160 mg.L^{-1}(left to right), at surface, mid water and nearbed levels (top to bottom) for* ***TSHD*** *dredging at* ***site 1a,*** *over the* ***proposed bathymetry.*** *Results are shown for the* ***sandy silt****. The dredger is assumed to dredge continuously over the 1-month simulation period. Results were masked below 1%.*

TSHD (Site 1a) ***CSD (Site 1a)*** ***BHD (Site Berth Pocket)***

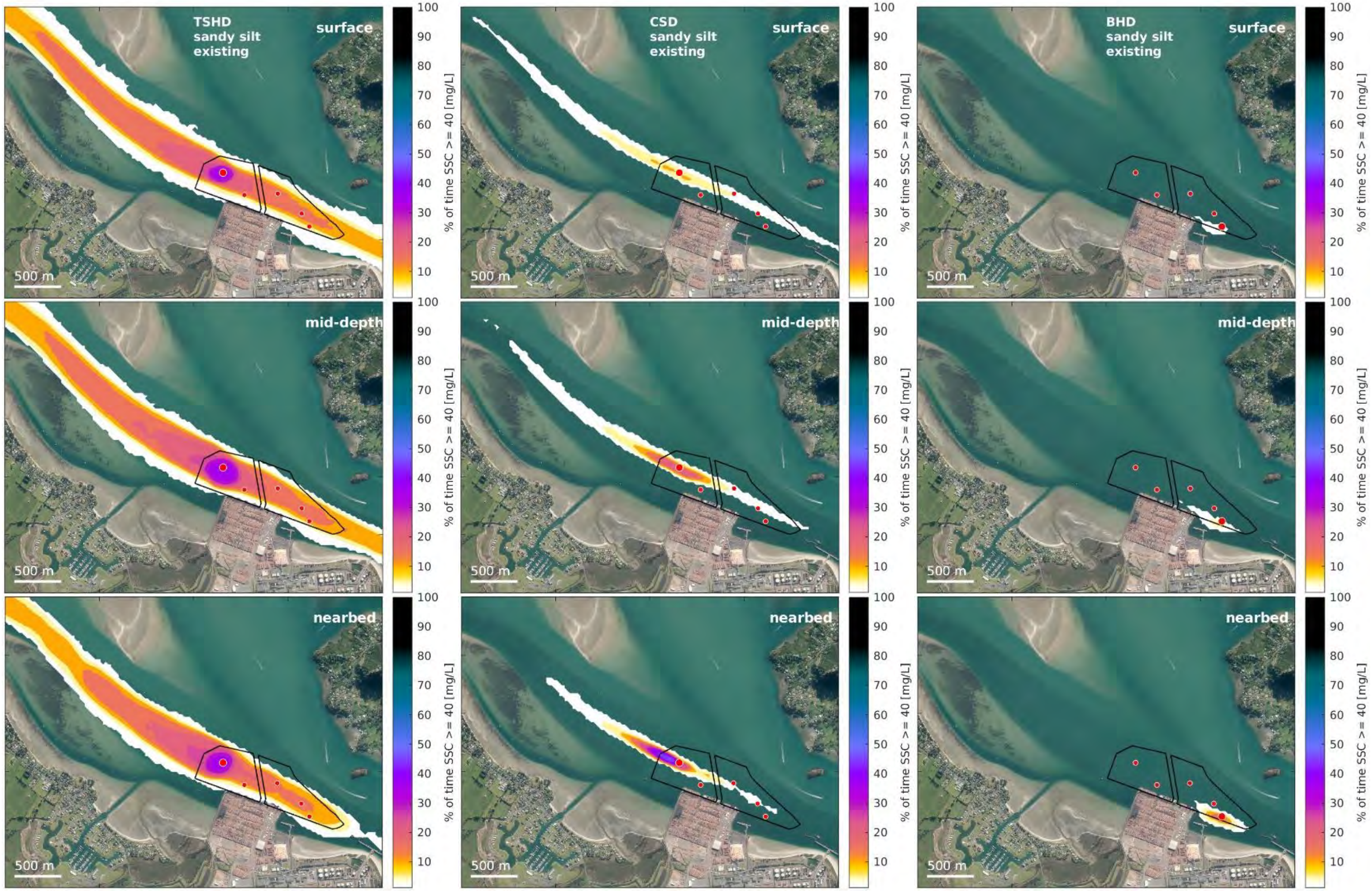

Figure 3-23 ***Percentage of time*** *total suspended sediment concentrations [mg.L^{-1}] are above thresholds of 40 mg.L^{-1}(left to right), at surface, mid water and nearbed levels (top to bottom) for* ***TSHD*** *and* ***CSD*** *dredging at* ***site 1a, and BHD*** *dredging at site* ***BerthPocket*** *over the* ***existing bathymetry.*** *Results are shown for the* ***sandy silt****. The dredger is assumed to dredge continuously over the 1-month simulation period. Results were masked below 1%.*

3.2.4 Discussion on potential for sediment resuspension

The cumulative deposition footprints obtained from the simulations assume that sediments stay in place once they settled on the seabed. In reality, some sediment resuspension is possible, with modulations with respect to the sediment type, notably percentage of fines and corresponding critical shear stress, degree of consolidation and ambient bed shear stress magnitude. In that sense, the presented deposition maps inform on the initial sediment deposition patterns. They can be considered relatively conservative since subsequent sediment resuspension and further dispersion is possible, thus potentially reducing the initial deposition thickness. That being, it is also possible that some local accumulation areas could develop notably in low flow regions, which could locally increase deposition thickness relative to the "initial-deposition" maps.

Examples of high and low bed shear stress maps obtained from MOS (2022b) are shown in Figure 3-24. Guidance on expected critical bed shear stresses for sand-mud mixtures, as a function of the percentage of fines (d_{50}<62 microns), is provided in Figure 3-25. Provided the sediment will be weakly consolidated due to the recent dredging, Figure 3-25 suggests critical bed shear stress of 0.6 N/m^2 for the sandy silt (48% fines), and 0.3 N/m^2 for the silty sand (13.5% fines). Given the bed shear stress magnitudes throughout harbour (Figure 3-24), (form light yellow), it is likely that some redistribution of the sediment that initially settled within the main channel will occur, particularly where flows and shear stress are the largest. "Final" deposited location would be closer to the harbour channel edges where ambient flows become low enough to prevent subsequent resuspension. In contrast, there is limited potential for resuspension in the areas where ambient bed shear stresses are low due to the relative shelter from the stronger channel flows.

Besides the inherent uncertainties on effective critical bed shear stress, including the resuspension processes in Lagrangian particle-tracking model can be challenging due to the large number of particles that would need to remain in the domain to ensure a good representation of both the plume dispersion patterns (while particles are in the water column), and resuspension processes (where settled particles may be picked up again by ambient currents, disperse, re-settle etc..).

We also note that predicted deposition fields can show some local accumulation of sediment near the edges of the turning basin to be dredged (e.g. Figure 3-11, simulations on *proposed* bathymetry). In reality, a feedback loop would likely develop before reaching the final *proposed* bathymetry state where local deposition may locally increase flows and bed shear stresses, thus possibly allowing sediment re-suspension and advection to further calmer areas. Such an hydro-morphological feedback loop is not included in the present Lagrangian simulations therefore these depositional features should be interpreted with care, however they suggest potential modulation of the deposition patterns near the turning basin edges, especially to the northwest, with possible impacts on seabed stability and dredging effort.

To better characterise the outcome of resuspension processes in the harbour, solutions could include shorter Lagrangian plumes simulations including the full resuspension physics, or morphological model simulations (e.g. MOS, 2022b) with bathymetries updated over time to reflect the initial dredging-related deposition.

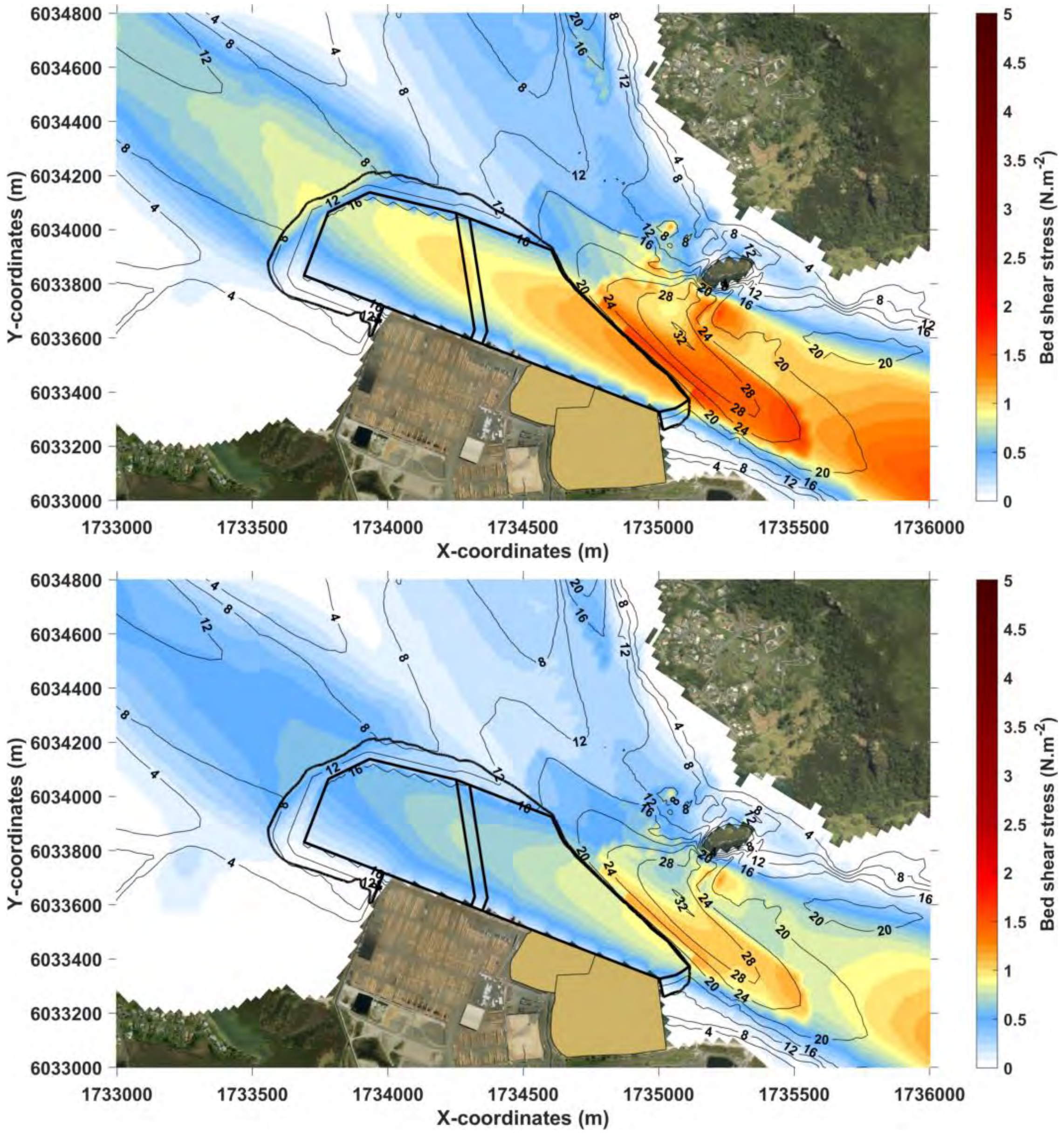

Figure 3-24 Examples of high and low bed shear stress fields in the harbour obtained from the morphological model implemented in (MOS, 2022b)

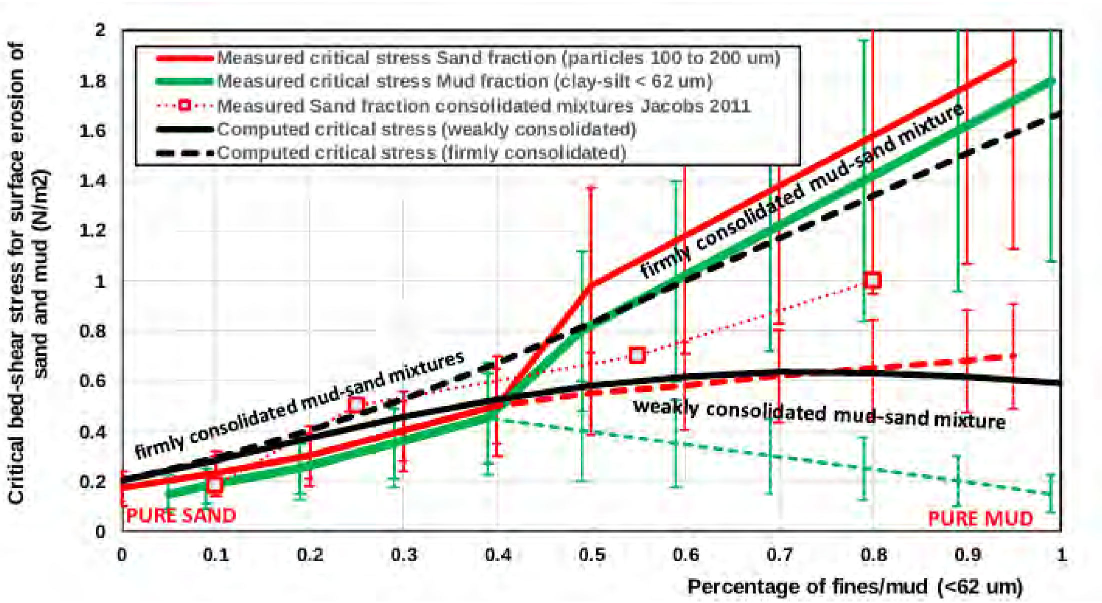

Figure 3-25 Empirical relationships between critical bed shear tress for surface erosion and percentage of fines (silt/clay) in the mud-sand mixture (from Van Rijn, 2016).

4. Conclusions

Northport is planning to expand the port's capacity by reclaiming land, building additional berths and dredging a larger turning basin

The present study characterizes the dispersion of the sediment plumes and deposition resulting from the required dredging works. Dredging is expected to be undertaken using a range of different methods, including Trailing Suction Hopper Dredger (TSHD) and Cutter Section Dredge (CSD) for the turning basin, and Backhoe Dredger (BHD) in the vicinity of the berths.

A large number of particle-tracking simulations was undertaken to investigate the effects of different dredging methods, dredging locations, and sediment size distributions on the dredging sediment plumes and sediment deposition. Simulations were reproduced for both the existing and proposed (i.e. post dredging and reclamation) bathymetries to assess relative changes and impacts.

In general, mean sediment plume and deposition footprints are elliptical, centred on the release sites, and follow a clear northwest-southeast-axis consistent with the ambient hydrodynamics dominated by tides and morphology of the main harbour channel. The predicted dispersion footprints indicate no significant dispersion towards secondary northward channel arm. In the turning basin, general dredging plume and sediment deposition footprints are more extended and have larger sediment concentration levels for the TSHD than for the CSD. This is notably due to the THSD's overflow phase which intermittently release significant amounts of sediment across the entire water column, and near the seabed. The BHD dredging near the berth results in comparatively smaller plumes and depositions.

The new eastern reclamation has a limited impact on general plume dispersion patterns with a slight flow deflection in its vicinity. Predicted deposition fields for the proposed bathymetry (i.e. .post-dredging) indicate possible sediment accumulation near the northwest and southeast edges of the new turning basin, with magnitude depending on dredging locations. The depositional features could impact the amount of dredging time required to reach the required depths over these areas.

5.References

Batchelor, G.K. (1952). Diffusion in a field of homogeneous turbulence. II. The relative motion of particles. Camb. Philos. Soc. 345–362. .

Becker, J., van Eekelen, E., van Wiechen, J., de Lange, W., Damsma, T., Smolders, T., and van Koningsveld, M. (2015). Estimating source terms for far field dredge plume modelling. J. Environ. Manage. *149*, 282–293. https://doi.org/10.1016/j.jenvman.2014.10.022.

Becker J., van Eekelen E., van Wiechen J., de Lange W., Damsma T., Smolders T., and van Koningsveld M. (2015). Estimating source terms for far field dredge plume modelling. J. Environ. Manage. *149*, 282–293. .

Bellasio, R., Bianconi,R, Mosca, S., and Zannetti, P. (2017). Formulation of the Lagrangian particle model LAPMOD and its evaluation against Kincaid SF6 and SO2 datasets. Atmos. Environ. *163*, 87–98. .

Botev, Z. I, Grotowski, J. F, and Kroese, D.P (2010). Kernel density estimation via diffusion. Ann. Stat. *38*, 2916–2957. .

Burt, T.N. (1996). Guidelines for the beneficial use of dredged materials - HR Wallingford.

Dagestad K.F, Röhrs J., Breivik O., and Ådlandsvik B. (2018). OpenDrift v1.0: a generic framework for trajectory modelling. Geosci. Model Dev. *11*, 1405–1420. .

List, E., Gartrell, G., and Winant, C. (1990). Diffusion and dispersion in coastal waters. J. Hydraul. Eng. *116(10)*, 1158–1179. .

MOS (2018a). Dredging Plumes for NorthPort Environment.

MOS (2018b). Hydrodynamic Modelling - Methodology, Validation and Simulations.

MOS (2018c). Morphodynamic Evolution Modelling for the Northport Environment - Five year morphological prediction of the swinging basin morphological response.

MOS (2018d). Morphodynamic Evolution Modelling for the Northport Environment - Morphological model calibration.

MOS (2018e). Northport Dredging Project - Dredging Plume Modelling.

MOS (2021a). Dredge Plume Modelling . Dredging sediment plume dispersion over existing and proposed port configurations.

MOS (2021b). Hydrodynamic Modelling - Effect of Proposed Reclamation Layouts on Hydrodynamics.

MOS (2021c). Morphodynamic Modelling for the Northport Environment. Modelling Update . Predicted morphological response to proposed capital dredging and land reclamation.

MOS (2022a). Hydrodynamic Modelling Update - Effect of Proposed Reclamation Layouts on Hydrodynamics.

MOS (2022b). Morphodynamic Modelling for the Northport Environment. Modelling Update . Predicted morphological response to proposed eastern land reclamation.

Okubo (1974). Some speculations on oceanic diffusion diagrams. Rapp. Procès-Verbaux Reun. Cons. Perm. Int. Pour L'Exploration Mer.

Okubo, A. (1971). Oceanic diffusion diagrams. Deep-Sea Res. *18*, 789–802. .

Richardson, L.F (1962). Atmospheric diffusion shown on a distance neighbour graph. Proc R Soc Lond. *Ser A,* 709-737. .

Röhrs et al. (2019). The effect of vertical mixing on the horizontal drift of oil spills. Ocean Sci. *14*, 1581–1601. .

Silverman, B.W (1986). Density Estimation for Statistics and Data Analysis (London).

Spearman, J., Bray, R.N., Land, J., Burt, T.N., Mead, C.T., and Scott, D. (2007). Plume dispersion modelling using dynamic representation of trailer dredger source terms. In Proceedings in Marine Science, L.P.S. and D.H.S. J.P.-Y. Maa, ed. (Elsevier), pp. 417–448.

Stommel, H. (1949). Horizontal diffusion due to oceanic turbulence. J. Mar. Res. 199–225. .

Van Rijn, L.C. (1993). Principles of sediment transport in rivers, estuaries and coastal seas (Aqua publications Amsterdam).

Van Rijn, L.C. (2016). Initiation of Motion and suspension; Critical Bed-Shear Stress for Sand-Mud Mistures.

Van Rijn, L.J. (2019). Land reclamation of dredged mud - consolidation of soft soils.

Visser A (1997). Using random walk models to simulate the vertical distribution of particles in a turbulent water column. Mar. Ecol.-Prog. Ser. 275–281. .

Vitali, L., Monforti, F., Bellasio, R., Bianconi, R., Sachero, V., Mosca, S., and Zanini, G. (2006). Validation of a Lagrangian dispersion model implementing different kernel methods for density reconstruction. Atmos. Environ. *40*, 8020–8033. .

Winterwerp, J.C. (2002). Near-field behavior of dredging spill in shallow water. J. Waterw. Port Coast. Ocean Eng. *128*, 96–98. .

Appendix A: TSHD source term estimation

Vessel and Cycle	Units	Variables names (Becker et al., 2015)		area_1a	area_1b	area_2ab
Capacity	[m3]		1860			
Dredging cycle						
Hopper infilling - total time	[hours]	t2-t0	1.25	1.1	2.1	1.2
Initial infilling with no overflow	[hours]	t1-t0	0.9375	0.2	0.2	0.2
subsquent infilling with overflow	[hours]	t2-t1	0.3125	0.9	1.9	1.0
Overflow loading ratio	[-]	(t2-t1)/(t2-t0)	0.25	0.8	0.9	0.8
Production Rate		**Reference daily production rate**	**9200**			
Amount of sediment removed **per cycle**	[m3]	Vt=Pr*(t2-t0)		1373.6	1437.5	1360.8
Amount of sediment removed **per cycle**	[kg]	Mt		2197777.8	2300000.0	2177333.3
Production Rate	[m3.s-1]	Pr		0.4	0.2	0.3
Production Rate	[kg.s-1]	Mt/ (t2-t0)		581.4	306.7	511.1
Source terms - masses over a cycle						
Propeller wash(3% of production rate)	[kg]	m_prop		65933.3	69000.0	65320.0
Drag head (3% of production rate)	[kg]	m_drag		65933.3	69000.0	65320.0
Surface losses (1% of production rate))	[kg]	m_surface		21977.8	23000.0	21773.3
Remaining mass transported in hopper	[kg]	Mh = Mt - m_prop -m_drag - m_surface		2043933.3	2139000.0	2024920.0
Mass exiting through overflow	[kg]	Mo =[[(t2-t1)/(t2-t0)]*(1-fsett)*(1-ftrap)] * Mh		1209935.5	1413986.0	1230459.8
Overflow passive plume (fac0 = 20%)	[kg]	m_overflow_watercolumn = fac0 *Mo		241987.1	282797.2	246092.0
Overflow density current (1-fac0=80%)	[kg]	m_overflow_denscur = (1-fac0) * Mo		967948.4	1131188.8	984367.8
Mass remaining in hopper at end of cycle	[kg]	M_remaining = Mh - Mo		833997.8	725014.1	794460.3
Source terms - mass fluxes						
Propeller wash(3%)	[kg.s-1]	m_prop/(t2-t0)		17.4	9.2	15.3
Drag head (3%)	[kg.s-1]	m_drag/(t2-t0)		17.4	9.2	15.3
Surface losses (1%)	[kg.s-1]	m_surface/(t2-t0)		5.8	3.1	5.1
Overflow passive plume (fac0 = 20%)	[kg.s-1]	m_overflow_watercolumn/(t2-t1)		79.1	41.7	69.5
Overflow density current (1-fac0 = 80%)	[kg.s-1]	m_overflow_denscur/(t2-t1)		316.3	166.8	278.1

Appendix B: Full set of plots for TSS and deposition field

All mean and 90th percentile TSS maps as well as final cumulative deposition fields are provided in Appendix B (as digital image files) for all scenarios considered:

- 3 different dredgers (TSHD, BHD and CSD, Figure 2-2 to Figure 2-4)

5 different sites (Figure 2-1 and Table 2-1)

- 1 month period (September 2010 - La Niña episode)

existing versus *proposed* bathymetries (Figure 2-1)

- *sandy silt* versus *silty sand* (PSD in Table 2-4 and Table 2-5)